Eur. Phys. J. C (2019) 79:836
https://doi.org/10.1140/epjc/s10052-019-7335-x

THE EUROPEAN PHYSICAL JOURNAL C

Regular Article - Experimental Physics

Identification of boosted Higgs bosons decaying into *b*-quark pairs with the ATLAS detector at 13 TeV

ATLAS Collaboration[⋆]

CERN, 1211 Geneva 23, Switzerland

Received: 27 June 2019 / Accepted: 23 September 2019 / Published online: 10 October 2019

Abstract This paper describes a study of techniques for identifying Higgs bosons at high transverse momenta decaying into bottom-quark pairs, $H \to b\bar{b}$, for proton–proton collision data collected by the ATLAS detector at the Large Hadron Collider at a centre-of-mass energy $\sqrt{s} = 13$ TeV. These decays are reconstructed from calorimeter jets found with the anti-k_t $R = 1.0$ jet algorithm. To tag Higgs bosons, a combination of requirements is used: b-tagging of $R = 0.2$ track-jets matched to the large-R calorimeter jet, and requirements on the jet mass and other jet substructure variables. The Higgs boson tagging efficiency and corresponding multijet and hadronic top-quark background rejections are evaluated using Monte Carlo simulation. Several benchmark tagging selections are defined for different signal efficiency targets. The modelling of the relevant input distributions used to tag Higgs bosons is studied in 36 fb^{-1} of data collected in 2015 and 2016 using $g \to b\bar{b}$ and $Z(\to b\bar{b})\gamma$ event selections in data. Both processes are found to be well modelled within the statistical and systematic uncertainties.

1 Introduction

The Large Hadron Collider (LHC) centre-of-mass energy of 13 TeV greatly extends the sensitivity of the ATLAS experiment [1] to heavy new particles. In several new physics scenarios [2–4], these heavy new particles may have decay chains including the Higgs boson [5,6]. The large mass-splitting between these resonances and their decay products results in a high-momentum Higgs boson, causing its decay products to be collimated. The decay of the Higgs boson into a $b\bar{b}$ pair has the largest branching fraction within the Standard Model (SM), and thus is a major decay mode to use when searching for resonances involving high-momentum Higgs bosons (see e.g. Ref. [7]), as well as for measuring the SM Higgs boson properties. The signature of a boosted Higgs boson decaying into a $b\bar{b}$ pair is a collimated flow of particles, in this document called a 'Higgs-jet', having an energy and angular distribution of the jet constituents consistent with a two-body decay and containing two b-hadrons. The techniques described in this paper to identify Higgs bosons decaying into bottom-quark pairs have been used successfully in several analyses [8–10] of 13 TeV proton–proton collision data recorded by ATLAS.

In order to identify, or tag, boosted Higgs bosons it is paramount to understand the details of b-hadron identification and the internal structure of jets, or jet substructure, in such an environment [11]. The approach to tagging presented in this paper is built on studies from LHC runs at $\sqrt{s} = 7$ and 8 TeV, including extensive studies of jet reconstruction and grooming algorithms [12], detailed investigations of track-jet-based b-tagging in boosted topologies [13], and the combination of substructure and b-tagging techniques applied in the Higgs boson pair search in the four-b-quark final state [14] and for discrimination of Z bosons from W bosons [15]. Gluon splitting into b-quark pairs at small opening angles has been studied at $\sqrt{s} = 13$ TeV by ATLAS [16]. The identification of Higgs bosons at high transverse momenta through the use of jet substructure has also been studied by the CMS Collaboration and their techniques are described in Refs. [17,18].

The Higgs boson tagging efficiency and background rejection for the two most common background processes, the multijet and hadronic top-quark backgrounds, are evaluated using Monte Carlo simulation. In addition, two processes with a topology similar to the signal, $Z \to b\bar{b}$ decays and $g \to b\bar{b}$ splitting, are used to validate Higgs-jet tagging techniques in data at $\sqrt{s} = 13$ TeV. In particular the modelling of relevant Higgs-jet properties in Monte Carlo simulation is compared with data. The $g \to b\bar{b}$ process allows the modelling of one of the main backgrounds to be validated. The $Z \to b\bar{b}$ process is a colour-singlet resonance with a mass close to the Higgs boson mass and thus very similar to the $H \to b\bar{b}$ signal.

After a brief description of the ATLAS detector in Sect. 2 and of the data and simulated samples in Sect. 3, the object reconstruction, selection and labelling is discussed in Sect. 4.

⋆ e-mail: atlas.publications@cern.ch

Section 5 describes relevant systematic uncertainties. The Higgs-jet tagging algorithm and its performance are presented in Sect. 6. Sections 7 and 8 discuss a comparison between relevant distributions in data control samples dominated by $g \to b\bar{b}$ and $Z(\to b\bar{b})\gamma$ and the corresponding simulated events, respectively. Finally, conclusions are presented in Sect. 9.

2 ATLAS detector

The ATLAS detector [1] at the LHC covers nearly the entire solid angle around the collision point.[1] It consists of an inner tracking detector surrounded by a thin superconducting solenoid, electromagnetic and hadronic calorimeters, and a muon spectrometer incorporating three large superconducting toroid magnets. The inner-detector system (ID) is immersed in a 2 T axial magnetic field and provides charged-particle tracking in the range $|\eta| < 2.5$.

Preceding data-taking at a centre-of-mass energy of 13 TeV, the high-granularity silicon pixel detector was equipped with a new barrel layer, located at a smaller radius (of about 34 mm) than the other layers [19,20]. The upgraded pixel detector covers the vertex region and typically provides four measurements for tracks originating from the luminous region. It is followed by a silicon microstrip tracker, which usually provides four space points per track. These silicon detectors are complemented by a transition radiation tracker, which enables radially extended track reconstruction up to $|\eta| = 2.0$. The transition radiation tracker also provides electron identification information based on the fraction of hits above a certain energy deposit threshold corresponding to transition radiation.

The calorimeter system covers the pseudorapidity range $|\eta| < 4.9$. Within the region $|\eta| < 3.2$, electromagnetic calorimetry is provided by barrel and endcap high-granularity lead/liquid-argon (LAr) calorimeters, with an additional thin LAr presampler covering $|\eta| < 1.8$ to correct for energy loss in material upstream of the calorimeters. Hadronic calorimeter within $|\eta| < 1.7$ is provided by a steel/scintillating-tile calorimeter, segmented into three barrel structures, and two copper/LAr hadronic endcap calorimeters covering $1.5 < |\eta| < 3.2$. The solid angle coverage is completed with forward copper/LAr and tungsten/LAr calorimeter modules optimised for electromagnetic and hadronic measurements respectively.

The muon spectrometer (MS) comprises separate triggering and high-precision tracking chambers measuring the deflection of muons in a magnetic field generated by superconducting air-core toroids. The precision chamber system covers the region $|\eta| < 2.7$ with three layers of monitored drift tubes, complemented by cathode strip chambers in the forward region, where the background is highest. The muon trigger system covers the range $|\eta| < 2.4$ with resistive plate chambers in the barrel, and thin gap chambers in the endcap regions.

A two-level trigger system is used to select interesting events [21]. The level-1 trigger is implemented in hardware and uses a subset of detector information to reduce the event rate to a design value of at most 100 kHz. This is followed by a software-based high-level trigger, which reduces the event rate further to an average of 1 kHz.

3 Data and simulated event samples

The data used in this paper were recorded with the ATLAS detector during the 2015 and 2016 LHC proton–proton (pp) collision runs, and correspond to a total integrated luminosity of 36.1 fb^{-1} at $\sqrt{s} = 13$ TeV. This integrated luminosity is calculated after the imposition of data quality requirements, which ensure that the ATLAS detector was in good operating condition.

Several Monte Carlo (MC) simulated event samples were used for the optimisation of the Higgs boson tagger, estimation of its performance, and the comparisons between data and simulation.

Simulated events with a broad transverse momentum (p_{T}) spectrum of Higgs bosons were generated as decay products of Randall–Sundrum gravitons G^* in a benchmark model with a warped extra dimension [2], $G^* \to HH \to b\bar{b}b\bar{b}$, over a range of graviton masses between 300 and 6000 GeV. The events were simulated using the MadGraph5_aMC@NLO generator [22]. Parton showering, hadronisation and the underlying event were simulated with Pythia8 [23] using the leading-order (LO) NNPDF2.3 parton distribution function (PDF) set [24] and the ATLAS A14 [25] set of tuned parameters.

Events containing the $Z(\to b\bar{b})\gamma$ and γ + jets processes were simulated with the Sherpa v2.1.1 [26–29] LO generator. The matrix elements were configured to allow up to three partons in the final state in addition to the Z boson or the photon. The Z boson was produced on-shell and required to decay hadronically. The CT10 next-to-leading-order (NLO) PDF set [30,31] was used. The $t\bar{t}\gamma$ MC events were modelled by MadGraph interfaced with Pythia8 for showering, hadronisation and the underlying event with the LO

[1] ATLAS uses a right-handed coordinate system with its origin at the nominal interaction point (IP) in the centre of the detector and the z-axis along the beam pipe. The x-axis points from the IP to the centre of the LHC ring, and the y-axis points upwards. Cylindrical coordinates (r, ϕ) are used in the transverse plane, ϕ being the azimuthal angle around the z-axis. The pseudorapidity is defined in terms of the polar angle θ as $\eta = -\ln\tan(\theta/2)$. Angular distance is measured in units of $\Delta R \equiv \sqrt{(\Delta\eta)^2 + (\Delta\phi)^2}$.

NNPDF2.3 PDF set and the A14 underlying-event tune. Simulated events of hadronically decaying $W\gamma$ were generated using SHERPA v2.1.1, with the same configuration as the one used for the $Z\gamma$ sample.

To cover a large range of top-quark transverse momenta, hadronically decaying top quarks were generated using Z' bosons decaying into $t\bar{t}$ pairs over a range of Z' boson masses between 400 and 5000 GeV. These samples were simulated using PYTHIA8 with the LO NNPDF2.3 PDF set and the A14 underlying-event tune.

Finally, inclusive multijet events were generated using PYTHIA8, with the LO NNPDF2.3 PDF set and the A14 underlying-event tune; and with Herwig++ [32], with the CTEQ [33] PDF set and the UEEE [34] underlying event tune. To increase the number of simulated events with semimuonically decaying hadrons for the $g \to b\bar{b}$ analysis, samples of multijet events filtered to have at least one muon with p_{T} above 3 GeV and $|\eta| < 2.8$ were produced with PYTHIA8 and Herwig++ using the same PDF set and underlying-event tunes as the unfiltered multijet samples.

In all cases except events generated using SHERPA, EvtGen [35] was used to model the decays of b- and c-hadrons. All simulated event samples included the effect of multiple pp interactions in the same and neighbouring bunch crossings ('pile-up') by overlaying simulated minimum-bias events on each simulated hard-scatter event. The minimum-bias events were simulated with the single-, double- and non-diffractive pp processes of PYTHIA8 using the A2 tune [36] and the MSTW2008 LO PDF [37–39]. The detector response to the generated events was simulated with GEANT 4 [40,41].

4 Object and event reconstruction

In this section the object reconstruction, associations among the objects, jet labelling, and the procedure to determine the heavy-flavour content of jets are described.

4.1 Calorimeter jets

Calorimeter-based jets are built from noise-suppressed topological clusters and are reconstructed using FASTJET [42] with the anti-k_t algorithm [43] with a radius parameter of $R = 1.0$ (large-R jets) or $R = 0.4$ (small-R jets). The topological clusters of the large-R jets are brought to the hadronic energy scale using the local hadronic cell weighting scheme [44]. The large-R jets are groomed using trimming [12,45] to discard the softer components of jets that originate from initial-state radiation, pile-up interactions or the underlying event. This is done by reclustering the constituents of the initial jet, using the k_t algorithm [46,47], into subjets of radius parameter $R_{\mathrm{sub}} = 0.2$ and removing any subjet that has a p_{T} less than 5% of the parent jet p_{T}. The simulation-based calibration of the trimmed jet p_{T} and mass is described in Ref. [48]. Large-R jets are required to have $p_{\mathrm{T}} > 250$ GeV and $|\eta| < 2.0$. Small-R jets are calibrated with a series of simulation-based corrections and in situ techniques, including corrections to account for pile-up energy entering the jet area, as described in Ref. [49]. They are required to have $p_{\mathrm{T}} > 20$ GeV and $|\eta| < 2.5$. To reduce the number of small-R jets originating from pile-up interactions, these jets are required to pass the jet vertex tagger (JVT) [50] requirement if the jets are in the range $p_{\mathrm{T}} < 60$ GeV and $|\eta| < 2.4$. The JVT requirement has an inclusive hard-scatter efficiency of about 97% in that kinematic region.

4.2 Truth jets

Truth jets are built in simulated events by using 'truth' information from MC generator's event record to cluster stable particles with a lifetime τ_0 in the rest frame such that $c\tau_0 > 10$ mm. Particles such as muons and neutrinos which do not leave significant energy deposits in the calorimeter are excluded. The same jet-clustering algorithm and trimming procedure as for calorimeter jets are used to reconstruct truth jets.

4.3 Track-jets

Track-jets are built with the anti-k_t algorithm with a radius parameter of $R = 0.2$ [13] from at least two ID tracks with $p_{\mathrm{T}} > 0.4$ GeV and $|\eta| < 2.5$ that are either associated with the primary vertex or have a longitudinal impact parameter $|z_0 \sin(\theta)| < 3$ mm. Such requirements greatly reduce the number of tracks from pile-up vertices whilst being highly efficient for tracks from the hard-scatter vertex. Once the track-jet's axis is determined, tracks selected with looser impact parameter requirements are matched to the jet in order to collect the tracks needed to effectively run the jet flavour tagging algorithms. The tracks are matched to the jet by using the angular separation ΔR between the track and the track-jet's axis. The ΔR requirement varies as a function of jet p_{T}, being wide for low-p_{T} jets and narrower for high-p_{T} jets as described in Ref. [51]. Only track-jets with $p_{\mathrm{T}} > 10$ GeV and $|\eta| < 2.5$ are used for the analysis.

4.4 Muons

Muons are reconstructed from a combination of measurements from the ID and the MS. They are required to pass identification requirements based on quality criteria applied to the ID and MS tracks. The 'Loose' identification working point defined in Ref. [52] is used. Muons selected for this analysis are required to have $p_{\mathrm{T}} > 5$ GeV and $|\eta| < 2.4$.

4.5 Photons

Photons are reconstructed from clusters of energy deposits in the electromagnetic calorimeter. Clusters without matching tracks are classified as unconverted photon candidates. A photon candidate that can be matched to a reconstructed vertex or track consistent with a photon conversion is considered as a converted photon candidate [53]. The photon energy estimate is described in Ref. [54]. Requirements on the shower shape in the electromagnetic calorimeter and on the energy fraction measured in the hadronic calorimeter are used to identify photons; the 'Tight' identification working point is applied in the analysis [53]. In order to select prompt photons, the photons are required to fulfil the 'Tight' isolation criteria. The photons are required to have $|\eta| < 1.37$ or $1.52 < |\eta| < 2.37$ and $E_{\mathrm{T}} > 175$ GeV. The latter requirement is applied to insure efficient triggering.

4.6 Track-jet ghost association

In events with a dense hadronic environment an ambiguity often exists when matching track-jets to calorimeter jets. The track-jet matching to large-R jets is performed by applying ghost association [12,55,56]: the large-R jet clustering process using the anti-k_t algorithm with $R = 1.0$ is repeated with the addition of 'ghost' versions of the track-jets that have the same direction but infinitesimally small p_{T}, so that they do not change the properties of the large-R calorimeter jets. A track-jet is associated with the large-R jets if its ghost version is contained in the jet after reclustering. The reclustering is applied to the untrimmed large-R jets. The reclustered jets are identical to the jets before the reclustering, with the addition of the matched track-jets retained as associated objects. This provides a robust matching procedure, and matching to jets with irregular boundaries can be achieved in a way that is less ambiguous than a simple geometric matching.

4.7 Jet labelling

The performance of the tagger is evaluated on the basis of labelled large-R jets. Higgs-jets are defined as calorimeter-based large-R jets with a Higgs boson and the corresponding two b-hadrons from the Higgs boson decay found in the MC event record within $\Delta R = 1$ of the large-R jet. Only the Higgs boson with the highest p_{T} in the event is considered and it is required to have $p_{\mathrm{T}} > 250$ GeV and $|\eta| < 2.0$. The b-hadron must have p_{T} above 5 GeV and $|\eta| < 2.5$. Configurations where more than one Higgs boson is found within the large-R jet are excluded. Top-jets are defined as large-R jets in which exactly one top quark is found in the MC event record within $\Delta R = 1$ of the large-R jet.

4.8 Jet flavour labelling

The labelling of the flavour of the track-jets in simulation is done by geometrically matching the jet with truth hadrons. If a weakly decaying b-hadron with p_{T} above 5 GeV is found within $\Delta R = 0.2$ of the track-jet's direction, the track-jet is labelled as a b-jet. In the case that the b-hadron could match more than one track-jet, only the closest track-jet is labelled as a b-jet. If no b-hadron is found, the procedure is repeated for weakly decaying c-hadrons to label c-jets. If no c-hadron is found, the procedure is repeated for τ-leptons to label τ-jets. A jet for which no such matching can be made is labelled as a light-flavour jet.

4.9 b-jet identification

Track-jets containing b-hadrons are identified using a multivariate MV2c10 algorithm [51,57], which exploits the information about the jet kinematics, the impact parameters of tracks within jets, and the presence of displaced vertices. The training is performed on jets from $t\bar{t}$ events with b-jets as signal, and a mix of approximately 93% light-flavour jets and 7% c-jets as background. A particular b-tagging requirement on MV2c10 results in a given efficiency, known as an efficiency working point (WP). The efficiency WP is calculated from the inclusive p_{T} and η spectra of jets from an inclusive $t\bar{t}$ sample. For example a WP with 70% efficiency corresponds to a factor of 120 in the light-quark/gluon-track-jet rejection and a factor of seven in the c-track-jet rejection. Different WPs (60%, 70%, 77% and 85%) are studied in the analyses presented in this paper and jets satisfying a particular MV2c10 criterion WP are referred to as 'b-tagged jets'.

4.10 Large-R jet mass

To overcome the limited angular resolution for the energy deposits used to reconstruct the calorimeter-based jet mass (m^{calo}), an independent jet mass estimate using tracking information is developed, the 'track-assisted jet mass', m^{TA} [48]. A weighted combination of calorimeter-based and track-assisted jet masses, m^{comb} [48], is used in the analysis. The m^{comb} resolution is very similar to the m^{calo} resolution at Higgs-jet p_{T} below 700 GeV and improves with increasing p_{T}. Muons from semileptonic b-hadron decays do not leave significant energy deposits in the calorimeter, so they are considered separately in the calculation of the m^{comb} observable. The resulting neutrinos are not taken into account because they are not measured by the detector directly. The four-momentum of the closest muon candidate within $\Delta R = 0.2$ of the b-tagged track-jet is added to the four-momentum of the large-R-jet after subtraction of the muon energy loss in the calorimeter. Only the calorimeter-based component of the m^{comb} observable is corrected [58]. The resolution of

the muon-corrected Higgs-jet mass, m^{corr}, is improved by about 10% at transverse momenta below 500 GeV, while the improvement is not as pronounced at higher p_{T}, as was shown in Ref. [59].

5 Systematic uncertainties

5.1 Large-R jets

The uncertainties in the jet energy, mass, and substructure scales are evaluated by comparing the ratio of calorimeter-based to track-based measurements in dijet data and simulation [48]. The sources of uncertainty in these measurements are treated as fully correlated among p_{T}, mass, and substructure scales. The resolution uncertainty of the large-R jet observables is evaluated in measurements documented in Ref. [48] and is assessed by applying an additional smearing to these observables. The jet energy resolution uncertainty is estimated by degrading the nominal resolution by an absolute 2%. Similarly, the jet mass resolution is degraded by a relative 20% to estimate the jet mass resolution uncertainty. The parton-shower-related uncertainty for the $g \to b\bar{b}$ analysis is estimated by comparing the nominal PYTHIA8 multijet sample with Herwig++ samples.

5.2 Flavour tagging

The flavour-tagging efficiency and its uncertainty for b- and c-jets is estimated in $t\bar{t}$ events, while the light-flavour-jet misidentification rate and uncertainty is determined using dijet events [60–62]. Correction factors are applied to the simulated event samples to compensate for differences between data and simulation in the b-tagging efficiency for track-jets with $p_{\text{T}} < 250$ GeV. Correction factors and uncertainties for c-jets and light-flavour jets are derived for calorimeter-based jets and extrapolated to track-jets using MC simulation. An additional term is included to extrapolate the measured uncertainties to p_{T} above 250 GeV. This term is estimated from simulated events by varying the quantities affecting the flavour-tagging performance such as the impact parameter resolution, percentage of poorly measured tracks, description of the detector material, and track multiplicity per jet. The total uncertainties are 1–10%, 15–50%, and 50–100% for b-jets, c-jets, and light-flavour jets respectively.

5.3 Muon

The uncertainties in the muon momentum scale and resolution are derived from data events with dimuon decays of J/ψ and Z bosons. In total, there are three independent components: one corresponding to the uncertainty in the inner detector track p_{T} resolution, one corresponding to the uncertainty in the muon spectrometer p_{T} resolution, and one corresponding to the momentum scale uncertainty [52].

5.4 Photon

The uncertainties in the reconstruction, identification, and isolation efficiency for photons are determined from data samples of $Z \to \ell\ell\gamma$, $Z \to ee$, and inclusive photon events [53]. Uncertainties in the electromagnetic shower energy scale and resolution are taken into account as well [54].

5.5 Background modelling uncertainties for $t\bar{t}\gamma$, γ+jets and $W(\to q\bar{q})\gamma$

These correspond to the main backgrounds in the $Z(\to b\bar{b})\gamma$ studies presented in Sect. 8. The background modelling uncertainty for the γ+jets sample was estimated with the alternative MC generator, PYTHIA8 using the LO NNPDF2.3 PDF set and the A14 underlying event tune. The alternative sample includes LO photon plus jet events from the hard process and photon bremsstrahlung in dijet events.

In the case of the $W(\to q\bar{q})\gamma$ background, the nominal samples were compared with samples produced using the MADGRAPH5_aMC@NLO generator interfaced with PYTHIA8. For the $t\bar{t}\gamma$ background three different sources of modelling uncertainty were considered: uncertainty due to the parton shower and hadronisation estimated by comparing the nominal samples produced using MADGRAPH interfaced with PYTHIA8, with samples from MADGRAPH interfaced with HERWIG7 [32,63]; uncertainty due to different initial- and final-state radiation conditions from PYTHIA8 tunes with high or low QCD radiation activity; and uncertainty due to the choice of renormalisation and factorisation scales.

Uncertainties related to the photons and the γ+jets, $W(\to q\bar{q})\gamma$, and $t\bar{t}\gamma$ background modelling are applied only in the $Z(\to b\bar{b})\gamma$ analysis.

6 Higgs-jet tagger

The Higgs-jet tagger algorithm consists of several reconstruction steps. First, the Higgs boson candidate is reconstructed as a large-R jet. Second, the b-tagging requirement is applied to track-jets associated with the large-R jet in order to select candidates corresponding to $H \to b\bar{b}$ decays. Third, the b-tagged large-R jet mass can be required to be around the SM Higgs boson mass of 125 GeV. Finally, a requirement on other large-R jet substructure variables can be applied depending on the Higgs-jet tagger working point.

The signal acceptance for the first reconstruction step where the Higgs boson candidate is reconstructed as a large-R jet depends strongly on its transverse momentum.

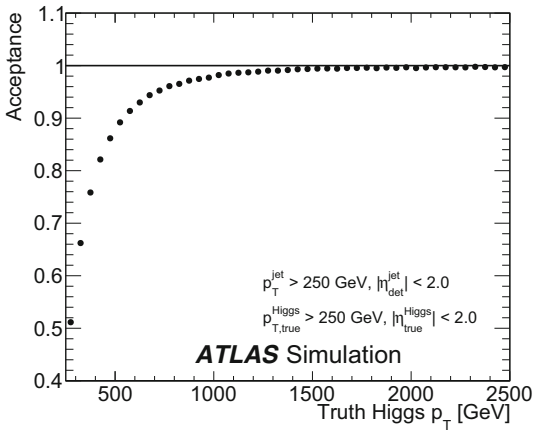

Fig. 1 Fraction of Higgs bosons in simulation which are reconstructed and labelled as a Higgs-jet following the definition in Sect. 4, as a function of Higgs boson p_{T}. Only Higgs bosons with $p_{\mathrm{T}} > 250$ GeV, $|\eta| < 2.0$ and with associated b-hadrons from its decay are considered. Same p_{T} and η requirements are applied to the Higgs-jets

The angular separation between Higgs boson decay products can be approximated as $\Delta R \approx 2m_H/p_{\mathrm{T}}$. Therefore, in most of the cases the Higgs boson decay products will fall within a single large-R jet with a radius parameter of $R = 1.0$ if the Higgs boson p_{T} is at least 250 GeV. The signal acceptance shown in Fig. 1 is determined as the fraction of Higgs bosons in simulation which are reconstructed and labelled as a Higgs-jet following the definition in Sect. 4. Only Higgs bosons with $p_{\mathrm{T}} > 250$ GeV, $|\eta| < 2.0$, and associated b-hadrons from its decay that have $p_{\mathrm{T}} > 5$ GeV and $|\eta| < 2.5$ are considered. The Higgs boson acceptance is around 50% at 250 GeV, where the jet p_{T} resolution have a significant impact as well, and increases to 95% for transverse momenta above 750 GeV.

The Higgs-jet tagging efficiency is defined as the number of Higgs-jets passing a given selection requirement divided by the total number of Higgs-jets. The background rejection is defined as the inverse of the efficiency for a background jet to pass the given selection requirement.

6.1 Two-step sample reweighting

To construct the signal sample, all graviton samples are combined. To allow a valid comparison between the signal efficiency and the background rejection, the large-R jet p_{T} spectrum of the combined graviton sample is reweighted to the reconstructed multijet p_{T} spectrum for the Higgs boson tagger performance studies in a two-step procedure. The same two-step reweighting procedure is also applied to the $Z' \to t\bar{t}$ background sample. The multijet spectrum is chosen as a reference because of its smoothly falling p_{T} spectrum being representative for many analyses. During the first step of the reweighting the highest-p_{T} truth Higgs-jet is used, whereas for the second reweighting step the highest-p_{T} reconstructed Higgs-jet is used. The reconstructed Higgs-jet and the truth Higgs-jet must both contain the highest-p_{T} Higgs boson to mitigate effects from initial-state radiation (ISR).

In the first step, the p_{T} spectrum of the truth Higgs-jet in the combined signal sample is reweighted to the p_{T} spectrum of the reconstructed large-R jet in the multijet sample. In the second step, the reconstructed Higgs-jet p_{T} spectrum is reweighted to the reconstructed large-R jet p_{T} spectrum in the multijet sample. A one-step reweighting using the reconstructed Higgs-jet p_{T} spectrum results in large weights for jets with p_{T} much larger or smaller than half of the graviton mass. Furthermore, the reconstructed Higgs-jet can contain additional energy which does not stem from the Higgs boson decay, such as ISR, energy missing due to neutrinos, 'out-of-cone' effects, or trimming. The frequency of these effects depends on the Higgs boson boost, i.e. on the graviton mass, introducing a dependence on the choice of simulated graviton masses used in the combined signal sample. The second step is needed to account for a residual difference between reconstructed and truth Higgs-jet transverse momenta.

6.2 Flavour-tagging working points

To apply b-tagging to identify $H \to b\bar{b}$ decays, the track-jets are matched to the large-R jets by ghost association as described in Sect. 4. At least two track-jets must be matched to the large-R jet for the double-b-tagging benchmarks, and at least one track-jet in the case of single-b-tagging benchmarks. The track-jet is considered to be b-tagged if its MV2c10 b-tagging discriminant value is larger than a given threshold value. These threshold values are defined for several b-tagging working points: 60%, 70%, 77% and 85% b-jet tagging efficiencies.

The following b-tagging benchmarks are studied:

- double b-tagging: the two highest-p_{T} track-jets must both pass a given b-tagging requirement;
- asymmetric b-tagging: the track-jet which is more consistent with the interpretation of being a b-jet must pass a given fixed 60%, 70%, 77%, or 85% working point, while the b-tagging requirement on the second track-jet is varied;
- single b-tagging: at least one of the two highest-p_{T} track-jets must pass the b-tagging requirement;
- leading single b-tagging: the highest-p_{T} track-jet must pass the b-tagging requirement.

The Higgs-jet efficiencies and background rejections as a function of the jet p_{T} for the 70% double-b-tagging benchmark are shown in Fig. 2. The signal efficiency varies from 52% at low p_{T} to about 5% for $1500 < p_{\mathrm{T}} < 2500$ GeV. The drop in efficiency at high transverse momenta due to the

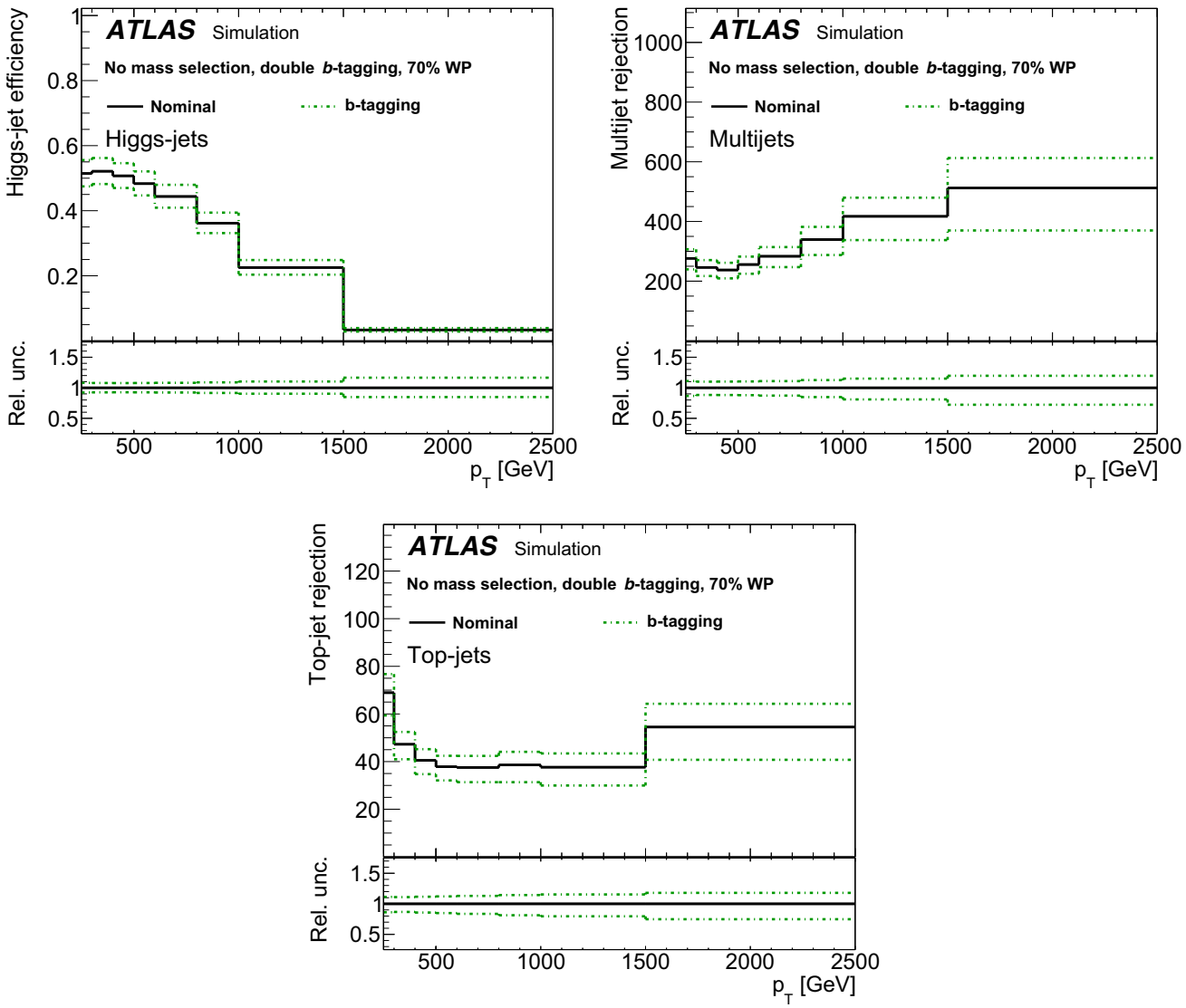

Fig. 2 The Higgs-jet efficiency (top left) and rejection against multijet (top right) and top-jet backgrounds (bottom) as a function of the jet p_{T} for the 70% double-b-tagging working point. The nominal curves correspond to the requirement on the MV2c10 discriminant described in Sect. 6.2. The b-tagging-related uncertainties defined in Sect. 5 are shown

increasing collimation and eventual merging of the two b-jets can be partially recovered using single-b-tagging working points as indicated in Fig. 6. The multijet (top-jet) rejection is relatively constant over the whole p_{T} range and is about 250 (60) at low p_{T} and 500 (50) at high p_{T}.

The multijet and top-quark background rejections as a function of the Higgs tagging efficiency for various b-tagging benchmarks are shown in Fig. 3. Plots on the left show the performance for Higgs-jet p_{T} above 250 GeV and plots on the right show the performance for Higgs-jet p_{T} above 1000 GeV. The double-b-tagging and asymmetric-b-tagging selections give the best background rejection in a large range of Higgs tagging efficiencies. At high Higgs-jet efficiencies above $\sim$90% ($\sim$55%) for Higgs-jet transverse momenta above 250 (1000) GeV the single-b-tagging benchmark shows a higher multijet and top-quark background rejection. To achieve such a high Higgs-jet efficiency, a very loose double-b-tagging or asymmetric-b-tagging requirement is needed, which results in a low light-flavour jet rejection. The double-b-tagging and asymmetric b-tagging working points do not reach an efficiency of 100% due to a requirement of at least two track-jets. In the case of asymmetric b-tagging, Higgs tagging efficiencies are below 100% because of the fixed b-tagging working point requirement on one of the track-jets. The drop in performance is pronounced at high jet transverse momenta due to the lower efficiency to reconstruct two subjets and the decrease in the MV2c10 b-tagging performance [64].

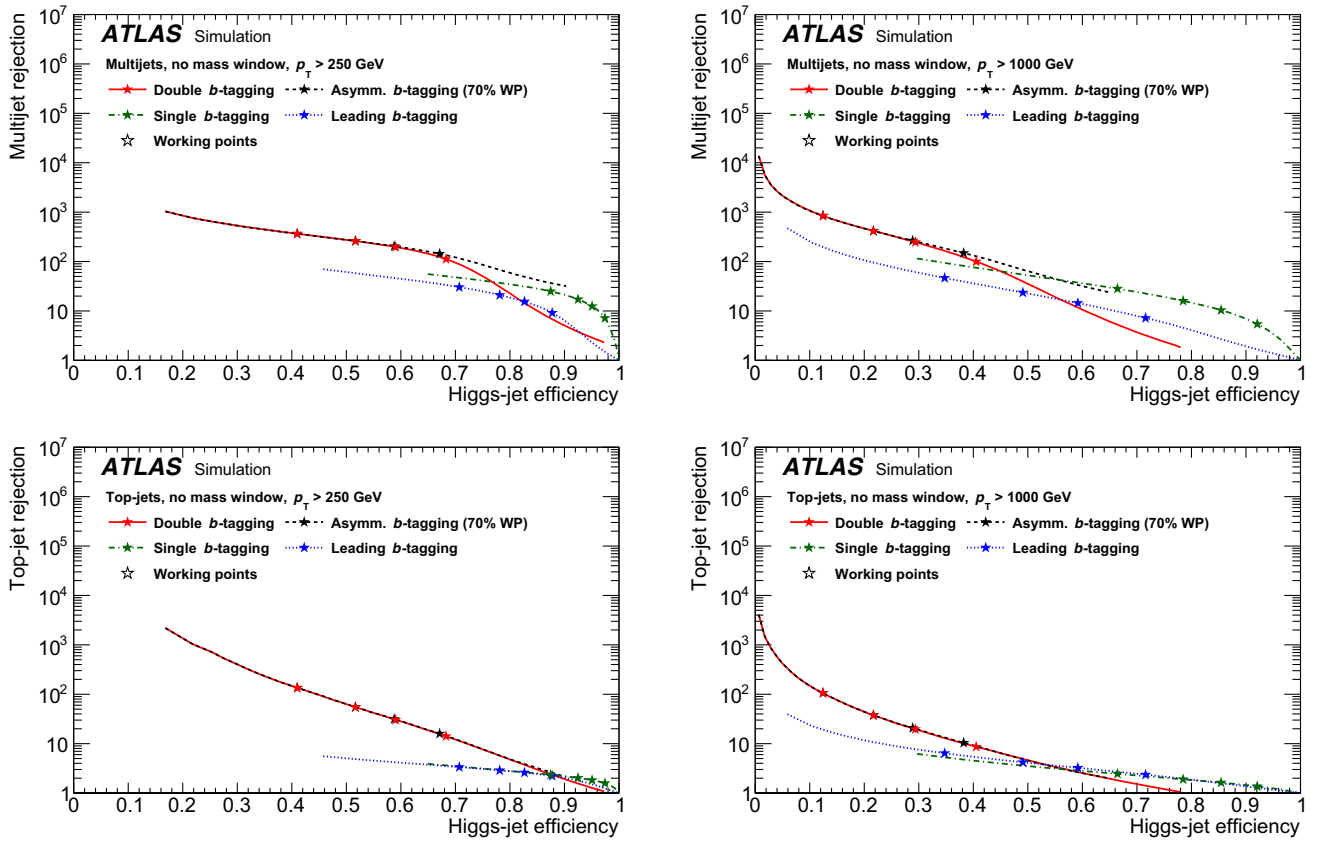

Fig. 3 The multijet (top) and the top-jet (bottom) rejection as a function of the Higgs tagging efficiency for large-R jet p_{T} above 250 GeV (left) and above 1000 GeV (right) for various b-tagging benchmarks defined in Sect. 6.2. The stars correspond to the 60%, 70%, 77% and 85% b-tagging WPs (from left to right). The curves for the double-b-tagging and asymmetric-b-tagging working points coincide over a large range of Higgs-jet efficiency

6.3 Mass window optimisation

The reconstructed Higgs boson mass distribution provides a powerful way to distinguish the Higgs boson signal from background processes. The muon-corrected combined mass described in Sect. 4 is used to impose the Higgs boson mass requirement and select large-R jets with a mass around the SM Higgs boson mass. The Higgs boson mass resolution, σ_m, varies as a function of the reconstructed large-R jet p_{T}, so the mass window is optimised and parameterised as a function of Higgs-jet p_{T}. Two working points are defined:

- tight mass window, containing 68% of Higgs-jets;
- loose mass window, containing 80% of Higgs-jets.

The mass window is defined as the smallest window containing the given fraction of Higgs-jets. The out-of-cone effects, ISR and the missing neutrinos from semileptonic b-hadron decays have an impact on the mass resolution that is similar to their impact on the p_{T} response; therefore, the mass window optimisation depends on the applied Higgs-jet selection and on the Higgs-jet p_{T} spectrum.

Figure 4 shows the reconstructed Higgs boson mass distribution for Higgs-jets with a p_{T} in the range 350 to 500 GeV. The mass region below 50 GeV is affected by grooming and out-of-cone effects. In the case of asymmetric $H \to b\bar{b}$ decays, where one of the b-hadrons carries a large fraction of the Higgs boson p_{T}, the large-R jet's axis is close to the direction of the higher-p_{T} b-hadron. The decay products of the lower-p_{T} b-hadron could be removed by grooming or not fully captured in the large-R jet. That leads to smaller Higgs-jet masses. The mass region above 150 GeV suffers from additional contributions from initial-state radiation. A large fraction of the ISR is suppressed by selecting the reconstructed Higgs-jet containing the highest-p_{T} Higgs boson candidate. However, the high mass tails are still substantial in high Higgs-jet p_{T} regions and affect the Higgs boson mass window definition.

In order to suppress the impact of the tails on the mass window definition, a fit of the mass distribution is performed. The fit function is chosen empirically to describe the core of

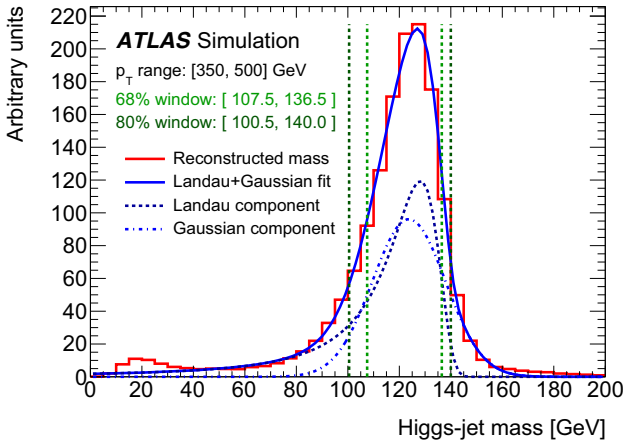

Fig. 4 The Higgs-jet mass distribution for jet transverse momenta in the range 350 to 500 GeV after reweighting the p_{T} spectrum. The dotted and dash-dotted blue curves correspond to the two components of the fit function, while the solid blue curve shows the combination thereof. The vertical lines indicate the boundaries of the mass ranges for 68% (light green) and 80% (dark green) containment

the mass distribution, while mitigating the tails. The chosen function is a linear combination of a Landau function to describe the low mass part of the distribution and a Gaussian function to describe the high mass part.

The fit is performed in 12 Higgs-jet p_{T} bins across the entire range of transverse momentum from 250 to 2500 GeV.

A toy MC simulation is used as input to model the mass window and to estimate the statistical uncertainty on the mass window determination. This toy MC simulation samples the fit functions mentioned above and is performed many times in each p_{T} slice. For each toy MC sample, the mass window is calculated by selecting the smallest window containing the required signal fraction. The final upper and lower boundaries for a given p_{T} slice are found by averaging over the upper and lower boundaries from the corresponding toy MC samples. The mean defines the position and the RMS the uncertainty of the window boundaries in each p_{T} slice. Using the mean and RMS from the toy MC samples as input, the mass window is parameterised as a function of the Higgs-jet p_{T} using the fit function: $f(p_{\mathrm{T}}) = \sqrt{(a + b/p_{\mathrm{T}})^2 + (c \cdot p_{\mathrm{T}} + d)^2}$. The jet mass depends primarily on the energies of the jet constituents and their angular separations. Consequently, there are two competing effects: the improving precision of the calorimeter energy scale with increasing jet p_{T} and the decreasing ability of the calorimeter granularity to resolve individual energy deposits due to increasing decay collimation with increasing jet p_{T}. Fit results are shown in Fig. 5 for tight and loose mass window working points.

The Higgs boson acceptance times efficiency is presented in Fig. 6. In addition to the truth-matching requirements defined for Fig. 1, the double- and single-b-tagging, tight, loose and no mass window working points are applied. The double-b-tagging requirement in particular leads to a significant drop in the Higgs boson acceptance times efficiency at high Higgs boson transverse momenta, where the efficiency to reconstruct two track-jets and the double-b-tagging efficiency decrease quickly.

Figure 7 shows the rejection of the multijet background as a function of the Higgs-jet p_{T}. Applying a combination of loose mass window and double-b-tagging requirements improves the rejection by a factor of about four relative to the corresponding benchmark without the mass requirement shown in Fig. 2. The tight mass window requirement leads to an additional improvement of about 30–50% in the background rejection. The efficiency of the mass window requirements changes by a few percent after the application of the double b-tagging-requirement due to the dependence of the b-tagging efficiency on the jet kinematics.

The corresponding rejection of the multijet background as a function of the Higgs-jet efficiency is shown in Fig. 8

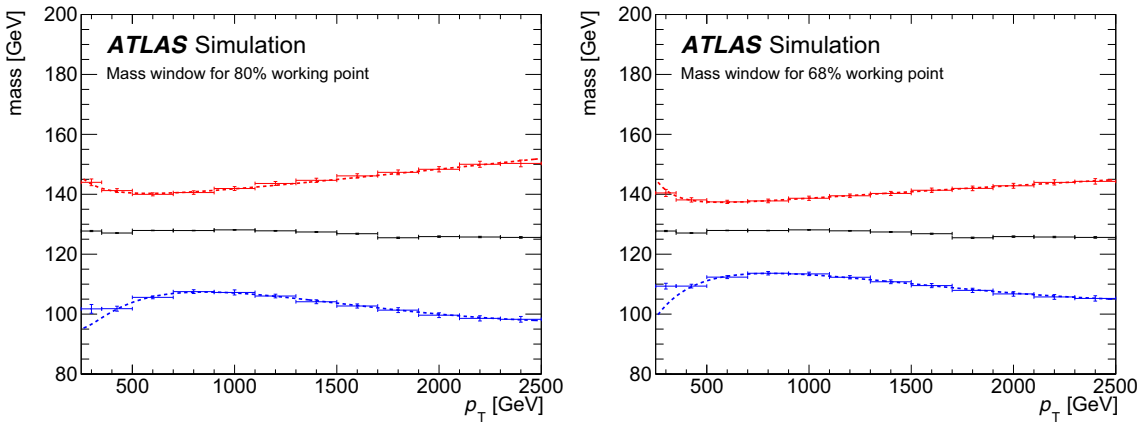

Fig. 5 The Higgs-jet mass window interval for a loose (left) and a tight (right) working point. The dashed lines show a fit to the derived intervals (blue and red markers) as a function of the Higgs-jet p_{T}. The black markers show the position of the maximum of the Higgs-jet mass distribution

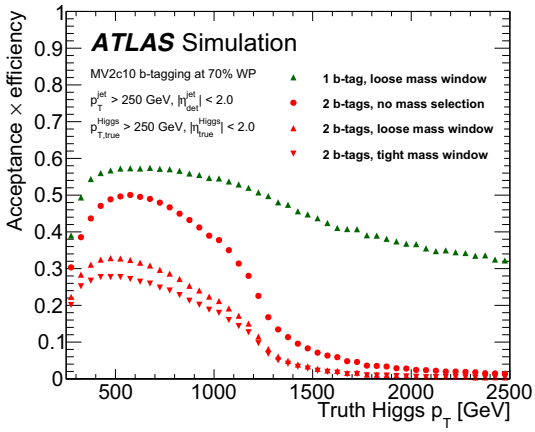

Fig. 6 The Higgs boson acceptance times efficiency is shown for a few working points: the double and single b-tagging with the loose mass window requirement and the double b-tagging with the tight, loose and no mass window requirements

for different Higgs-jet p_{T} ranges, b-tagging benchmarks, and mass window requirements. Application of the mass window requirement improves the performance of the tagger substantially. For a fixed signal efficiency of 40% and large-R jet p_{T} above 250 GeV, the multijet rejection rises from roughly 360 after applying the double-b-tagging requirement to about 1480 (1670) for the combination of the double-b-tagging and loose (tight) mass window requirements.

Figure 9 shows the hadronic top-quark background rejection as a function of the Higgs-jet p_{T} for combinations of mass window and b-tagging benchmarks. The background rejection is higher for multijets than for hadronically decaying top quarks. The rejection varies between 120 (170) at low p_{T} and 1000 (1300) at high p_{T} for the loose (tight) mass window and double-b-tagging benchmark. In comparison with the benchmarks without the mass window requirement, the rejection is improved by about one order of magnitude, but the shape as function of p_{T} is fundamentally different. At low p_{T}, not all decay products of the top quark are contained in the large-R jet. Thus the reconstructed jet mass has a long tail towards low jet masses with a substantial fraction of jets within the mass window of the tagger. Hence, the rejection at low jet p_{T} is not improved as much as at high jet p_{T}. The tight mass window requirement further improves the background rejection by 15–40% as function of p_{T}.

The rejection of the hadronic top-quark background as a function of the Higgs tagging efficiency is shown in Fig. 10. For the loose mass window requirement, an improvement from 140 to 200 is found at a fixed Higgs-jet efficiency of 40%, whereas for the tight mass window a smaller improvement from 140 to 160 is observed relative to no mass requirement for large-R jet p_{T} above 250 GeV. The rejection values are lower for double b-tagging and asymmetric b-tagging for large-R jet p_{T} above 1 TeV, and for high Higgs tagging efficiency single and single leading b-tagging are better options.

6.4 Jet substructure

Sections 6.2 and 6.3 present the performance of the Higgs-jet tagger based on the b-tagging and jet mass requirements designed to distinguish large-R jets produced by Higgs boson decays from backgrounds. This section discusses the possibility of improving the background rejection with the help of

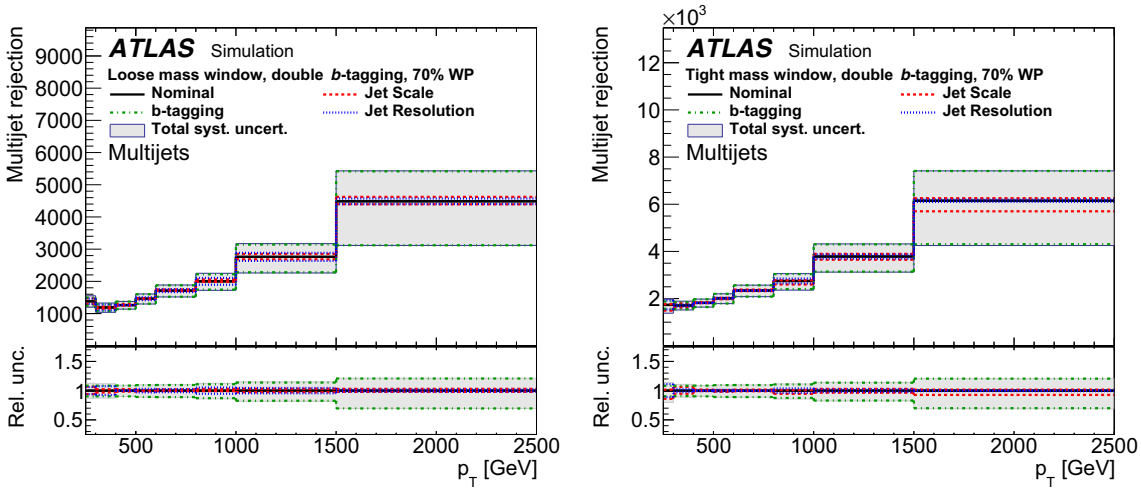

Fig. 7 Rejection of multijet background as a function of the Higgs-jet p_{T} for the loose (left) and tight (right) mass window requirements, in combination with the 70% double-b-tagging working point. The nominal curves correspond to the requirement on the MV2c10 discriminant described in Sect. 6.2. Systematic uncertainties defined in Sect. 5 as well as their sum in quadrature (total uncertainty) are shown. 'Jet Scale' refers to the sum in quadrature of the jet energy and mass scale uncertainties and 'Jet Resolution' refers to the sum in quadrature of the jet energy and mass resolution uncertainties

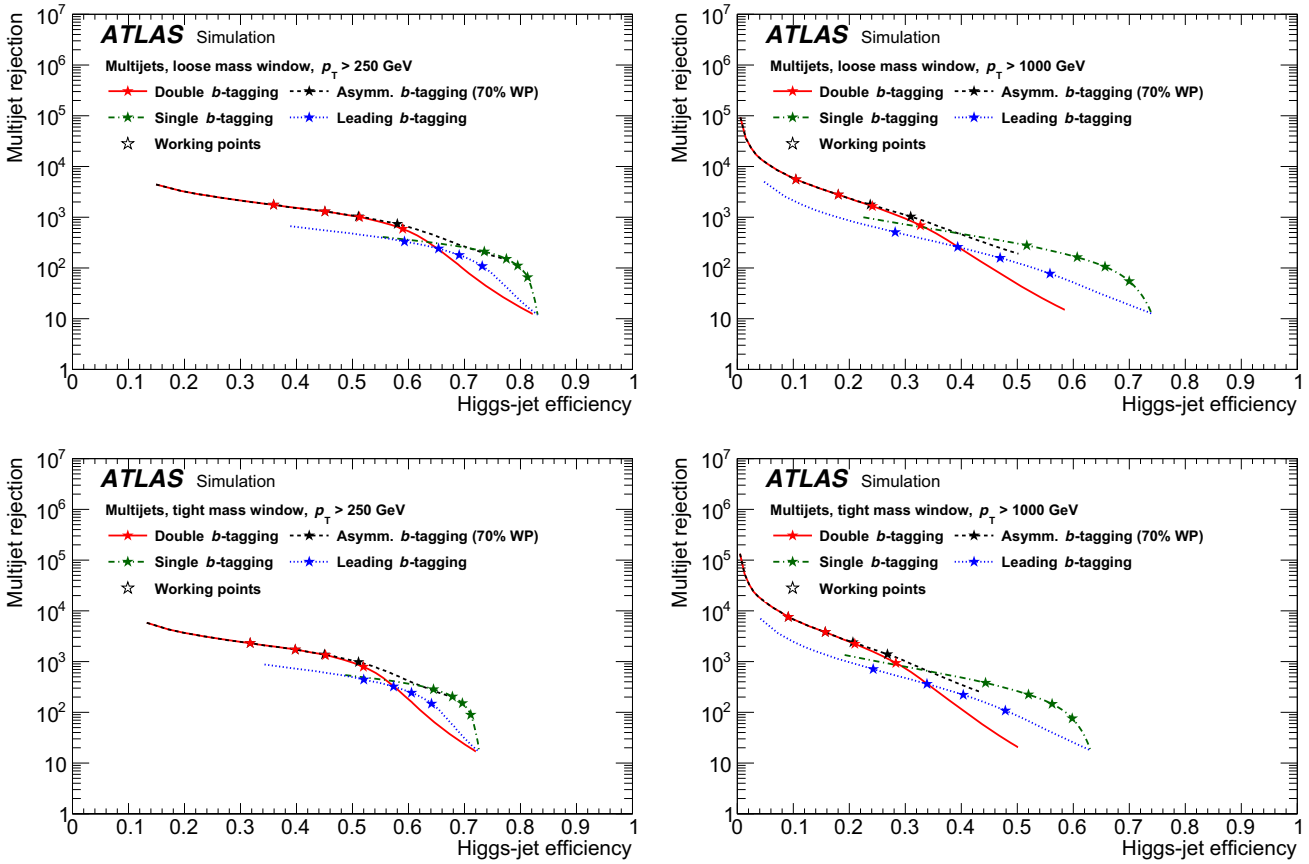

Fig. 8 Rejection of multijet background as a function of the Higgs boson tagging efficiency for loose (top) and tight (bottom) mass window requirements for large-R jet p_{T} above 250 GeV (left) and above 1000 GeV (right) for various b-tagging benchmarks. The stars correspond to the 60%, 70%, 77% and 85% b-tagging WPs (from left to right). The curves for the double- and asymmetric-b-tagging working points coincide over a large range of Higgs-jet efficiency

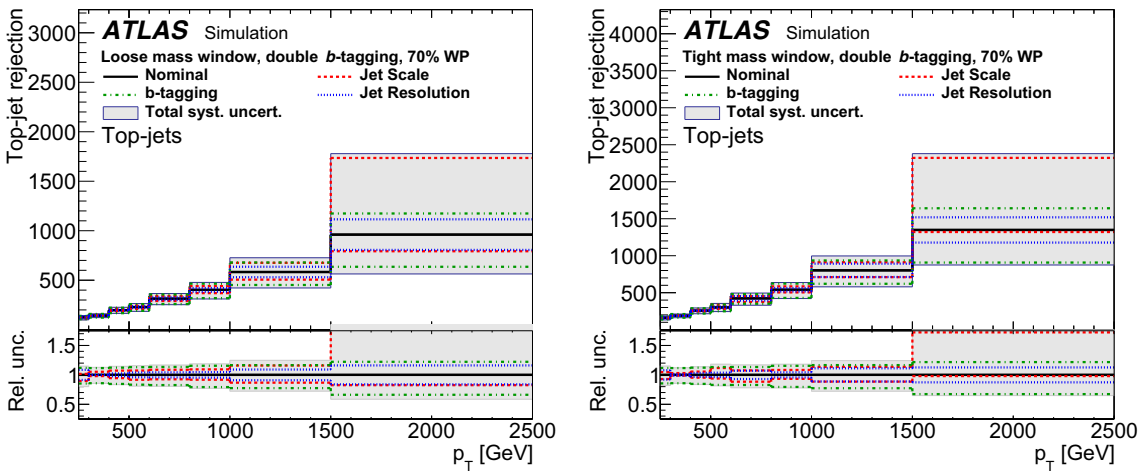

Fig. 9 Rejection of the top-jet background as a function of the Higgs-jet p_{T} for the loose (left) and tight (right) mass window requirements, in combination with the 70% double-b-tagging working point. The nominal curves correspond to the requirement on the MV2c10 discriminant described in Sect. 6.2. Systematic uncertainties defined in Sect. 5 as well as their sum in quadrature (total uncertainty) are shown. 'Jet Scale' refers to the sum in quadrature of the jet energy and mass scale uncertainties and 'Jet Resolution' refers to the sum in quadrature of the jet energy and mass resolution uncertainties

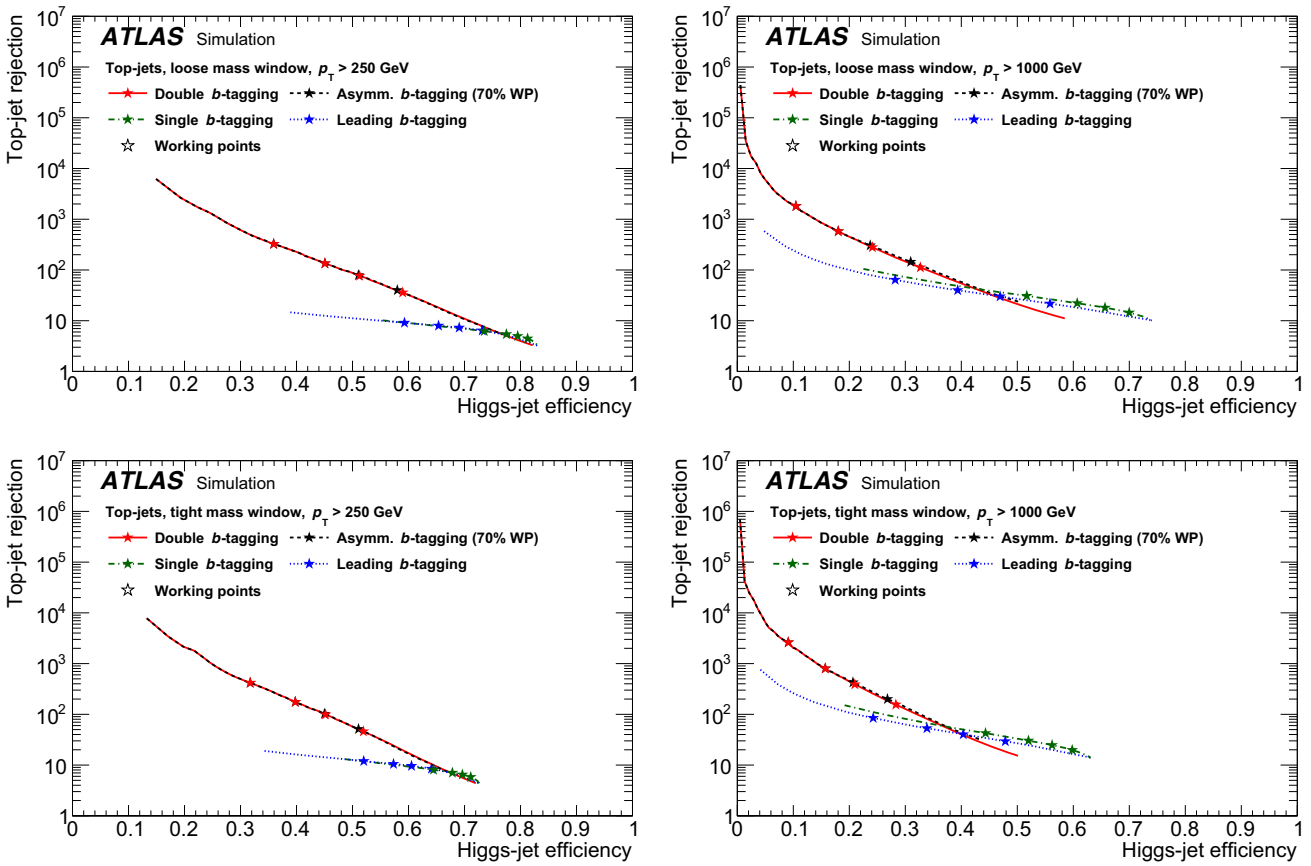

Fig. 10 Rejection of the top-jet background as a function of the Higgs tagging efficiency for loose (top) and tight (bottom) mass window requirements for large-R jet p_{T} above 250 GeV (left) and above 1000 GeV (right) for various b-tagging benchmarks. The stars correspond to the 60%, 70%, 77% and 85% b-tagging WPs (from left to right). The curves for the double- and asymmetric-b-tagging working points coincide over a large range of Higgs-jet efficiency

other jet substructure variables and tighter selections on jet mass and b-tagging applied on top of the previously defined jet mass window and b-tagging benchmark working points. These additional selections are referred to as secondary selections.

Many jet substructure variables exist that can capture features of a jet's internal structure and can potentially give additional discrimination power against backgrounds from multijet production and top-quark decays. They are based on the jet constituents and exploit quantities such as transverse momentum and angular distance between the constituents. They give information about different jet attributes such as shape (e.g. sphericity, aplanarity) or number of axes (e.g. two-subjettiness τ_2). Ratios are often used to avoid scale dependence of substructure variables. Table 1 lists the jet substructure variables that are investigated in this study, together with a short description and references. Secondary selections on jet mass and the flavour-tagging discriminant for the track-jets, MV2c10, are also considered relative to the previously defined mass window and b-tagging benchmark working points and their performance is compared with that achieved by the application of additional jet substructure variables to these benchmarks. Two categories of secondary selections are used for the b-tagging discriminant MV2c10, and these exploit the potential of tighter b-tagging working points where the criteria are tightened for both track-jets (double b-tagging) or for only one track-jet (single b-tagging).

For all secondary selection variables an optimal two-sided range is chosen for each variable and each benchmark working point. Searches of new-physics resonances typically use tagging definitions with relatively high signal efficiency, around 40% (75%) for Higgs-jets with $p_{\mathrm{T}} = 500$ GeV for double (single) b-tagging and a mass requirement. Hence, the two-sided range for a secondary variable which contains the smallest fraction of background but at least 80% of signal events is determined. Figures 11 and 12 show the background rejection for a 80% retention of signal efficiency relative to the jet mass and b-tagging benchmark working points for multijet and hadronic top-quark backgrounds, respec-

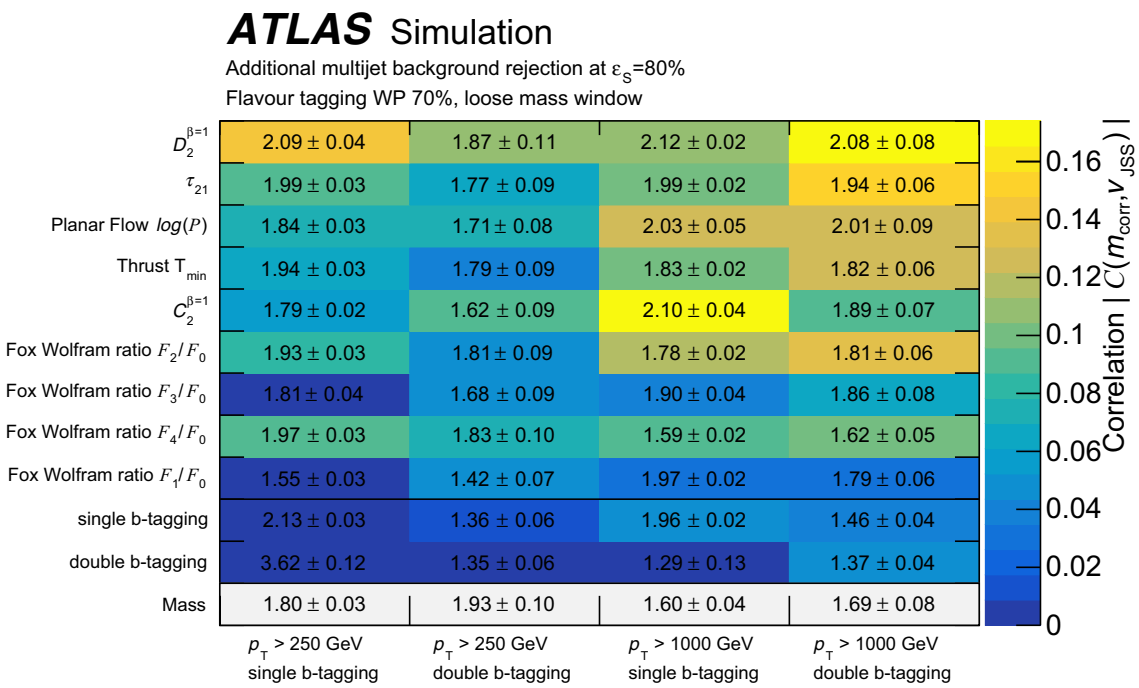

Fig. 11 Multijet background rejection at 80% signal efficiency ($\varepsilon_S = 80\%$) for a variety of substructure variables using different benchmarks in terms of b-tagging strategy and transverse momentum range. The z-axis colour scale represents the absolute value of the linear-correlation coefficient, $|C(m_{corr}, v_{JSS})|$, between the jet mass and the jet substructure variables. The selection efficiency is determined relative to the mass window and b-tagging benchmark working points defined in Sects. 6.3 and 6.2 respectively

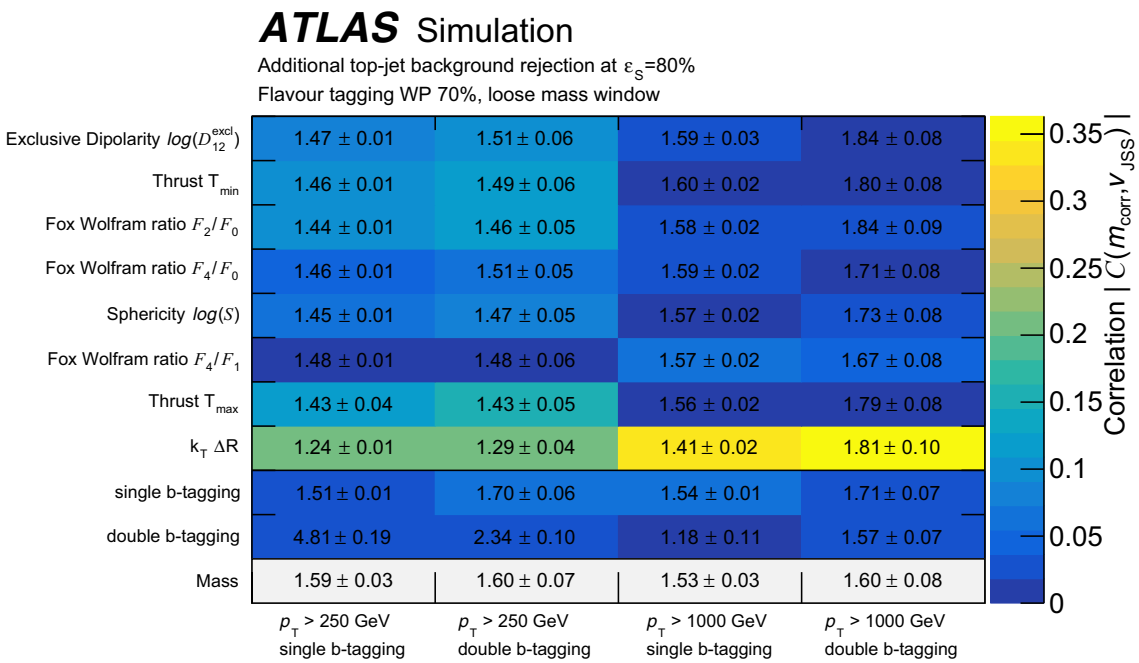

Fig. 12 Hadronic top-quark background rejection at 80% signal efficiency ($\varepsilon_S = 80\%$) for a variety of substructure variables using different benchmarks in terms of b-tagging strategy and transverse momentum range. The z-axis colour scale represents the absolute value of the linear-correlation coefficient, $|C(m_{corr}, v_{JSS})|$, between the jet mass and the jet substructure variables. The selection efficiency is determined relative to the mass window and b-tagging benchmark working points defined in Sects. 6.3 and 6.2 respectively

Table 1 Overview of jet substructure variables. A short description of these substructure variables can be found in Refs. [65,66]. (*) Exclusive dipolarity forces the jet to have exactly two subjets from the k_t algorithm to begin with, which is different from the dipolarity, which runs k_t clustering and then takes all jets with p_{T} above 5 GeV

Symbol	Description	References
Energy correlation functions		
$E_{\mathrm{CF}i}$	i-th energy correlation function	[67,68]
$C_2^{\beta=1}$	$E_{\mathrm{CF3}} \cdot E_{\mathrm{CF1}}/E_{\mathrm{CF2}}$	
$D_2^{\beta=1}$	$E_{\mathrm{CF3}} \cdot (E_{\mathrm{CF1}}/E_{\mathrm{CF2}})^3$	
n-subjettiness		
τ_n	n-subjettiness	[69,70]
τ_n^{wta}	n-subjettiness variant *winner takes all* (wta)	
τ_{ji}, τ_{ji}^{wta}	τ_j/τ_i or $\tau_j^{\mathrm{wta}}/\tau_i^{\mathrm{wta}}$, $j > i$	
Centre-of-mass observables		
$\mathcal{F}_i$	i-th Fox–Wolfram moment	[71]
Dipolarity		
$\mathcal{D}^{\mathrm{excl}}$	Exclusive dipolarity(*)	[72]
Cluster sequence		
$k_t \Delta R$	ΔR of two subjets within the large-R jet	[46]
μ_{12}	k_t mass drop	[11]
Splitting measures		
$\sqrt{d_{ij}}$	k_t splitting scale from $i \to j$ splitting	[73,74]
Thrust		
T_{min}, T_{max}	Thrust	[75]
Shape		
A	Aplanarity	[76]
$\mathcal{P}$	Planar flow	[77]
S	Sphericity	[76]
Other		
a_3	Angularity	[78]

tively. The matrices in Figs. 11 and 12 show the background rejection for substructure variables, secondary jet mass, and MV2c10 b-tagging discriminant on the y-axis for the four benchmark points of the Higgs-jet tagger on the x-axis. The z-axis colour scale represents the absolute value of the linear-correlation coefficient of the substructure variable and the jet mass for the corresponding background. For each benchmark, five variables with the largest background rejection are selected and all selected variables for every benchmark are shown.

In general, there are improvements across the various benchmark points. The background rejection is often higher for the multijet background than for the hadronically decaying top quarks. The secondary b-tagging discriminant is very powerful, and there are only a few areas of phase space where substructure yields larger improvements than an optimised b-tagging working point. However, substructure variables are an interesting alternative to tighter b-tagging working points for large-R jet p_{T} above 1 TeV. For the multijet background (Fig. 11), a tighter requirement on the double b-tagging achieves a background rejection of 3.62 (1.35) in the inclusive range $p_{\mathrm{T}} > 250$ GeV for the single-b-tagging (double-b-tagging) working point. In contrast, the improvement from the double-b-tagging discriminant is small for working points for $p_{\mathrm{T}} > 1000$ GeV, achieving a background rejection of 1.29 (1.37) for the single-b-tagging (double-b-tagging) working point. At large p_{T} the background rejection for substructure variables varies between 2.12 ($D_2^{\beta=1}$) and 1.55 (Fox–Wolfram ratio $\mathcal{F}_1/\mathcal{F}_0$) for a signal efficiency of 80%. In general, correlations with the jet mass greater than 10% are observed for most of the jet substructure variables. The Fox–Wolfram ratios $\mathcal{F}_3/\mathcal{F}_0$ and $\mathcal{F}_1/\mathcal{F}_0$ show the lowest correlations: less than 1% for most of the benchmarks.

The room for improvement is smaller if secondary jet substructure selections on top of the jet mass window and b-tagging benchmark working points are used in the case of the hadronic top-quark background (Fig. 12). A tighter double-b-tagging working point reaches a factor of 4.81 (2.34) background rejection in the inclusive range $p_{\mathrm{T}} > 250$ GeV for the single-b-tagging (double-b-tagging) working point. In contrast, the improvement from the double-b-tagging discriminant is small at large p_{T}, achieving a background rejection of 1.18 (1.57) for the single-b-tagging (double-b-tagging) working point. The background rejection for other variables

varies between 1.84 (Fox–Wolfram ratio $\mathcal{F}_2/\mathcal{F}_0$ and exclusive dipolarity) and 1.24 ($k_t\Delta R$) for a signal efficiency of 80%. Compared with the multijet background the correlations between the jet mass and the jet substructure variables are smaller in the case of the top-quark background, especially for $p_{\mathrm{T}} > 1000$ GeV. The Fox–Wolfram ratio $\mathcal{F}_4/\mathcal{F}_1$ shows the lowest correlation: less than 1% for most of the benchmarks.

In conclusion, the application of jet substructure variables improves the background rejection moderately, while better improvements are observed for high transverse momenta. Furthermore, it is important to take into account the correlation between the large-R jet mass and the substructure variables since requirements on the substructure variables sculpt the jet mass distribution [79,80].

7 Modelling tests in $g \to b\bar{b}$ data

Multijet events enriched in b-jets, which predominately originate from gluon to $b\bar{b}$ production, are used to evaluate the b-tagging efficiency in data and simulation as well as the modelling of jet substructure variables. The multijet background is one of the main backgrounds for searches in fully hadronic final states, for example the Higgs boson pair search in the four-b-quark final state [81]. This background also provides a unique opportunity to validate the modelling of the double-b-jets in a large data sample. Events with one large-R jet with two ghost-associated track-jets ('$g \to b\bar{b}$ candidate jet') and one recoiling ISR small-R jet ('recoil jet', j_{recoil}) are used for this study.

7.1 Event selection

Events are required to have a primary vertex that has at least two tracks, each with $p_{\mathrm{T}} > 500$ MeV [82]. The primary vertex with the highest p_{T}^2 sum of associated tracks is selected. A single-small-R-jet trigger with an online E_{T} threshold of 380 GeV was used to collect the data. An offline $R = 0.4$ recoil jet with p_{T} above 500 GeV is matched to the jet which fired the trigger.

Non-collision backgrounds originating from calorimeter noise, beam-halo interactions, or cosmic rays can lead to spurious calorimeter signals. This effect is suppressed by applying the criteria described in Ref. [83].

Selected events are required to have at least one large-R jet with $p_{\mathrm{T}} > 500$ GeV and $|\eta| < 2.0$, for which the small-R jet trigger is fully efficient and unbiased. The large-R jet must have at least two ghost-associated $R = 0.2$ track-jets. To enrich the event sample in jets containing b-hadrons, it is required that at least one of the ghost-associated track-jets be matched to a muon. The highest-p_{T} track-jet matched to a muon is called the muon-tagged jet, j_{μ}^{trk}. The matching is performed using a geometric $\Delta R < 0.2$ requirement between the track-jet's axis and the muon. The highest-p_{T} jet among the remaining track-jets matched by ghost association to the large-R jet is called the non-muon jet, $j_{\text{non-}\mu}^{\mathrm{trk}}$. The highest-$p_{\mathrm{T}}$ large-R jet satisfying these criteria is selected as gluon-jet candidate. Furthermore, the event must satisfy $\Delta R(j_{\mathrm{recoil}}, j_{\mu}^{\mathrm{trk}}) > 1.5$. This requirement ensures that the triggering jet and the gluon-jet candidate are well separated.

7.2 Flavour fraction corrections

To reduce discrepancies between data and MC simulation in the flavour composition of the large-R jet, the flavour fractions of the sample are determined from the data before applying b-tagging. Each large-R jet carries two flavours, that of j_{μ}^{trk} and $j_{\text{non-}\mu}^{\mathrm{trk}}$, leaving nine possible flavour combinations for the large-R jet (each track-jet can be a b-jet, c-jet, or light-flavour jet; B, C and L abbreviations are used in the following). The long decay length of b- and c-hadrons makes the signed impact parameter significance, s_{d_0}, of tracks associated with a jet a good discriminating variable for different jet flavours. The s_{d_0} of a track is defined as:

$$s_{d_0} = \frac{d_0}{\sigma(d_0)} s_j,$$

where d_0 is the track's transverse impact parameter relative to the primary vertex, $\sigma(d_0)$ is the uncertainty in the d_0 measurement, and s_j is the sign of d_0 relative to the track-jet's axis, depending on whether the track crosses the track-jet's axis in front of or behind the primary vertex. For a given track-jet, the average $\langle s_{d_0} \rangle$ is built from the three highest-p_{T} tracks associated with the track-jet. The tracks from b- and c-hadron decays are expected to have higher p_{T} than tracks in light-flavour jets, because the heavy-flavour hadrons carry on average a larger fraction of the jet energy. The requirement that $\langle s_{d_0} \rangle$ is built from the three highest-p_{T} tracks helps to distinguish them from light-flavour jets, which may have tracks with large s_{d_0} values, e.g. from Λ and K_{s} decays.

The impact parameter resolution depends on the intrinsic track resolution, the traversed detector material, the detector alignment, and other effects. To determine the impact parameter resolution in data, minimum-bias, dijet, and Z+jets events are used. The impact parameter resolution is extracted in fine bins of track p_{T} and η with an iterative method described in Ref. [51]. The simulation is corrected to match the measured impact parameter resolution as a function of track p_{T} and η by using a Gaussian function to smear the impact parameter resolution in the simulation.

The $\langle s_{d_0} \rangle$ values of j_{μ}^{trk} and $j_{\text{non-}\mu}^{\mathrm{trk}}$ are found to be uncorrelated and thus the one-dimensional distributions of each jet's $\langle s_{d_0} \rangle$ are fit simultaneously. Furthermore, the flavour combinations of $(j_{\mu}^{\mathrm{trk}}, j_{\text{non-}\mu}^{\mathrm{trk}}) = \{(\mathrm{B,C}), (\mathrm{C,B}), (\mathrm{L,C}), (\mathrm{L,B})\}$ are pre-

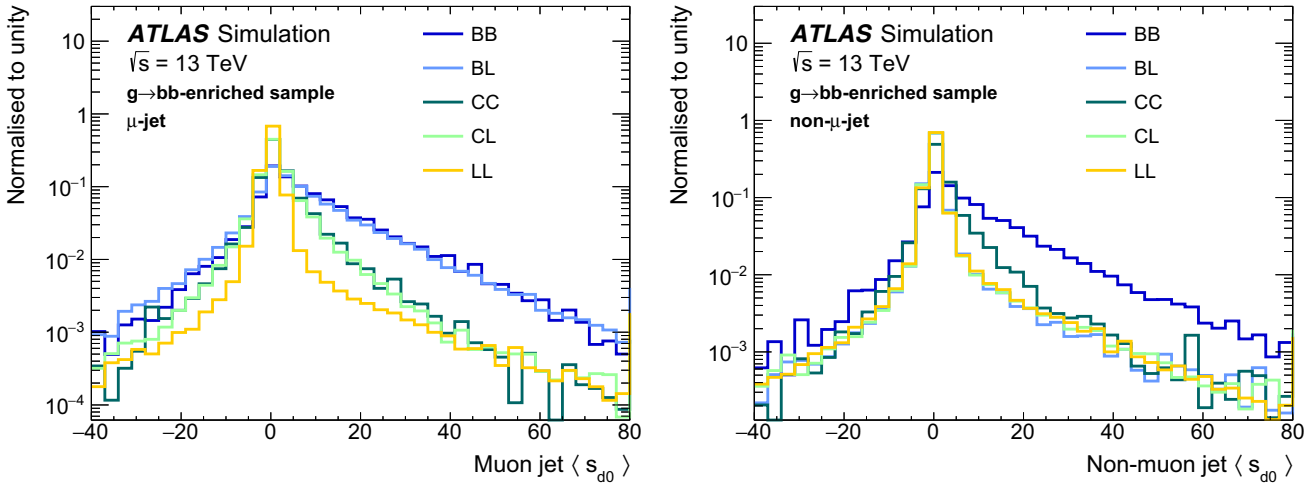

Fig. 13 Averaged impact parameter significance, $\langle s_{d_0} \rangle$, distributions for the muon (left) and non-muon jets (right) inclusive in j_{μ}^{trk} and $j_{\text{non-}\mu}^{\text{trk}}$ transverse momenta. The double flavour labels denote the true flavour of the jet pair, with the j_{μ}^{trk} given first

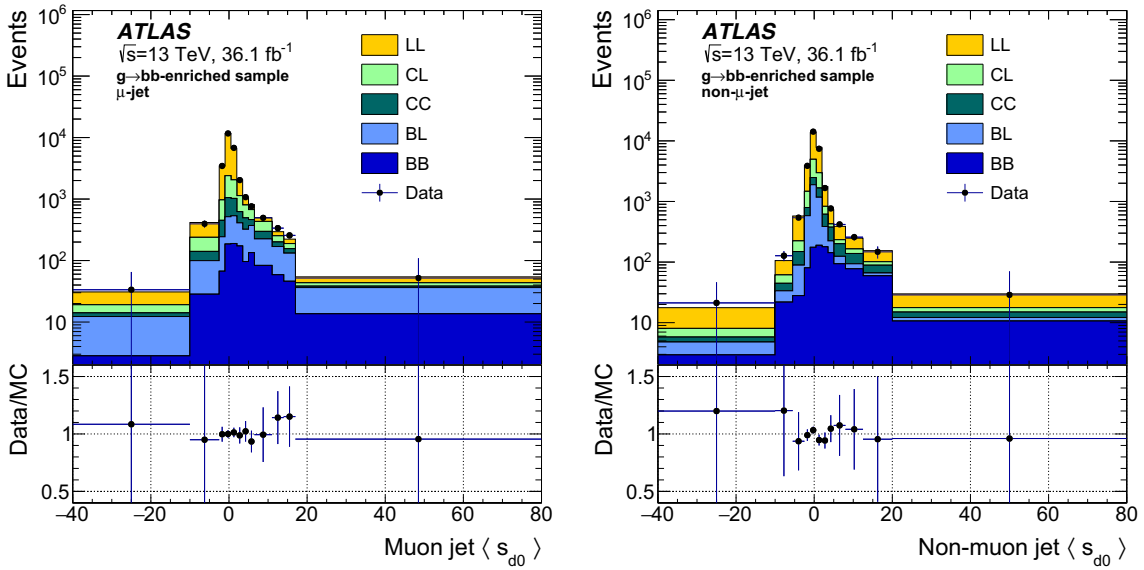

Fig. 14 Averaged impact parameter significance, $\langle s_{d_0} \rangle$, distributions of the muon (left) and non-muon jet (right) in the (100–200) GeV bin of the j_{μ}^{trk} and $j_{\text{non-}\mu}^{\text{trk}}$ transverse momenta

dicted to be less than 1% of the total, so they are merged with other flavour categories which have the closest shape. The shape similarity is determined using the χ^2-statistic. Thus a total of five flavour categories are used, $(j_{\mu}^{\text{trk}}, j_{\text{non-}\mu}^{\text{trk}}) = \{(\text{B,B}), (\text{B,L}), (\text{C,C}), (\text{C,L}), (\text{L,L})\}$. Figure 13 shows the templates inclusive in p_{T}.

Since the flavour fractions vary with p_{T}, the flavour fraction fits to the data are performed in bins of p_{T} of the two track-jets. For each jet p_{T} bin, individual MC templates are used. The following jet-p_{T} bins are considered: j_{μ}^{trk} p_{T} bins = {(0–100), (100–200), >200} GeV and $j_{\text{non-}\mu}^{\text{trk}}$ p_{T} bins = {(0–100), (100–200), (200–300), >300} GeV. Figure 14 shows an example of the flavour fraction fit to the s_{d_0} distributions of j_{μ}^{trk} and $j_{\text{non-}\mu}^{\text{trk}}$ for one particular bin of the track-jet transverse momenta. The fit uncertainty includes the statistical uncertainty of the templates and is evaluated using toy MC simulations. The flavour fraction corrections relative to the simulated fractions vary between 0.7 and 1.7 in the jet p_{T} bins with a statistical uncertainty below 10%.

After correcting for the observed flavour-pair fractions the level of agreement between data and MC simulation is evaluated in the selected event sample before and after b-tagging is applied to the track-jets. The 70% double-b-tagging working point is used.

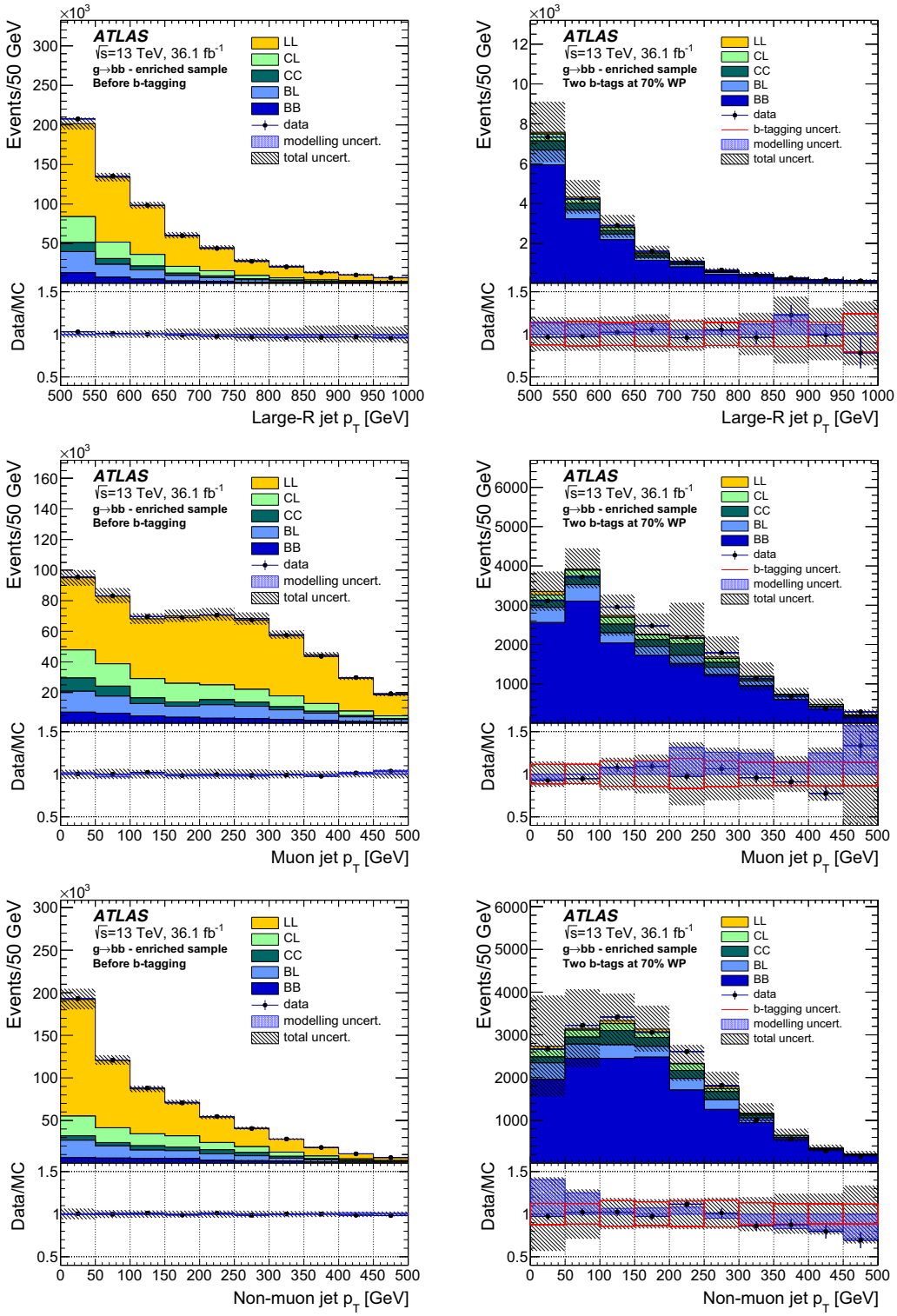

Fig. 15 Transverse momentum distributions of the large-R jet (top), j_{μ}^{trk} (middle) and $j_{\text{non-}\mu}^{\mathrm{trk}}$ (bottom) before (left) and after (right) double b-tagging. The flavour-tagging correction factors and the flavour-fit corrections have been applied. The two largest systematic uncertainties, generator modelling and the b-tagging-related uncertainties, are shown as well. The total uncertainty includes all systematic uncertainties listed in Sect. 5 and the fit uncertainty summed in quadrature

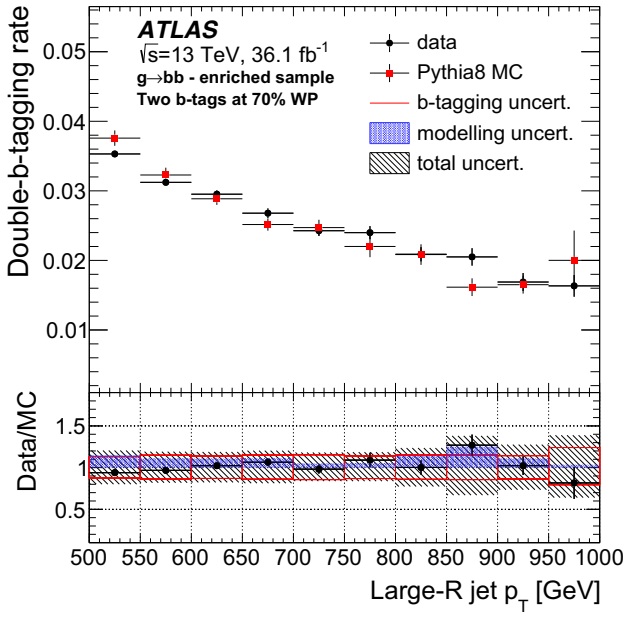

Fig. 16 Comparison of data and MC simulation double-b-tagging rates as a function of the large-R jet p_{T}. The flavour-tagging correction factors and the flavour-fit corrections have been applied. The two largest systematic uncertainties, generator modelling and the b-tagging-related uncertainties, are shown as well. The total uncertainty includes all systematic uncertainties listed in Sect. 5 and the fit uncertainty summed in quadrature. The size of the flavour-fit uncertainty is below 1%

7.3 b-tagging results

Since the flavour fractions are corrected in the MC simulation, differences between the data and predictions after the b-tagging can be attributed to a difference between data and MC simulation in the dependence of the b-tagging performance on the large-R jet topology, in particular on the topology with two closely spaced track-b-jets.

Figure 15 shows the flavour-fit-corrected p_{T} spectrum of the large-R jet as well the j_{μ}^{trk} and $j_{\text{non-}\mu}^{\mathrm{trk}}$ before and after b-tagging. As seen in the ratio plots, there is good agreement within uncertainties between data and MC simulation. The shape differences between data and MC simulations especially for the $j_{\text{non-}\mu}^{\mathrm{trk}}$ transverse momentum can be partially explained by the difference observed between Pythia8 and Herwig++ MC simulations. The double-b-tagging rate is defined as the number of selected large-R jets with at least two track-jets, two of which are b-tagged, divided by the number of all selected large-R jets with at least two track-jets. Figure 16 shows the double-b-tagging rate as a function of the large-R jet p_{T}. Data and MC simulation agree within the uncertainties. The performance of the double b-tagging applied to two track-jets seems not to depend on the large-R jet topology with two closely spaced track-b-jets, and the default b-tagging calibration described in Sect. 5 can be applied for this analysis.

7.4 Jet substructure results

As possible variations of Higgs taggers may make use of the large-R jet p_{T}, and substructure variables such as mass, n-subjettiness, or $D_2^{\beta=1}$, it is important to ensure that these variables are well modelled by MC simulations. The distributions of kinematic and substructure variables are shown in Fig. 17, for double-b-tagged jets after the flavour-fit correction. As seen in the ratio plots, there is acceptable agreement within uncertainties between data and MC simulations.

The relative impact of the systematic uncertainties on the yields of signal and background are presented in Table 2. The dominant signal uncertainty is the modelling uncertainty followed by the b-tagging-related uncertainties. The b-tagging-related uncertainties (misidentification of light-flavour jets and c-jets as b-jets) are dominant for background. The dominant uncertainties are shown separately in Fig. 17. The difference in the shapes between data and MC simulations can be partially explained by the difference observed between Pythia8 and Herwig++ MC simulations.

8 Modelling tests in $Z \to b\bar{b}$ data

As mentioned in the introduction, the $Z \to b\bar{b}$ process is a colour-singlet resonance with a mass close to the Higgs boson mass, so kinematic properties of the $Z \to b\bar{b}$ and $H \to b\bar{b}$ events are expected to be similar. Events with one double-b-tagged large-R jet ('$Z \to b\bar{b}$ candidate jet') and a photon that are back-to-back are used for this study. The photon requirement improves the signal-to-background ratio in comparison with the fully hadronic final state.

8.1 Event selection

Events are selected using a single-photon trigger with a transverse energy (E_{T}) threshold of 140 GeV and loose photon identification requirements [21]. This trigger is non-prescaled for the entire data-taking period and is fully efficient for offline photons with $E_{\mathrm{T}} > 175$ GeV. The same primary vertex and jet-cleaning requirements are applied as for the $g \to b\bar{b}$ study, described in Sect. 7.

Exactly one photon and at least one large-R jet are required to be present in the event. The large-R jet is required to have $p_{\mathrm{T}} > 200$ GeV, $|\eta| < 2.0$, and mass greater than 30 GeV. A jet–photon overlap removal procedure is applied, removing photons within $\Delta R = 1.0$ of the large-R jet. The large-R jet with the highest p_{T} is chosen as the $Z \to b\bar{b}$ candidate. The two highest-p_{T} track-jets that are associated with the $Z \to b\bar{b}$ candidate are required to be identified as b-jets using the 70% working point.

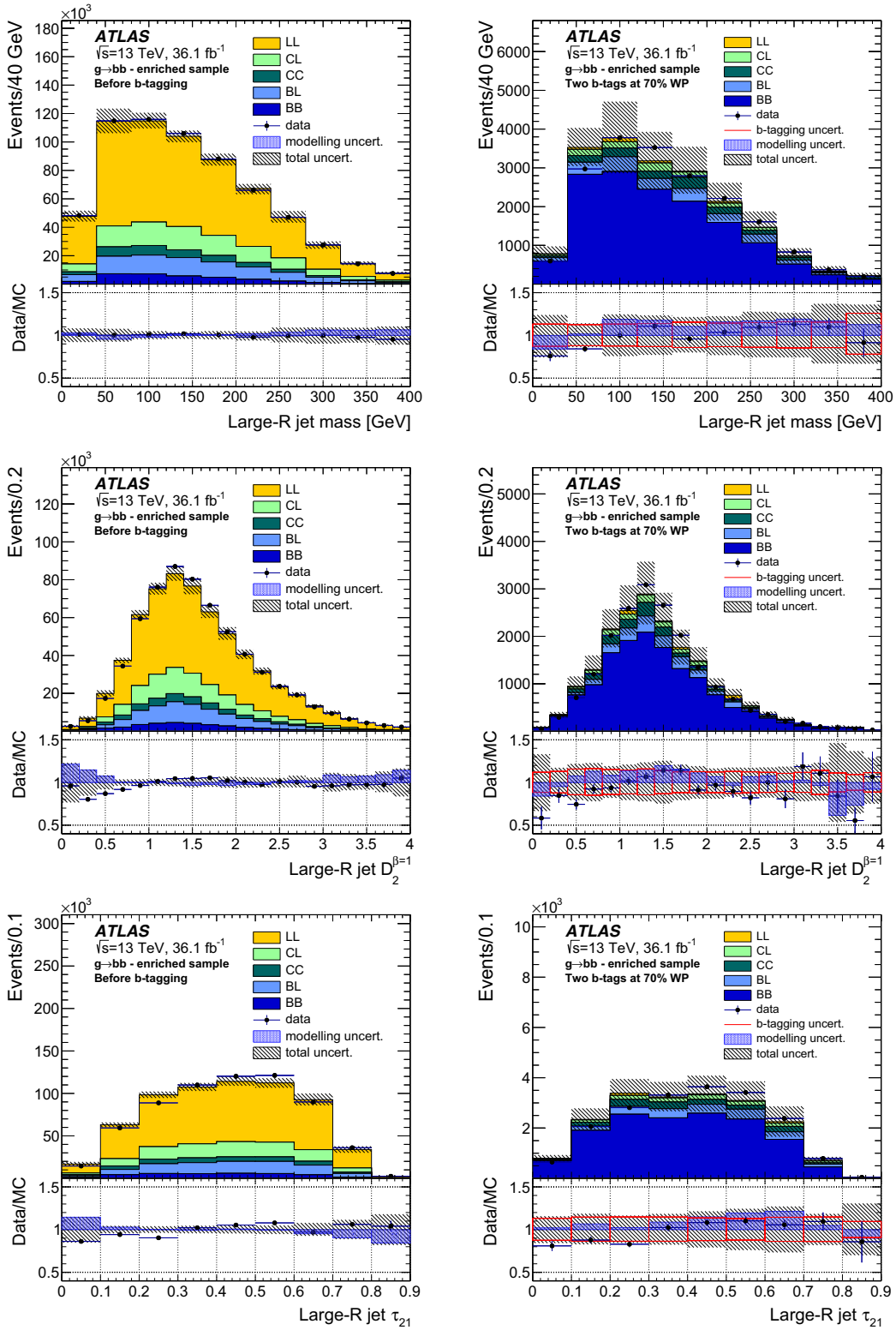

Fig. 17 Distributions of large-R jet mass (top), $D_2^{\beta=1}$ (middle) and τ_{21} (bottom) before (left) and after (right) double b-tagging. The flavour-tagging correction factors and the flavour-fit corrections have been applied. The two largest systematic uncertainties, generator modelling and the b-tagging-related uncertainties, are shown as well. The total uncertainty includes all systematic uncertainties listed in Sect. 5 and the fit uncertainty summed in quadrature. The $D_2^{\beta=1}$ and τ_{21} uncertainty bands include additional substructure variable uncertainties [48]

Table 2 Relative impact of the systematic uncertainties on the yields of signal and the main background for the $g \to b\bar{b}$ analysis. Multiple independent components have been combined into groups of systematic uncertainties. 'Jet scales' refers to the sum in quadrature of the jet energy, mass and substructure scale uncertainties

Source	Signal (B, B) (%)	Background (non-B, non-B) (%)
Jet scales	9.0	7.3
Jet energy resolution	1.0	1.8
Jet mass resolution	0.1	0.2
JVT	0.01	0.01
b-tagging related	9.5	27
Modelling	23	13
Fit statistics	1.0	0.1

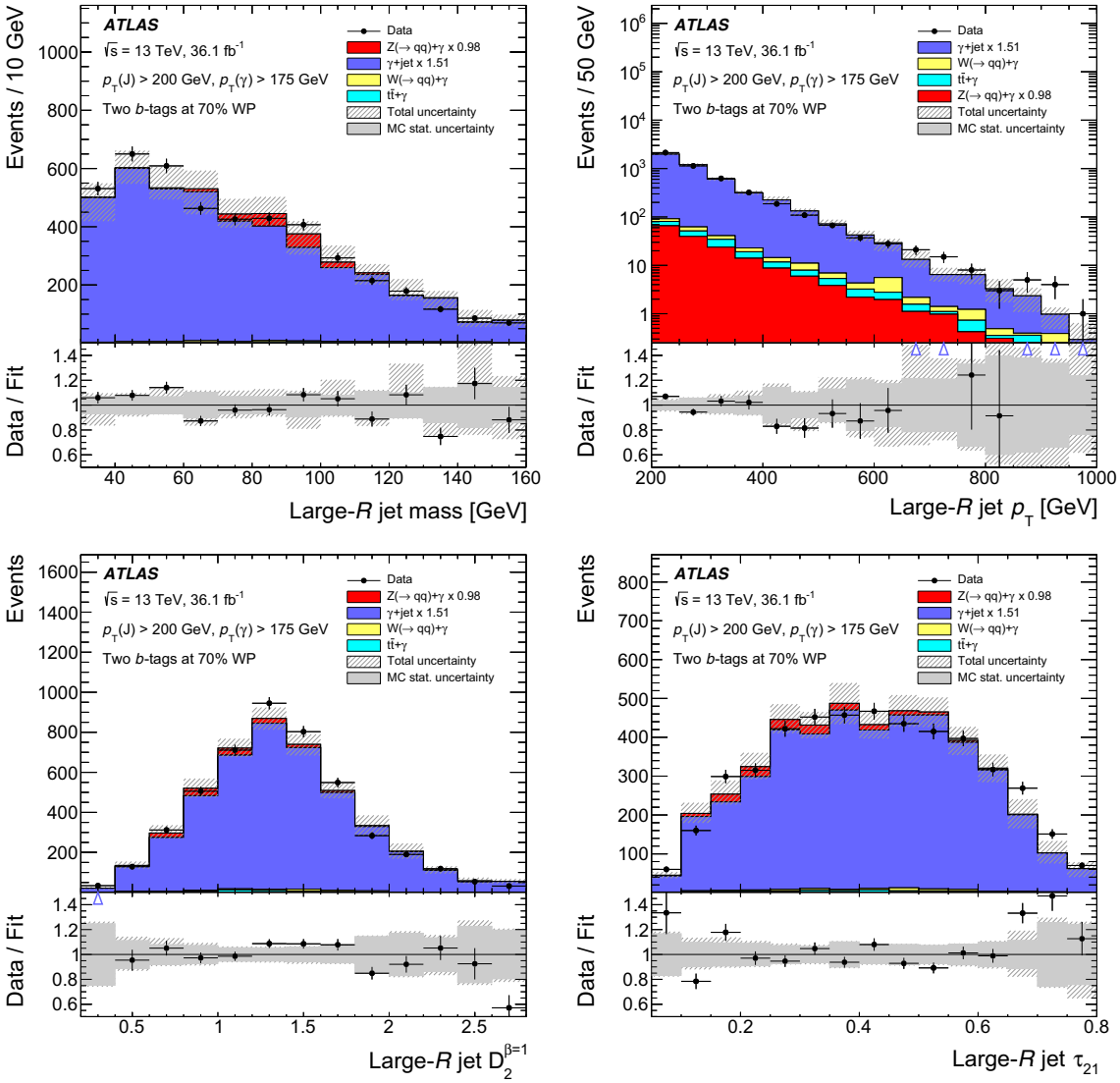

Fig. 18 Jet mass, p_{T}, $D_2^{\beta=1}$ and τ_{21} distributions. Events with two b-tagged track-jets are used. The γ+ jets background and the $Z \to b\bar{b}$ signal are normalised to data by applying a scale factor of 1.51 and 0.98, respectively. The upward- or downward-pointing arrows indicate that the Data/Fit ratio is out of the histogram range for these bins

Table 3 Relative impact of the systematic uncertainties on the $Z \to b\bar{b}$ and γ+jets yields . Multiple independent components have been combined into groups of systematic uncertainties. 'Jet scales' refers to the sum in quadrature of the jet energy, mass and substructure scale uncertainties

Source	$Z\gamma$ (%)	γ+ jets (%)
Photon related	1.3	0.1
b-tagging related	23	1.4
Muon related	0.9	0.1
Jet scales	59	2.1
Jet energy resolution	25	1.0
Jet mass resolution	42	1.7
γ+ jets modelling	40	8.3
$t\bar{t} + \gamma$ related	4.0	0.2
$W\gamma$ related	0.6	0.7
Fit statistics	37	2.1

8.2 Background estimate

The dominant SM background in this analysis is γ+jets with gluon-to-$b\bar{b}$ splitting. The contribution from the Standard Model $t\bar{t}\gamma$ and $W\gamma$ processes is smaller than that from the γ + jets process. Other background contributions such as jets faking photons, electrons faking photons, and $t\bar{t}$ are found to be negligible. To extract the $Z \to b\bar{b}$ and γ+jets normalisations, the $Z \to b\bar{b}$ candidate jet mass distribution is fitted to data. Both templates are taken from the MC simulation as described in Sect. 3. The $t\bar{t} + \gamma$ and $W(q\bar{q}) + \gamma$ background contributions estimated from MC simulation are subtracted before the fit to data. The jet mass variable is used in the fit because the difference between the shapes of the $Z \to b\bar{b}$ and γ+jets templates is larger than for other substructure variables. The extracted normalisations are applied to all other distributions.

8.3 Jet substructure results

Figure 18 shows the $Z \to b\bar{b}$ candidate jet mass, p_{T}, $D_2^{\beta=1}$, and τ_{21} distributions in data and MC simulation. Systematic uncertainties summarised in Sect. 5 are applied to the templates, and for each systematic variation the fit to data is performed. The fit uncertainty and the contribution for each of the systematic uncertainties summed in quadrature are presented in Fig. 18. The relative impact of the systematic uncertainties on the $Z \to b\bar{b}$ and γ+jets yields are presented in Table 3. The observed data/MC discrepancies are covered by systematic uncertainties.

Further requirements on the jet substructure variables can improve the purity of the selection. Figure 19 shows the $Z \to b\bar{b}$ candidate jet mass after further selections: $\tau_{21} < 0.45$ or $D_2^{\beta=1} < 1.3$. Figure 20 shows the $D_2^{\beta=1}$ and τ_{21} distributions after requiring the $Z \to b\bar{b}$ candidate jet mass to be between 70 and 110 GeV.

The $Z(\to b\bar{b})\gamma$ process provides a unique possibility to validate the Higgs-jet tagging algorithm given the similarity of the $H \to b\bar{b}$ and $Z \to b\bar{b}$ processes. For the current integrated luminosity of 36 fb^{-1}, the dominant uncertainties are the statistical and systematic uncertainties of the jet scales and jet mass for the $Z \to b\bar{b}$ process and the γ+jets modelling uncertainties. To reduce the dominant uncertainties, a larger dataset is needed. Within the uncertainties the studied jet substructure variables are modelled well by the signal plus background MC simulations.

9 Conclusions

Techniques to identify Higgs bosons at high transverse momenta decaying into bottom-quark pairs are described in this paper. The identification is based on the b-tagging of $R = 0.2$ track-jets matched to the Higgs-jet and requirements placed on the Higgs-jet mass and other substructure variables. The modelling of the relevant input distributions is studied in 36 fb^{-1} of 13 TeV proton–proton collision data recorded by the ATLAS detector at the LHC in 2015 and 2016.

The choice of b-tagging working point for an analysis depends on the required background rejection rate and on the Higgs-jet p_{T} range relevant for the analysis. The double-b-tagging working points give the best background rejection for a large range of the Higgs-jet-tagging efficiency but the efficiency decreases faster with increasing Higgs-jet p_{T} than it does for single-b-tagging working points. At high efficiencies above $\sim$ 90% ($\sim$ 55%) for Higgs-jet p_{T} above 250 (1000) GeV the single-b-tagging selection provides better background rejection.

Application of the Higgs boson mass window requirement improves the performance of the Higgs-jet tagger substantially. The multijet background rejection improves by a factor of about five by adding a loose (corresponding to 80% signal efficiency) mass window requirement on top of the double-b-tagging requirement. The tight (corresponding to 68% signal efficiency) mass window requirement leads to an additional 30–50% improvement in the multijet background rejection. The multijet background rejection has a weak dependence on the jet p_{T} for both mass window requirements. The hadronic top-quark rejection depends strongly on the jet p_{T}. The rejection varies between 60 and 230 for the loose mass window and double-b-tagging working points. The largest improvement in the top-quark rejection for the tight mass window is about 70% and corresponds to the high p_{T} and double-b-tagging working point.

The performance of the additional jet substructure variables depends on the chosen Higgs-jet tagger working point.

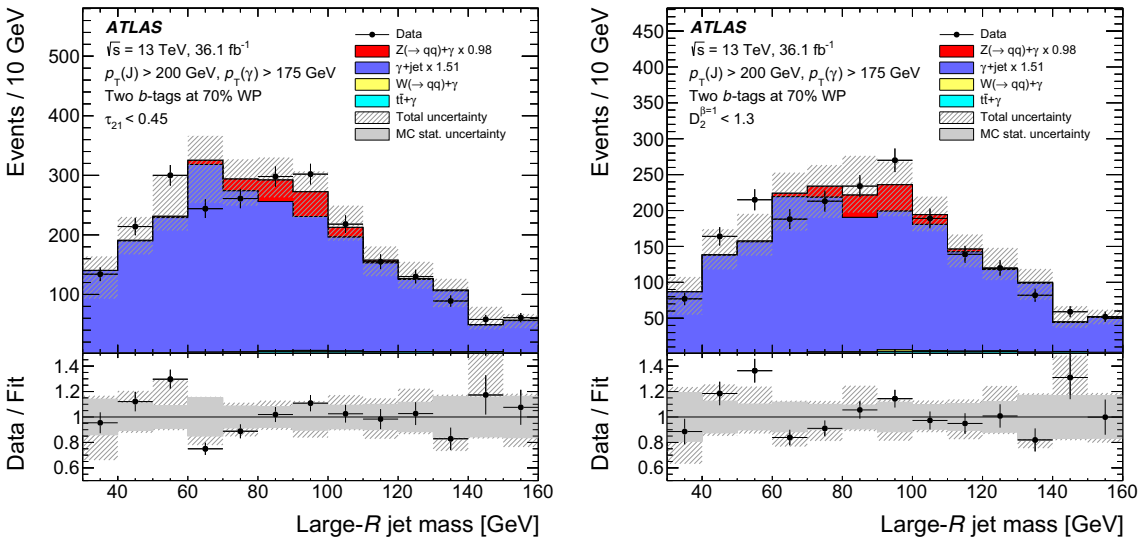

Fig. 19 $Z \to b\bar{b}$ candidate jet mass after applying the $\tau_{21} < 0.45$ (left) or $D_2^{\beta=1} < 1.3$ (right) requirement. Events with two b-tagged track-jets are used. The $\gamma+$ jets background and the $Z \to b\bar{b}$ signal are normalised to data by applying a scale factor of 1.51 and 0.98, respectively

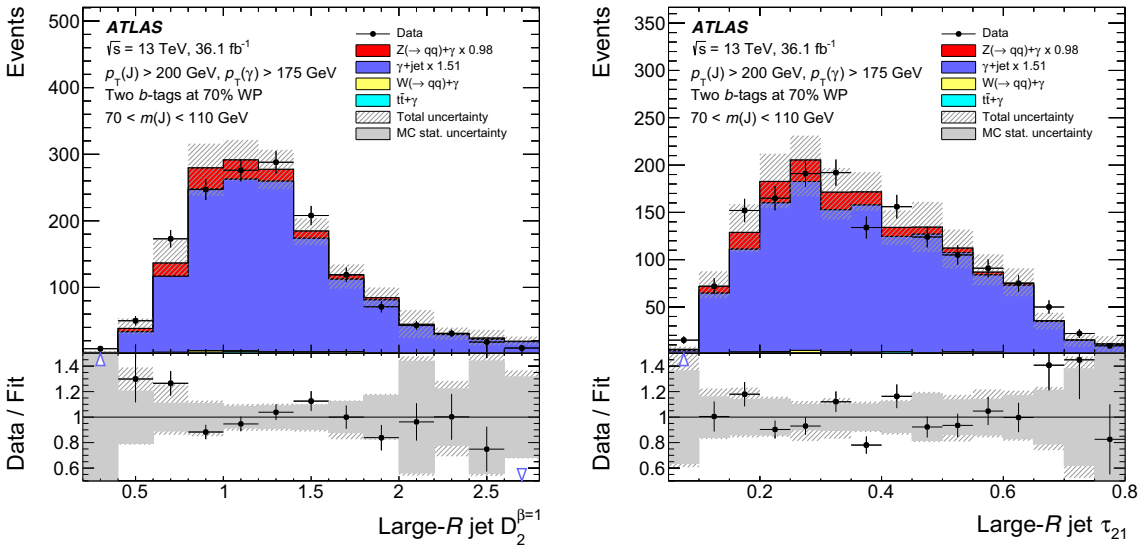

Fig. 20 $Z \to b\bar{b}$ candidate $D_2^{\beta=1}$ and τ_{21} distributions after requiring the $Z \to b\bar{b}$ candidate jet mass to be between 70 and 110 GeV. Events with two b-tagged track-jets are used. The $\gamma+$ jets background and the $Z \to b\bar{b}$ signal are normalised to data by applying a scale factor of 1.51 and 0.98, respectively. The upward- or downward-pointing arrows indicate that the Data/Fit ratio is out of the histogram range for these bins

The jet mass and other substructure variables are often correlated and the double-b-tagging requirement enforces a two-prong structure. In general, the background rejection is larger for the multijet background than for hadronically decaying top quarks but still below two for the individual variables and the loose mass window working point. The b-tagging discriminant is very powerful but the jet substructure variables offer an alternative to the b-tagging working points. Especially at high Higgs-jet p_{T} the efficiency to reconstruct two track-jets and the double-b-tagging efficiency decrease quickly. A combination of several substructure variables using multivariate methods could potentially increase the gain in performance in this phase space.

The modelling of representative Higgs-jet properties is tested in ATLAS data for $g \to b\bar{b}$ and $Z(\to b\bar{b})\gamma$ event selections. Good modelling is observed given the size of the available data sample and the systematic uncertainties. In particular, the use of jet substructure variables is shown to improve the purity of the $Z(\to b\bar{b})\gamma$ event selection.

Acknowledgements We thank CERN for the very successful operation of the LHC, as well as the support staff from our institutions without whom ATLAS could not be operated efficiently. We acknowledge the support of ANPCyT, Argentina; YerPhI, Armenia; ARC, Australia; BMWFW and FWF, Austria; ANAS, Azerbaijan; SSTC, Belarus; CNPq and FAPESP, Brazil; NSERC, NRC and CFI, Canada; CERN; CONICYT, Chile; CAS, MOST and NSFC, China; COLCIEN-

CIAS, Colombia; MSMT CR, MPO CR and VSC CR, Czech Republic; DNRF and DNSRC, Denmark; IN2P3-CNRS, CEA-DRF/IRFU, France; SRNSFG, Georgia; BMBF, HGF, and MPG, Germany; GSRT, Greece; RGC, Hong Kong SAR, China; ISF and Benoziyo Center, Israel; INFN, Italy; MEXT and JSPS, Japan; CNRST, Morocco; NWO, The Netherlands; RCN, Norway; MNiSW and NCN, Poland; FCT, Portugal; MNE/IFA, Romania; MES of Russia and NRC KI, Russian Federation; JINR; MESTD, Serbia; MSSR, Slovakia; ARRS and MIZŠ, Slovenia; DST/NRF, South Africa; MINECO, Spain; SRC and Wallenberg Foundation, Sweden; SERI, SNSF and Cantons of Bern and Geneva, Switzerland; MOST, Taiwan; TAEK, Turkey; STFC, UK; DOE and NSF, USA. In addition, individual groups and members have received support from BCKDF, CANARIE, CRC and Compute Canada, Canada; COST, ERC, ERDF, Horizon 2020, and Marie Skłodowska-Curie Actions, European Union; Investissements d' Avenir Labex and Idex, ANR, France; DFG and AvH Foundation, Germany; Herakleitos, Thales and Aristeia programmes co-financed by EU-ESF and the Greek NSRF, Greece; BSF-NSF and GIF, Israel; CERCA Programme Generalitat de Catalunya, Spain; The Royal Society and Leverhulme Trust, UK. The crucial computing support from all WLCG partners is acknowledged gratefully, in particular from CERN, the ATLAS Tier-1 facilities at TRIUMF (Canada), NDGF (Denmark, Norway, Sweden), CC-IN2P3 (France), KIT/GridKA (Germany), INFN-CNAF (Italy), NL-T1 (The Netherlands), PIC (Spain), ASGC (Taiwan), RAL (UK) and BNL (USA), the Tier-2 facilities worldwide and large non-WLCG resource providers. Major contributors of computing resources are listed in Ref. [84].

Data Availability Statement This manuscript has no associated data or the data will not be deposited. [Authors' comment: "All ATLAS scientific output is published in journals, and preliminary results are made available in Conference Notes. All are openly available, without restriction on use by external parties beyond copyright law and the standard conditions agreed by CERN. Data associated with journal publications are also made available: tables and data from plots (e.g. cross section values, likelihood profiles, selection efficiencies, cross section limits, ...) are stored in appropriate repositories such as HEPDATA (http://hepdata.cedar.ac.uk/). ATLAS also strives to make additional material related to the paper available that allows a reinterpretation of the data in the context of new theoretical models. For example, an extended encapsulation of the analysis is often provided for measurements in the framework of RIVET (http://rivet.hepforge.org/)." This information is taken from the ATLAS Data Access Policy, which is a public document that can be downloaded from http://opendata.cern.ch/record/413 [opendata.cern.ch].]

Funded by SCOAP[3].

References

1. ATLAS Collaboration, The ATLAS Experiment at the CERN Large Hadron Collider, JINST **3**, S08003 (2008)
2. L. Randall, R. Sundrum, Large Mass Hierarchy from a Small Extra Dimension. Phys. Rev. Lett. **83**, 3370 (1999). arXiv:hep-ph/9905221
3. K. Matchev, K. Thomas, Higgs and Z-boson signatures of supersymmetry. Phys. Rev. D **62**, 077702 (2000). arXiv:hep-ph/9908482 [hep-ph]
4. G. Branco et al., Theory and phenomenology of two-Higgs-doublet models. Phys. Rept. **516**, 1 (2012). arXiv:1106.0034 [hep-ex]
5. ATLAS Collaboration, Observation of a new particle in the search for the Standard Model Higgs boson with the ATLAS detector at the LHC, Phys. Lett. B **716**, 1 (2012) arXiv:1207.7214 [hep-ex]
6. CMS Collaboration, Observation of a new boson at a mass of 125 GeV with the CMS experiment at the LHC. Phys. Lett. B **716**, 30 (2012). arXiv:1207.7235 [hep-ex]
7. B. Cooper, N. Konstantinidis, L. Lambourne, D. Wardrope, Boosted $hh \to b\bar{b}b\bar{b}$: A new topology in searches for TeV-scale resonances at the LHC. Phys. Rev. D **88**, 114005 (2013). arXiv:1307.0407 [hep-ex]
8. ATLAS Collaboration, Search for pair production of Higgs bosons in the $b\bar{b}b\bar{b}$ final state using proton–proton collisions at $\sqrt{s} = 13$ TeV with the ATLAS detector, JHEP **01**, 030, (2019) arXiv:1804.06174 [hep-ex]
9. ATLAS Collaboration, Search for heavy resonances decaying into a W or Z boson and a Higgs boson in final states with leptons and b-jets in 36 fb^{-1} of $\sqrt{s} = 13$ TeV pp collisions with the ATLAS detector, JHEP **03**, 174 (2018) arXiv:1712.06518 [hep-ex]
10. ATLAS Collaboration, Search for heavy resonances decaying to a W or Z boson and a Higgs boson in the $q\bar{q}^{(\prime)}b\bar{b}$ final state in pp collisions at $\sqrt{s} = 13$ TeV with the ATLAS detector, Phys. Lett. B **774**, 494, (2017) arXiv:1707.06958 [hep-ex]
11. J.M. Butterworth, A.R. Davison, M. Rubin, G.P. Salam, Jet Substructure as a New Higgs-Search Channel at the Large Hadron Collider. Phys. Rev. Lett. **100**, 242001 (2008). arXiv:0802.2470 [hep-ph]
12. ATLAS Collaboration, Performance of jet substructure techniques for large-R jets in proton–proton collisions at $\sqrt{s} = 7$ TeV using the ATLAS detector, JHEP **09**, 076 (2013) arXiv:1306.4945 [hep-ex]
13. ATLAS Collaboration, Flavor Tagging with Track-Jets in Boosted Topologies with the ATLAS Detector, ATL-PHYS-PUB-2014-013, (2014), https://cds.cern.ch/record/1750681
14. ATLAS Collaboration, Search for Higgs boson pair production in the $b\bar{b}b\bar{b}$ final state from pp collisions at $\sqrt{s} = 8$ TeV with the ATLAS detector, Eur. Phys. J. C **75**, 412 (2015) arXiv:1506.00285 [hep-ex]
15. ATLAS Collaboration, A new method to distinguish hadronically decaying boosted Z bosons from W bosons using the ATLAS detector, Eur. Phys. J. C **76**, 238 (2016) arXiv:1509.04939 [hep-ex]
16. ATLAS Collaboration, Properties of $g \to b\bar{b}$ at small opening angles in pp collisions with the ATLAS detector at $\sqrt{s} = 13$ TeV, Phys. Rev. D **99**, 052004 (2019) arXiv:1812.09283 [hep-ex]
17. CMS Collaboration, Identification of heavy-flavour jets with the CMS detector in pp collisions at 13 TeV. JINST **13**, P05011 (2018). arXiv:1712.07158 [hep-ex]
18. CMS Collaboration, Inclusive Search for a Highly Boosted Higgs Boson Decaying to a Bottom Quark–Antiquark Pair. Phys. Rev. Lett. **120**, 071802 (2018). arXiv:1709.05543 [hep-ex]
19. ATLAS Collaboration, ATLAS Insertable B-Layer Technical Design Report, ATLAS-TDR-19, 2010, https://cds.cern.ch/record/1291633, ATLAS Insertable B-Layer Technical Design Report Addendum, ATLAS-TDR-19-ADD-1, (2012), https://cds.cern.ch/record/1451888
20. ATLAS IBL Collaboration, Production and integration of the ATLAS Insertable B-Layer, JINST **13**, T05008 (2018) arXiv:1803.00844 [physics.ins-det]
21. ATLAS Collaboration, Performance of the ATLAS trigger system in 2015, Eur. Phys. J. C **77**, 317 (2017) arXiv:1611.09661 [hep-ex]
22. J. Alwall, R. Frederix, S. Frixione, V. Hirschi, F. Maltoni et al., The automated computation of tree-level and next-to-leading order differential cross sections, and their matching to parton shower simulations. JHEP **07**, 079 (2014). arXiv:1405.0301 [hep-ph]

23. T. Sjöstrand et al., An Introduction to PYTHIA 8.2. Comput. Phys. Commun. **191**, 159 (2015). arXiv:1410.3012 [hep-ph]
24. R.D. Ball et al., Parton distributions with LHC data. Nucl. Phys. B **867**, 244 (2013). arXiv:1207.1303 [hep-ph]
25. ATLAS Collaboration, ATLAS Pythia 8 tunes to 7 TeV data, ATL-PHYS-PUB-2014-021, (2014), https://cds.cern.ch/record/1966419
26. T. Gleisberg, S. Höche, F. Krauss, M. Schönherr, S. Schumann et al., Event generation with SHERPA 1.1. JHEP **02**, 007 (2009). arXiv:0811.4622 [hep-ph]
27. S. Höche, F. Krauss, S. Schumann, F. Siegert, QCD matrix elements and truncated showers. JHEP **05**, 053 (2009). arXiv:0903.1219 [hep-ph]
28. T. Gleisberg, S. Höche, Comix, a new matrix element generator. JHEP **12**, 039 (2008). arXiv:0808.3674 [hep-ph]
29. S. Schumann, F. Krauss, A Parton shower algorithm based on Catani-Seymour dipole factorisation. JHEP **03**, 038 (2008). arXiv:0709.1027 [hep-ph]
30. H.-L. Lai et al., New parton distributions for collider physics. Phys. Rev. D **82**, 074024 (2010). arXiv:1007.2241 [hep-ph]
31. J. Gao et al., CT10 next-to-next-to-leading order global analysis of QCD. Phys. Rev. D **89**, 033009 (2014)
32. M. Bahr et al., Herwig++ Physics and Manual. Eur. Phys. J. C **58**, 639 (2008). arXiv:0803.0883 [hep-ph]
33. J. Pumplin et al., New generation of parton distributions with uncertainties from global QCD analysis. JHEP **07**, 012 (2002). arXiv:hep-ph/0201195
34. S. Gieseke, C. Rohr, A. Siodmok, Colour reconnections in Herwig++. Eur. Phys. J. C **72**, 2225 (2012). arXiv:1206.0041 [hep-ph]
35. D.J. Lange, The EvtGen particle decay simulation package. Nucl. Instr. Meth. A **462**, 152 (2001)
36. ATLAS Collaboration, Summary of ATLAS Pythia 8 tunes, ATL-PHYS-PUB-2012-003, (2012), https://cds.cern.ch/record/1474107
37. A.D. Martin, W.J. Stirling, R.S. Thorne, G. Watt, Parton distributions for the LHC. Eur. Phys. J. C **63**, 189 (2009). arXiv:0901.0002 [hep-ph]
38. A.D. Martin, W.J. Stirling, R.S. Thorne, G. Watt, Uncertainties on α_S in global PDF analyses and implications for predicted hadronic cross sections. Eur. Phys. J. C **64**, 653 (2009). arXiv:0905.3531 [hep-ph]
39. A.D. Martin, W.J. Stirling, R.S. Thorne, G. Watt, Heavy-quark mass dependence in global PDF analyses and 3- and 4-flavour parton distributions. Eur. Phys. J. C **70**, 51 (2010). arXiv:1007.2624 [hep-ph]
40. S. Agostinelli et al., GEANT4: A Simulation toolkit. Nucl. Instrum. Meth. A **506**, 250 (2003)
41. ATLAS Collaboration, The ATLAS Simulation Infrastructure, Eur. Phys. J. C **70**, 823 (2010) arXiv:1005.4568 [physics.ins-det]
42. M. Cacciari, G.P. Salam, G. Soyez, FastJet User Manual. Eur. Phys. J. C **72**, 1896 (2012). arXiv:1111.6097 [hep-ph]
43. M. Cacciari, G.P. Salam, G. Soyez, The anti-k_t jet clustering algorithm. JHEP **04**, 063 (2008). arXiv:0802.1189 [hep-ph]
44. ATLAS Collaboration, Topological cell clustering in the ATLAS calorimeters and its performance in LHC Run 1, Eur. Phys. J. C **77**, 490 (2017) arXiv:1603.02934 [hep-ex]
45. D. Krohn, J. Thaler, L.-T. Wang, Jet Trimming. JHEP **02**, 084 (2010). arXiv:0912.1342 [hep-ph]
46. S. Catani, Y.L. Dokshitzer, M.H. Seymour, B.R. Webber, Longitudinally invariant K_t clustering algorithms for hadron hadron collisions. Nucl. Phys. B **406**, 187 (1993)
47. S.D. Ellis, D.E. Soper, Successive combination jet algorithm for hadron collisions. Phys. Rev. D **48**, 3160 (1993). arXiv:hep-ph/9305266 [hep-ph]
48. ATLAS Collaboration, In situ calibration of large-radius jet energy and mass in 13 TeV proton–proton collisions with the ATLAS detector, Eur. Phys. J. C **79**, 135 (2019) arXiv:1807.09477 [hep-ex]
49. ATLAS Collaboration, Jet energy scale measurements and their systematic uncertainties in proton–proton collisions at $\sqrt{s} = 13$ TeV with the ATLAS detector, Phys. Rev. D **96**, 072002 (2017) arXiv:1703.09665 [hep-ex]
50. ATLAS Collaboration, Performance of pile-up mitigation techniques for jets in pp collisions at $\sqrt{s} = 8$ TeV using the ATLAS detector, Eur. Phys. J. C **76**, 581 (2016) arXiv:1510.03823 [hep-ex]
51. ATLAS Collaboration, Performance of b-jet identification in the ATLAS experiment, JINST **11**, P04008 (2016) arXiv:1512.01094 [hep-ex]
52. ATLAS Collaboration, Muon reconstruction performance of the ATLAS detector in proton–proton collision data at $\sqrt{s} = 13$ TeV, Eur. Phys. J. C **76**, 292 (2016) arXiv:1603.05598 [hep-ex]
53. ATLAS Collaboration, Measurement of the photon identification efficiencies with the ATLAS detector using LHC Run 2 data collected in 2015 and 2016, Eur. Phys. J. C **79**, 205 (2019) arXiv:1810.05087 [hep-ex]
54. ATLAS Collaboration, Electron and photon energy calibration with the ATLAS detector using 2015–2016 LHC proton–proton collision data, JINST **14**, P03017 (2019) arXiv:1812.03848 [hep-ex]. 34
55. M. Cacciari, G.P. Salam, G. Soyez, The Catchment Area of Jets. JHEP **04**, 005 (2008). arXiv:0802.1188 [hep-ph]
56. M. Cacciari, G.P. Salam, Pileup subtraction using jet areas. Phys. Lett. B **659**, 119 (2008). arXiv:0707.1378 [hep-ph]
57. ATLAS Collaboration, Optimisation of the ATLAS b-tagging performance for the 2016 LHC Run, ATL-PHYS-PUB-2016-012, (2016), https://cds.cern.ch/record/2160731
58. ATLAS Collaboration, Boosted Higgs ($\rightarrow b\bar{b}$) Boson Identification with the ATLAS Detector at $\sqrt{s} = 13$ TeV, ATLAS-CONF-2016-039, (2016), https://cds.cern.ch/record/2206038
59. ATLAS Collaboration, Expected Performance of Boosted Higgs ($\rightarrow b\bar{b}$) Boson Identification with the ATLAS Detector at $\sqrt{s} = 13$ TeV, ATL-PHYS-PUB-2015-035, (2015), https://cds.cern.ch/record/2042155
60. ATLAS Collaboration, Measurement of b-tagging efficiency of c-jets in $t\bar{t}$ events using a likelihood approach with the ATLAS detector, ATLAS-CONF-2018-001, (2018), https://cds.cern.ch/record/2306649
61. ATLAS Collaboration, Measurements of b-jet tagging efficiency with the ATLAS detector using $t\bar{t}$ events at $\sqrt{s} = 13$ TeV, JHEP **08**, 089 (2018) arXiv:1805.01845 [hep-ex]
62. ATLAS Collaboration, Calibration of light-flavour b-jet mistagging rates using ATLAS proton–proton collision data at $\sqrt{s} = 13$ TeV, ATLAS-CONF-2018-006, (2018), https://cds.cern.ch/record/2314418
63. J. Bellm et al., Herwig 7.0/Herwig++ 3.0 release note. Eur. Phys. J. C **76**, 196 (2016). arXiv:1512.01178 [hep-ph]
64. ATLAS Collaboration, Variable Radius, Exclusive-k_T , and Center-of-Mass Subjet Reconstruction for Higgs($\rightarrow b\bar{b}$) Tagging in ATLAS, ATL-PHYS-PUB-2017-010, (2017), https://cds.cern.ch/record/2268678
65. ATLAS Collaboration, Identification of boosted, hadronically decaying W bosons and comparisons with ATLAS data taken at $\sqrt{s} = 8$ TeV, Eur. Phys. J. C **76**, 154 (2016) arXiv:1510.05821 [hep-ex]
66. ATLAS Collaboration, Identification of high transverse momentum top quarks in pp collisions at $\sqrt{s} = 8$ TeV with the ATLAS detector, JHEP **06**, 093 (2016) arXiv:1603.03127 [hep-ex]
67. A.J. Larkoski, G.P. Salam, J. Thaler, Energy Correlation Functions for Jet Substructure. JHEP **06**, 108 (2013). arXiv:1305.0007 [hep-ph]

68. A.J. Larkoski, I. Moult, D. Neill, Power Counting to Better Jet Observables. JHEP **12**, 009 (2014). arXiv:1409.6298 [hep-ph]
69. J. Thaler, K. Van Tilburg, Identifying boosted objects with N-subjettiness. JHEP **03**, 015 (2011). arXiv:1011.2268 [hep-ph]
70. J. Thaler, K. Van Tilburg, Maximizing boosted top identification by minimizing N-subjettiness. JHEP **02**, 093 (2012). arXiv:1108.2701 [hep-ph]
71. G.C. Fox, S. Wolfram, Observables for the Analysis of Event Shapes in e^+e^- Annihilation and Other Processes. Phys. Rev. Lett. **41**, 1581 (1978)
72. A. Hook, M. Jankowiak, J.G. Wacker, Jet dipolarity: top tagging with color flow. JHEP **04**, 007 (2012). arXiv:1102.1012 [hep-ph]
73. J.M. Butterworth, B.E. Cox, J.R. Forshaw, WW scattering at the CERN LHC. Phys. Rev. D **65**, 096014 (2002). arXiv:hep-ph/0201098 [hep-ph]
74. ATLAS Collaboration, Measurement of k_T splitting scales in W $\rightarrow \ell\nu$ events at $\sqrt{s} = 7$ TeV with the ATLAS detector, Eur. Phys. J. C **73**, 2432 (2013) arXiv:1302.1415 [hep-ex]
75. S. Brandt, C. Peyrou, R. Sosnowski, A. Wroblewski, The Principal axis of jets. An Attempt to analyze high-energy collisions as two-body processes. Phys. Lett. **12**, 57 (1964)
76. C. Chen, New approach to identifying boosted hadronically-decaying particle using jet substructure in its center-of-mass frame. Phys. Rev. D **85**, 034007 (2012). arXiv:1112.2567 [hep-ph]
77. L.G. Almeida et al., Top quark jets at the LHC. Phys. Rev. D **79**, 074012 (2009). arXiv:0810.0934 [hep-ph]
78. ATLAS Collaboration, ATLAS measurements of the properties of jets for boosted particle searches, Phys. Rev. D **86**, 072006 (2012) arXiv:1206.5369 [hep-ex]
79. ATLAS Collaboration, Performance of top-quark and W-boson tagging with ATLAS in Run 2 of the LHC, (2018), arXiv:1808.07858 [hep-ex]
80. ATLAS Collaboration, Performance of mass-decorrelated jet substructure observables for hadronic two-body decay tagging in ATLAS, ATL-PHYS-PUB-2018-014, (2018), https://cds.cern.ch/record/2630973
81. ATLAS Collaboration, Search for pair production of Higgs bosons in the $b\bar{b}b\bar{b}$ final state using proton–proton collisions at $\sqrt{s} = 13$ TeV with the ATLAS detector, Phys. Rev. D **94**, 052002 (2016) arXiv:1606.04782 [hep-ex]
82. ATLAS Collaboration, Vertex Reconstruction Performance of the ATLAS Detector at $\sqrt{s} = 13$ TeV, ATL-PHYS-PUB-2015-026, (2015), https://cds.cern.ch/record/2037717
83. ATLAS Collaboration, Characterisation and mitigation of beam-induced backgrounds observed in the ATLAS detector during the 2011 proton–proton run, JINST **8**, P07004 (2013) arXiv:1303.0223 [hep-ex]
84. ATLAS Collaboration, ATLAS Computing Acknowledgements, ATL-GEN-PUB-2016-002, https://cds.cern.ch/record/2202407

ATLAS Collaboration

G. Aad[101], B. Abbott[128], D. C. Abbott[102], O. Abdinov[13,*], A. Abed Abud[70a,70b], K. Abeling[53], D. K. Abhayasinghe[93], S. H. Abidi[167], O. S. AbouZeid[40], N. L. Abraham[156], H. Abramowicz[161], H. Abreu[160], Y. Abulaiti[6], B. S. Acharya[66a,66b,o], B. Achkar[53], S. Adachi[163], L. Adam[99], C. Adam Bourdarios[132], L. Adamczyk[83a], L. Adamek[167], J. Adelman[121], M. Adersberger[114], A. Adiguzel[12c,aj], S. Adorni[54], T. Adye[144], A. A. Affolder[146], Y. Afik[160], C. Agapopoulou[132], M. N. Agaras[38], A. Aggarwal[119], C. Agheorghiesei[27c], J. A. Aguilar-Saavedra[140a,140f,ai], F. Ahmadov[79], W. S. Ahmed[103], X. Ai[15a], G. Aielli[73a,73b], S. Akatsuka[85], T. P. A. Åkesson[96], E. Akilli[54], A. V. Akimov[110], K. Al Khoury[132], G. L. Alberghi[23a,23b], J. Albert[176], M. J. Alconada Verzini[88], S. Alderweireldt[36], M. Aleksa[36], I. N. Aleksandrov[79], C. Alexa[27b], D. Alexandre[19], T. Alexopoulos[10], A. Alfonsi[120], M. Alhroob[128], B. Ali[142], G. Alimonti[68a], J. Alison[37], S. P. Alkire[148], C. Allaire[132], B. M. M. Allbrooke[156], B. W. Allen[131], P. P. Allport[21], A. Aloisio[69a,69b], A. Alonso[40], F. Alonso[88], C. Alpigiani[148], A. A. Alshehri[57], M. Alvarez Estevez[98], D. Álvarez Piqueras[174], M. G. Alviggi[69a,69b], Y. Amaral Coutinho[80b], A. Ambler[103], L. Ambroz[135], C. Amelung[26], D. Amidei[105], S. P. Amor Dos Santos[140a], S. Amoroso[46], C. S. Amrouche[54], F. An[78], C. Anastopoulos[149], N. Andari[145], T. Andeen[11], C. F. Anders[61b], J. K. Anders[20], A. Andreazza[68a,68b], V. Andrei[61a], C. R. Anelli[176], S. Angelidakis[38], A. Angerami[39], A. V. Anisenkov[122a,122b], A. Annovi[71a], C. Antel[61a], M. T. Anthony[149], M. Antonelli[51], D. J. A. Antrim[171], F. Anulli[72a], M. Aoki[81], J. A. Aparisi Pozo[174], L. Aperio Bella[36], G. Arabidze[106], J. P. Araque[140a], V. Araujo Ferraz[80b], R. Araujo Pereira[80b], C. Arcangeletti[51], A. T. H. Arce[49], F. A. Arduh[88], J-F. Arguin[109], S. Argyropoulos[77], J.-H. Arling[46], A. J. Armbruster[36], L. J. Armitage[92], A. Armstrong[171], O. Arnaez[167], H. Arnold[120], A. Artamonov[111,*], G. Artoni[135], S. Artz[99], S. Asai[163], N. Asbah[59], E. M. Asimakopoulou[172], L. Asquith[156], K. Assamagan[29], R. Astalos[28a], R. J. Atkin[33a], M. Atkinson[173], N. B. Atlay[151], H. Atmani[132], K. Augsten[142], G. Avolio[36], R. Avramidou[60a], M. K. Ayoub[15a], A. M. Azoulay[168b], G. Azuelos[109,ay], M. J. Baca[21], H. Bachacou[145], K. Bachas[67a,67b], M. Backes[135], F. Backman[45a,45b], P. Bagnaia[72a,72b], M. Bahmani[84], H. Bahrasemani[152], A. J. Bailey[174], V. R. Bailey[173], J. T. Baines[144], M. Bajic[40], C. Bakalis[10], O. K. Baker[183], P. J. Bakker[120], D. Bakshi Gupta[8], S. Balaji[157], E. M. Baldin[122a,122b], P. Balek[180], F. Balli[145], W. K. Balunas[135], J. Balz[99], E. Banas[84], A. Bandyopadhyay[24], Sw. Banerjee[181,j], A. A. E. Bannoura[182], L. Barak[161], W. M. Barbe[38], E. L. Barberio[104], D. Barberis[55a,55b], M. Barbero[101], T. Barillari[115], M-S. Barisits[36], J. Barkeloo[131], T. Barklow[153], R. Barnea[160], S. L. Barnes[60c], B. M. Barnett[144], R. M. Barnett[18], Z. Barnovska-Blenessy[60a], A. Baroncelli[60a], G. Barone[29], A. J. Barr[135], L. Barranco Navarro[45a,45b], F. Barreiro[98], J. Barreiro Guimarães da Costa[15a], S. Barsov[138], R. Bartoldus[153], G. Bartolini[101], A. E. Barton[89], P. Bartos[28a], A. Basalaev[46], A. Bassalat[132,ar], R. L. Bates[57], S. J. Batista[167], S. Batlamous[35e], J. R. Batley[32], B. Batool[151], M. Battaglia[146], M. Bauce[72a,72b],

F. Bauer[145], K. T. Bauer[171], H. S. Bawa[31,m], J. B. Beacham[49], T. Beau[136], P. H. Beauchemin[170], F. Becherer[52], P. Bechtle[24], H. C. Beck[53], H. P. Beck[20,s], K. Becker[52], M. Becker[99], C. Becot[46], A. Beddall[12d], A. J. Beddall[12a], V. A. Bednyakov[79], M. Bedognetti[120], C. P. Bee[155], T. A. Beermann[76], M. Begalli[80b], M. Begel[29], A. Behera[155], J. K. Behr[46], F. Beisiegel[24], A. S. Bell[94], G. Bella[161], L. Bellagamba[23b], A. Bellerive[34], P. Bellos[9], K. Beloborodov[122a,122b], K. Belotskiy[112], N. L. Belyaev[112], D. Benchekroun[35a], N. Benekos[10], Y. Benhammou[161], D. P. Benjamin[6], M. Benoit[54], J. R. Bensinger[26], S. Bentvelsen[120], L. Beresford[135], M. Beretta[51], D. Berge[46], E. Bergeaas Kuutmann[172], N. Berger[5], B. Bergmann[142], L. J. Bergsten[26], J. Beringer[18], S. Berlendis[7], N. R. Bernard[102], G. Bernardi[136], C. Bernius[153], T. Berry[93], P. Berta[99], C. Bertella[15a], I. A. Bertram[89], G. J. Besjes[40], O. Bessidskaia Bylund[182], N. Besson[145], A. Bethani[100], S. Bethke[115], A. Betti[24], A. J. Bevan[92], J. Beyer[115], R. Bi[139], R. M. Bianchi[139], O. Biebel[114], D. Biedermann[19], R. Bielski[36], K. Bierwagen[99], N. V. Biesuz[71a,71b], M. Biglietti[74a], T. R. V. Billoud[109], M. Bindi[53], A. Bingul[12d], C. Bini[72a,72b], S. Biondi[23a,23b], M. Birman[180], T. Bisanz[53], J. P. Biswal[161], A. Bitadze[100], C. Bittrich[48], K. Bjørke[134], K. M. Black[25], T. Blazek[28a], I. Bloch[46], C. Blocker[26], A. Blue[57], U. Blumenschein[92], G. J. Bobbink[120], V. S. Bobrovnikov[122a,122b], S. S. Bocchetta[96], A. Bocci[49], D. Boerner[46], D. Bogavac[14], A. G. Bogdanchikov[122a,122b], C. Bohm[45a], V. Boisvert[93], P. Bokan[53,172], T. Bold[83a], A. S. Boldyrev[113], A. E. Bolz[61b], M. Bomben[136], M. Bona[92], J. S. Bonilla[131], M. Boonekamp[145], H. M. Borecka-Bielska[90], A. Borisov[123], G. Borissov[89], J. Bortfeldt[36], D. Bortoletto[135], V. Bortolotto[73a,73b], D. Boscherini[23b], M. Bosman[14], J. D. Bossio Sola[103], K. Bouaouda[35a], J. Boudreau[139], E. V. Bouhova-Thacker[89], D. Boumediene[38], S. K. Boutle[57], A. Boveia[126], J. Boyd[36], D. Boye[33b,as], I. R. Boyko[79], A. J. Bozson[93], J. Bracinik[21], N. Brahimi[101], G. Brandt[182], O. Brandt[61a], F. Braren[46], B. Brau[102], J. E. Brau[131], W. D. Breaden Madden[57], K. Brendlinger[46], L. Brenner[46], R. Brenner[172], S. Bressler[180], B. Brickwedde[99], D. L. Briglin[21], D. Britton[57], D. Britzger[115], I. Brock[24], R. Brock[106], G. Brooijmans[39], W. K. Brooks[147b], E. Brost[121], J. H. Broughton[21], P. A. Bruckman de Renstrom[84], D. Bruncko[28b], A. Bruni[23b], G. Bruni[23b], L. S. Bruni[120], S. Bruno[73a,73b], B. H. Brunt[32], M. Bruschi[23b], N. Bruscino[139], P. Bryant[37], L. Bryngemark[96], T. Buanes[17], Q. Buat[36], P. Buchholz[151], A. G. Buckley[57], I. A. Budagov[79], M. K. Bugge[134], F. Bührer[52], O. Bulekov[112], T. J. Burch[121], S. Burdin[90], C. D. Burgard[120], A. M. Burger[129], B. Burghgrave[8], K. Burka[84], J. T. P. Burr[46], J. C. Burzynski[102], V. Büscher[99], E. Buschmann[53], P. J. Bussey[57], J. M. Butler[25], C. M. Buttar[57], J. M. Butterworth[94], P. Butti[36], W. Buttinger[36], A. Buzatu[158], A. R. Buzykaev[122a,122b], G. Cabras[23a,23b], S. Cabrera Urbán[174], D. Caforio[56], H. Cai[173], V. M. M. Cairo[153], O. Cakir[4a], N. Calace[36], P. Calafiura[18], A. Calandri[101], G. Calderini[136], P. Calfayan[65], G. Callea[57], L. P. Caloba[80b], S. Calvente Lopez[98], D. Calvet[38], S. Calvet[38], T. P. Calvet[155], M. Calvetti[71a,71b], R. Camacho Toro[136], S. Camarda[36], D. Camarero Munoz[98], P. Camarri[73a,73b], D. Cameron[134], R. Caminal Armadans[102], C. Camincher[36], S. Campana[36], M. Campanelli[94], A. Camplani[40], A. Campoverde[151], V. Canale[69a,69b], A. Canesse[103], M. Cano Bret[60c], J. Cantero[129], T. Cao[161], Y. Cao[173], M. D. M. Capeans Garrido[36], M. Capua[41a,41b], R. Cardarelli[73a], F. C. Cardillo[149], G. Carducci[41a,41b], I. Carli[143], T. Carli[36], G. Carlino[69a], B. T. Carlson[139], L. Carminati[68a,68b], R. M. D. Carney[45a,45b], S. Caron[119], E. Carquin[147b], S. Carrá[46], J. W. S. Carter[167], M. P. Casado[14,e], A. F. Casha[167], D. W. Casper[171], R. Castelijn[120], F. L. Castillo[174], V. Castillo Gimenez[174], N. F. Castro[140a,140e], A. Catinaccio[36], J. R. Catmore[134], A. Cattai[36], J. Caudron[24], V. Cavaliere[29], E. Cavallaro[14], M. Cavalli-Sforza[14], V. Cavasinni[71a,71b], E. Celebi[12b], F. Ceradini[74a,74b], L. Cerda Alberich[174], K. Cerny[130], A. S. Cerqueira[80a], A. Cerri[156], L. Cerrito[73a,73b], F. Cerutti[18], A. Cervelli[23a,23b], S. A. Cetin[12b], D. Chakraborty[121], S. K. Chan[59], W. S. Chan[120], W. Y. Chan[90], J. D. Chapman[32], B. Chargeishvili[159b], D. G. Charlton[21], T. P. Charman[92], C. C. Chau[34], S. Che[126], A. Chegwidden[106], S. Chekanov[6], S. V. Chekulaev[168a], G. A. Chelkov[79,ax], M. A. Chelstowska[36], B. Chen[78], C. Chen[60a], C. H. Chen[78], H. Chen[29], J. Chen[60a], J. Chen[39], S. Chen[137], S. J. Chen[15c], X. Chen[15b,aw], Y. Chen[82], Y-H. Chen[46], H. C. Cheng[63a], H. J. Cheng[15a,15d], A. Cheplakov[79], E. Cheremushkina[123], R. Cherkaoui El Moursli[35e], E. Cheu[7], K. Cheung[64], T. J. A. Chevalérias[145], L. Chevalier[145], V. Chiarella[51], G. Chiarelli[71a], G. Chiodini[67a], A. S. Chisholm[36,21], A. Chitan[27b], I. Chiu[163], Y. H. Chiu[176], M. V. Chizhov[79], K. Choi[65], A. R. Chomont[72a,72b], S. Chouridou[162], Y. S. Chow[120], M. C. Chu[63a], X. Chu[15a], J. Chudoba[141], A. J. Chuinard[103], J. J. Chwastowski[84], L. Chytka[130], K. M. Ciesla[84], D. Cinca[47], V. Cindro[91], I. A. Cioară[27b], A. Ciocio[18], F. Cirotto[69a,69b], Z. H. Citron[180], M. Citterio[68a], D. A. Ciubotaru[27b], B. M. Ciungu[167], A. Clark[54], M. R. Clark[39], P. J. Clark[50], C. Clement[45a,45b], Y. Coadou[101], M. Cobal[66a,66c], A. Coccaro[55b], J. Cochran[78], H. Cohen[161], A. E. C. Coimbra[36], L. Colasurdo[119], B. Cole[39], A. P. Colijn[120], J. Collot[58], P. Conde Muiño[140a,f], E. Coniavitis[52], S. H. Connell[33b], I. A. Connelly[57], S. Constantinescu[27b], F. Conventi[69a,az], A. M. Cooper-Sarkar[135], F. Cormier[175], K. J. R. Cormier[167], L. D. Corpe[94], M. Corradi[72a,72b], E. E. Corrigan[96], F. Corriveau[103,ae], A. Cortes-Gonzalez[36], M. J. Costa[174], F. Costanza[5], D. Costanzo[149], G. Cowan[93], J. W. Cowley[32], J. Crane[100], K. Cranmer[124], S. J. Crawley[57], R. A. Creager[137], S. Crépé-Renaudin[58], F. Crescioli[136], M. Cristinziani[24], V. Croft[120], G. Crosetti[41a,41b], A. Cueto[5], T. Cuhadar Donszelmann[149], A. R. Cukierman[153], S. Czekierda[84], P. Czodrowski[36], M. J. Da Cunha Sargedas De Sousa[60b], J. V. Da Fonseca Pinto[80b], C. Da Via[100], W. Dabrowski[83a], T. Dado[28a], S. Dahbi[35e], T. Dai[105], C. Dallapiccola[102],

M. Dam[40], G. D'amen[23a,23b], V. D'Amico[74a,74b], J. Damp[99], J. R. Dandoy[137], M. F. Daneri[30], N. P. Dang[181], N. D. Dann[100], M. Danninger[175], V. Dao[36], G. Darbo[55b], O. Dartsi[5], A. Dattagupta[131], T. Daubney[46], S. D'Auria[68a,68b], W. Davey[24], C. David[46], T. Davidek[143], D. R. Davis[49], I. Dawson[149], K. De[8], R. De Asmundis[69a], M. De Beurs[120], S. De Castro[23a,23b], S. De Cecco[72a,72b], N. De Groot[119], P. de Jong[120], H. De la Torre[106], A. De Maria[15c], D. De Pedis[72a], A. De Salvo[72a], U. De Sanctis[73a,73b], M. De Santis[73a,73b], A. De Santo[156], K. De Vasconcelos Corga[101], J. B. De Vivie De Regie[132], C. Debenedetti[146], D. V. Dedovich[79], A. M. Deiana[42], M. Del Gaudio[41a,41b], J. Del Peso[98], Y. Delabat Diaz[46], D. Delgove[132], F. Deliot[145,r], C. M. Delitzsch[7], M. Della Pietra[69a,69b], D. Della Volpe[54], A. Dell'Acqua[36], L. Dell'Asta[73a,73b], M. Delmastro[5], C. Delporte[132], P. A. Delsart[58], D. A. DeMarco[167], S. Demers[183], M. Demichev[79], G. Demontigny[109], S. P. Denisov[123], D. Denysiuk[120], L. D'Eramo[136], D. Derendarz[84], J. E. Derkaoui[35d], F. Derue[136], P. Dervan[90], K. Desch[24], C. Deterre[46], K. Dette[167], C. Deutsch[24], M. R. Devesa[30], P. O. Deviveiros[36], A. Dewhurst[144], S. Dhaliwal[26], F. A. Di Bello[54], A. Di Ciaccio[73a,73b], L. Di Ciaccio[5], W. K. Di Clemente[137], C. Di Donato[69a,69b], A. Di Girolamo[36], G. Di Gregorio[71a,71b], B. Di Micco[74a,74b], R. Di Nardo[102], K. F. Di Petrillo[59], R. Di Sipio[167], D. Di Valentino[34], C. Diaconu[101], F. A. Dias[40], T. Dias Do Vale[140a], M. A. Diaz[147a], J. Dickinson[18], E. B. Diehl[105], J. Dietrich[19], S. Díez Cornell[46], A. Dimitrievska[18], W. Ding[15b], J. Dingfelder[24], F. Dittus[36], F. Djama[101], T. Djobava[159b], J. I. Djuvsland[17], M. A. B. Do Vale[80c], M. Dobre[27b], D. Dodsworth[26], C. Doglioni[96], J. Dolejsi[143], Z. Dolezal[143], M. Donadelli[80d], B. Dong[60c], J. Donini[38], A. D'onofrio[92], M. D'Onofrio[90], J. Dopke[144], A. Doria[69a], M. T. Dova[88], A. T. Doyle[57], E. Drechsler[152], E. Dreyer[152], T. Dreyer[53], A. S. Drobac[170], Y. Duan[60b], F. Dubinin[110], M. Dubovsky[28a], A. Dubreuil[54], E. Duchovni[180], G. Duckeck[114], A. Ducourthial[136], O. A. Ducu[109], D. Duda[115], A. Dudarev[36], A. C. Dudder[99], E. M. Duffield[18], L. Duflot[132], M. Dührssen[36], C. Dülsen[182], M. Dumancic[180], A. E. Dumitriu[27b], A. K. Duncan[57], M. Dunford[61a], A. Duperrin[101], H. Duran Yildiz[4a], M. Düren[56], A. Durglishvili[159b], D. Duschinger[48], B. Dutta[46], D. Duvnjak[1], G. I. Dyckes[137], M. Dyndal[36], S. Dysch[100], B. S. Dziedzic[84], K. M. Ecker[115], R. C. Edgar[105], T. Eifert[36], G. Eigen[17], K. Einsweiler[18], T. Ekelof[172], H. El Jarrari[35e], M. El Kacimi[35c], R. El Kosseifi[101], V. Ellajosyula[172], M. Ellert[172], F. Ellinghaus[182], A. A. Elliot[92], N. Ellis[36], J. Elmsheuser[29], M. Elsing[36], D. Emeliyanov[144], A. Emerman[39], Y. Enari[163], J. S. Ennis[178], M. B. Epland[49], J. Erdmann[47], A. Ereditato[20], M. Errenst[36], M. Escalier[132], C. Escobar[174], O. Estrada Pastor[174], E. Etzion[161], H. Evans[65], A. Ezhilov[138], F. Fabbri[57], L. Fabbri[23a,23b], V. Fabiani[119], G. Facini[94], R. M. Faisca Rodrigues Pereira[140a], R. M. Fakhrutdinov[123], S. Falciano[72a], P. J. Falke[5], S. Falke[5], J. Faltova[143], Y. Fang[15a], Y. Fang[15a], G. Fanourakis[44], M. Fanti[68a,68b], A. Farbin[8], A. Farilla[74a], E. M. Farina[70a,70b], T. Farooque[106], S. Farrell[18], S. M. Farrington[50], P. Farthouat[36], F. Fassi[35e], P. Fassnacht[36], D. Fassouliotis[9], M. Faucci Giannelli[50], W. J. Fawcett[32], L. Fayard[132], O. L. Fedin[138,p], W. Fedorko[175], M. Feickert[42], S. Feigl[134], L. Feligioni[101], A. Fell[149], C. Feng[60b], E. J. Feng[36], M. Feng[49], M. J. Fenton[57], A. B. Fenyuk[123], J. Ferrando[46], A. Ferrante[173], A. Ferrari[172], P. Ferrari[120], R. Ferrari[70a], D. E. Ferreira de Lima[61b], A. Ferrer[174], D. Ferrere[54], C. Ferretti[105], F. Fiedler[99], A. Filipčič[91], F. Filthaut[119], K. D. Finelli[25], M. C. N. Fiolhais[140a], L. Fiorini[174], F. Fischer[114], W. C. Fisher[106], I. Fleck[151], P. Fleischmann[105], R. R. M. Fletcher[137], T. Flick[182], B. M. Flierl[114], L. F. Flores[137], L. R. Flores Castillo[63a], F. M. Follega[75a,75b], N. Fomin[17], J. H. Foo[167], G. T. Forcolin[75a,75b], A. Formica[145], F. A. Förster[14], A. C. Forti[100], A. G. Foster[21], M. G. Foti[135], D. Fournier[132], H. Fox[89], P. Francavilla[71a,71b], S. Francescato[72a,72b], M. Franchini[23a,23b], S. Franchino[61a], D. Francis[36], L. Franconi[20], M. Franklin[59], A. N. Fray[92], B. Freund[109], W. S. Freund[80b], E. M. Freundlich[47], D. C. Frizzell[128], D. Froidevaux[36], J. A. Frost[135], C. Fukunaga[164], E. Fullana Torregrosa[174], E. Fumagalli[55a,55b], T. Fusayasu[116], J. Fuster[174], A. Gabrielli[23a,23b], A. Gabrielli[18], G. P. Gach[83a], S. Gadatsch[54], P. Gadow[115], G. Gagliardi[55a,55b], L. G. Gagnon[109], C. Galea[27b], B. Galhardo[140a], G. E. Gallardo[135], E. J. Gallas[135], B. J. Gallop[144], P. Gallus[142], G. Galster[40], R. Gamboa Goni[92], K. K. Gan[126], S. Ganguly[180], J. Gao[60a], Y. Gao[90], Y. S. Gao[31,m], C. García[174], J. E. García Navarro[174], J. A. García Pascual[15a], C. Garcia-Argos[52], M. Garcia-Sciveres[18], R. W. Gardner[37], N. Garelli[153], S. Gargiulo[52], V. Garonne[134], A. Gaudiello[55a,55b], G. Gaudio[70a], I. L. Gavrilenko[110], A. Gavrilyuk[111], C. Gay[175], G. Gaycken[24], E. N. Gazis[10], A. A. Geanta[27b], C. N. P. Gee[144], J. Geisen[53], M. Geisen[99], M. P. Geisler[61a], C. Gemme[55b], M. H. Genest[58], C. Geng[105], S. Gentile[72a,72b], S. George[93], T. Geralis[44], L. O. Gerlach[53], P. Gessinger-Befurt[99], G. Gessner[47], S. Ghasemi[151], M. Ghasemi Bostanabad[176], M. Ghneimat[24], A. Ghosh[132], A. Ghosh[77], B. Giacobbe[23b], S. Giagu[72a,72b], N. Giangiacomi[23a,23b], P. Giannetti[71a], A. Giannini[69a,69b], S. M. Gibson[93], M. Gignac[146], D. Gillberg[34], G. Gilles[182], D. M. Gingrich[3,ay], M. P. Giordani[66a,66c], F. M. Giorgi[23b], P. F. Giraud[145], G. Giugliarelli[66a,66c], D. Giugni[68a], F. Giuli[73a,73b], S. Gkaitatzis[162], I. Gkialas[9,h], E. L. Gkougkousis[14], P. Gkountoumis[10], L. K. Gladilin[113], C. Glasman[98], J. Glatzer[14], P. C. F. Glaysher[46], A. Glazov[46], M. Goblirsch-Kolb[26], S. Goldfarb[104], T. Golling[54], D. Golubkov[123], A. Gomes[140a,140b], R. Goncalves Gama[53], R. Gonçalo[140a,140b], G. Gonella[52], L. Gonella[21], A. Gongadze[79], F. Gonnella[21], J. L. Gonski[59], S. González de la Hoz[174], S. Gonzalez-Sevilla[54], G. R. Gonzalvo Rodriguez[174], L. Goossens[36], P. A. Gorbounov[111], H. A. Gordon[29], B. Gorini[36], E. Gorini[67a,67b], A. Gorišek[91], A. T. Goshaw[49], M. I. Gostkin[79], C. A. Gottardo[24], M. Gouighri[35b], D. Goujdami[35c], A. G. Goussiou[148], N. Govender[33b,a], C. Goy[5], E. Gozani[160],

I. Grabowska-Bold[83a], E. C. Graham[90], J. Gramling[171], E. Gramstad[134], S. Grancagnolo[19], M. Grandi[156], V. Gratchev[138], P. M. Gravila[27f], F. G. Gravili[67a,67b], C. Gray[57], H. M. Gray[18], C. Grefe[24], K. Gregersen[96], I. M. Gregor[46], P. Grenier[153], K. Grevtsov[46], C. Grieco[14], N. A. Grieser[128], J. Griffiths[8], A. A. Grillo[146], K. Grimm[31,l], S. Grinstein[14,y], J.-F. Grivaz[132], S. Groh[99], E. Gross[180], J. Grosse-Knetter[53], Z. J. Grout[94], C. Grud[105], A. Grummer[118], L. Guan[105], W. Guan[181], J. Guenther[36], A. Guerguichon[132], J. G. R. Guerrero Rojas[174], F. Guescini[115], D. Guest[171], R. Gugel[52], T. Guillemin[5], S. Guindon[36], U. Gul[57], J. Guo[60c], W. Guo[105], Y. Guo[60a,t], Z. Guo[101], R. Gupta[46], S. Gurbuz[12c], G. Gustavino[128], P. Gutierrez[128], C. Gutschow[94], C. Guyot[145], M. P. Guzik[83a], C. Gwenlan[135], C. B. Gwilliam[90], A. Haas[124], C. Haber[18], H. K. Hadavand[8], N. Haddad[35e], A. Hadef[60a], S. Hageböck[36], M. Hagihara[169], M. Haleem[177], J. Haley[129], G. Halladjian[106], G. D. Hallewell[101], K. Hamacher[182], P. Hamal[130], K. Hamano[176], H. Hamdaoui[35e], G. N. Hamity[149], K. Han[60a,al], L. Han[60a], S. Han[15a,15d], K. Hanagaki[81,w], M. Hance[146], D. M. Handl[114], B. Haney[137], R. Hankache[136], E. Hansen[96], J. B. Hansen[40], J. D. Hansen[40], M. C. Hansen[24], P. H. Hansen[40], E. C. Hanson[100], K. Hara[169], A. S. Hard[181], T. Harenberg[182], S. Harkusha[107], P. F. Harrison[178], N. M. Hartmann[114], Y. Hasegawa[150], A. Hasib[50], S. Hassani[145], S. Haug[20], R. Hauser[106], L. B. Havener[39], M. Havranek[142], C. M. Hawkes[21], R. J. Hawkings[36], D. Hayden[106], C. Hayes[155], R. L. Hayes[175], C. P. Hays[135], J. M. Hays[92], H. S. Hayward[90], S. J. Haywood[144], F. He[60a], M. P. Heath[50], V. Hedberg[96], L. Heelan[8], S. Heer[24], K. K. Heidegger[52], W. D. Heidorn[78], J. Heilman[34], S. Heim[46], T. Heim[18], B. Heinemann[46,at], J. J. Heinrich[131], L. Heinrich[36], C. Heinz[56], J. Hejbal[141], L. Helary[61b], A. Held[175], S. Hellesund[134], C. M. Helling[146], S. Hellman[45a,45b], C. Helsens[36], R. C. W. Henderson[89], Y. Heng[181], S. Henkelmann[175], A. M. Henriques Correia[36], G. H. Herbert[19], H. Herde[26], V. Herget[177], Y. Hernández Jiménez[33c], H. Herr[99], M. G. Herrmann[114], T. Herrmann[48], G. Herten[52], R. Hertenberger[114], L. Hervas[36], T. C. Herwig[137], G. G. Hesketh[94], N. P. Hessey[168a], A. Higashida[163], S. Higashino[81], E. Higón-Rodriguez[174], K. Hildebrand[37], E. Hill[176], J. C. Hill[32], K. K. Hill[29], K. H. Hiller[46], S. J. Hillier[21], M. Hils[48], I. Hinchliffe[18], F. Hinterkeuser[24], M. Hirose[133], S. Hirose[52], D. Hirschbuehl[182], B. Hiti[91], O. Hladik[141], D. R. Hlaluku[33c], X. Hoad[50], J. Hobbs[155], N. Hod[180], M. C. Hodgkinson[149], A. Hoecker[36], F. Hoenig[114], D. Hohn[52], D. Hohov[132], T. R. Holmes[37], M. Holzbock[114], L.B.A.H Hommels[32], S. Honda[169], T. Honda[81], T. M. Hong[139], A. Hönle[115], B. H. Hooberman[173], W. H. Hopkins[6], Y. Horii[117], P. Horn[48], L. A. Horyn[37], J-Y. Hostachy[58], A. Hostiuc[148], S. Hou[158], A. Hoummada[35a], J. Howarth[100], J. Hoya[88], M. Hrabovsky[130], J. Hrdinka[76], I. Hristova[19], J. Hrivnac[132], A. Hrynevich[108], T. Hryn'ova[5], P. J. Hsu[64], S.-C. Hsu[148], Q. Hu[29], S. Hu[60c], Y. Huang[15a], Z. Hubacek[142], F. Hubaut[101], M. Huebner[24], F. Huegging[24], T. B. Huffman[135], M. Huhtinen[36], R. F. H. Hunter[34], P. Huo[155], A. M. Hupe[34], N. Huseynov[79,ag], J. Huston[106], J. Huth[59], R. Hyneman[105], S. Hyrych[28a], G. Iacobucci[54], G. Iakovidis[29], I. Ibragimov[151], L. Iconomidou-Fayard[132], Z. Idrissi[35e], P. I. Iengo[36], R. Ignazzi[40], O. Igonkina[120,aa,*], R. Iguchi[163], T. Iizawa[54], Y. Ikegami[81], M. Ikeno[81], D. Iliadis[162], N. Ilic[119], F. Iltzsche[48], G. Introzzi[70a,70b], M. Iodice[74a], K. Iordanidou[168a], V. Ippolito[72a,72b], M. F. Isacson[172], M. Ishino[163], M. Ishitsuka[165], W. Islam[129], C. Issever[135], S. Istin[160], F. Ito[169], J. M. Iturbe Ponce[63a], R. Iuppa[75a,75b], A. Ivina[180], H. Iwasaki[81], J. M. Izen[43], V. Izzo[69a], P. Jacka[141], P. Jackson[1], R. M. Jacobs[24], B. P. Jaeger[152], V. Jain[2], G. Jäkel[182], K. B. Jakobi[99], K. Jakobs[52], S. Jakobsen[76], T. Jakoubek[141], J. Jamieson[57], K. W. Janas[83a], R. Jansky[54], J. Janssen[24], M. Janus[53], P. A. Janus[83a], G. Jarlskog[96], N. Javadov[79,ag], T. Javůrek[36], M. Javurkova[52], F. Jeanneau[145], L. Jeanty[131], J. Jejelava[159a,ah], A. Jelinskas[178], P. Jenni[52,b], J. Jeong[46], N. Jeong[46], S. Jézéquel[5], H. Ji[181], J. Jia[155], H. Jiang[78], Y. Jiang[60a], Z. Jiang[153,q], S. Jiggins[52], F. A. Jimenez Morales[38], J. Jimenez Pena[174], S. Jin[15c], A. Jinaru[27b], O. Jinnouchi[165], H. Jivan[33c], P. Johansson[149], K. A. Johns[7], C. A. Johnson[65], K. Jon-And[45a,45b], R. W. L. Jones[89], S. D. Jones[156], S. Jones[7], T. J. Jones[90], J. Jongmanns[61a], P. M. Jorge[140a], J. Jovicevic[36], X. Ju[18], J. J. Junggeburth[115], A. Juste Rozas[14,y], A. Kaczmarska[84], M. Kado[72a,72b], H. Kagan[126], M. Kagan[153], C. Kahra[99], T. Kaji[179], E. Kajomovitz[160], C. W. Kalderon[96], A. Kaluza[99], A. Kamenshchikov[123], L. Kanjir[91], Y. Kano[163], V. A. Kantserov[112], J. Kanzaki[81], L. S. Kaplan[181], D. Kar[33c], M. J. Kareem[168b], E. Karentzos[10], S. N. Karpov[79], Z. M. Karpova[79], V. Kartvelishvili[89], A. N. Karyukhin[123], L. Kashif[181], R. D. Kass[126], A. Kastanas[45a,45b], Y. Kataoka[163], C. Kato[60c,60d], J. Katzy[46], K. Kawade[82], K. Kawagoe[87], T. Kawaguchi[117], T. Kawamoto[163], G. Kawamura[53], E. F. Kay[176], V. F. Kazanin[122a,122b], R. Keeler[176], R. Kehoe[42], J. S. Keller[34], E. Kellermann[96], D. Kelsey[156], J. J. Kempster[21], J. Kendrick[21], O. Kepka[141], S. Kersten[182], B. P. Kerševan[91], S. Ketabchi Haghighat[167], M. Khader[173], F. Khalil-Zada[13], M. Khandoga[145], A. Khanov[129], A. G. Kharlamov[122a,122b], T. Kharlamova[122a,122b], E. E. Khoda[175], A. Khodinov[166], T. J. Khoo[54], E. Khramov[79], J. Khubua[159b], S. Kido[82], M. Kiehn[54], C. R. Kilby[93], Y. K. Kim[37], N. Kimura[66a,66c], O. M. Kind[19], B. T. King[90,*], D. Kirchmeier[48], J. Kirk[144], A. E. Kiryunin[115], T. Kishimoto[163], D. P. Kisliuk[167], V. Kitali[46], O. Kivernyk[5], E. Kladiva[28b,*], T. Klapdor-Kleingrothaus[52], M. Klassen[61a], M. H. Klein[105], M. Klein[90], U. Klein[90], K. Kleinknecht[99], P. Klimek[121], A. Klimentov[29], T. Klingl[24], T. Klioutchnikova[36], F. F. Klitzner[114], P. Kluit[120], S. Kluth[115], E. Kneringer[76], E. B. F. G. Knoops[101], A. Knue[52], D. Kobayashi[87], T. Kobayashi[163], M. Kobel[48], M. Kocian[153], P. Kodys[143], P. T. Koenig[24], T. Koffas[34], N. M. Köhler[115], T. Koi[153], M. Kolb[61b], I. Koletsou[5], T. Komarek[130], T. Kondo[81], N. Kondrashova[60c], K. Köneke[52], A. C. König[119], T. Kono[125], R. Konoplich[124,ao], V. Konstantinides[94],

N. Konstantinidis[94], B. Konya[96], R. Kopeliansky[65], S. Koperny[83a], K. Korcyl[84], K. Kordas[162], G. Koren[161], A. Korn[94], I. Korolkov[14], E. V. Korolkova[149], N. Korotkova[113], O. Kortner[115], S. Kortner[115], T. Kosek[143], V. V. Kostyukhin[24], A. Kotwal[49], A. Koulouris[10], A. Kourkoumeli-Charalampidi[70a,70b], C. Kourkoumelis[9], E. Kourlitis[149], V. Kouskoura[29], A. B. Kowalewska[84], R. Kowalewski[176], C. Kozakai[163], W. Kozanecki[145], A. S. Kozhin[123], V. A. Kramarenko[113], G. Kramberger[91], D. Krasnopevtsev[60a], M. W. Krasny[136], A. Krasznahorkay[36], D. Krauss[115], J. A. Kremer[83a], J. Kretzschmar[90], P. Krieger[167], F. Krieter[114], A. Krishnan[61b], K. Krizka[18], K. Kroeninger[47], H. Kroha[115], J. Kroll[141], J. Kroll[137], J. Krstic[16], U. Kruchonak[79], H. Krüger[24], N. Krumnack[78], M. C. Kruse[49], J. A. Krzysiak[84], T. Kubota[104], O. Kuchinskaia[166], S. Kuday[4b], J. T. Kuechler[46], S. Kuehn[36], A. Kugel[61a], T. Kuhl[46], V. Kukhtin[79], R. Kukla[101], Y. Kulchitsky[107,ak], S. Kuleshov[147b], Y. P. Kulinich[173], M. Kuna[58], T. Kunigo[85], A. Kupco[141], T. Kupfer[47], O. Kuprash[52], H. Kurashige[82], L. L. Kurchaninov[168a], Y. A. Kurochkin[107], A. Kurova[112], M. G. Kurth[15a,15d], E. S. Kuwertz[36], M. Kuze[165], A. K. Kvam[148], J. Kvita[130], T. Kwan[103], A. La Rosa[115], L. La Rotonda[41a,41b], F. La Ruffa[41a,41b], C. Lacasta[174], F. Lacava[72a,72b], D. P. J. Lack[100], H. Lacker[19], D. Lacour[136], E. Ladygin[79], R. Lafaye[5], B. Laforge[136], T. Lagouri[33c], S. Lai[53], S. Lammers[65], W. Lampl[7], C. Lampoudis[162], E. Lançon[29], U. Landgraf[52], M. P. J. Landon[92], M. C. Lanfermann[54], V. S. Lang[46], J. C. Lange[53], R. J. Langenberg[36], A. J. Lankford[171], F. Lanni[29], K. Lantzsch[24], A. Lanza[70a], A. Lapertosa[55a,55b], S. Laplace[136], J. F. Laporte[145], T. Lari[68a], F. Lasagni Manghi[23a,23b], M. Lassnig[36], T. S. Lau[63a], A. Laudrain[132], A. Laurier[34], M. Lavorgna[69a,69b], M. Lazzaroni[68a,68b], B. Le[104], E. Le Guirriec[101], M. LeBlanc[7], T. LeCompte[6], F. Ledroit-Guillon[58], C. A. Lee[29], G. R. Lee[17], L. Lee[59], S. C. Lee[158], S. J. Lee[34], B. Lefebvre[168a], M. Lefebvre[176], F. Legger[114], C. Leggett[18], K. Lehmann[152], N. Lehmann[182], G. Lehmann Miotto[36], W. A. Leight[46], A. Leisos[162,x], M. A. L. Leite[80d], C. E. Leitgeb[114], R. Leitner[143], D. Lellouch[180,*], K. J. C. Leney[42], T. Lenz[24], B. Lenzi[36], R. Leone[7], S. Leone[71a], C. Leonidopoulos[50], A. Leopold[136], G. Lerner[156], C. Leroy[109], R. Les[167], C. G. Lester[32], M. Levchenko[138], J. Levêque[5], D. Levin[105], L. J. Levinson[180], D. J. Lewis[21], B. Li[15b], B. Li[105], C-Q. Li[60a], F. Li[60c], H. Li[60a], H. Li[60b], J. Li[60c], K. Li[153], L. Li[60c], M. Li[15a], Q. Li[15a,15d], Q. Y. Li[60a], S. Li[60c,60d], X. Li[46], Y. Li[46], Z. Li[60b], Z. Liang[15a], B. Liberti[73a], A. Liblong[167], K. Lie[63c], S. Liem[120], C. Y. Lin[32], K. Lin[106], T. H. Lin[99], R. A. Linck[65], J. H. Lindon[21], A. L. Lionti[54], E. Lipeles[137], A. Lipniacka[17], M. Lisovyi[61b], T. M. Liss[173,av], A. Lister[175], A. M. Litke[146], J. D. Little[8], B. Liu[78,ad], B. L. Liu[6], H. B. Liu[29], H. Liu[105], J. B. Liu[60a], J. K. K. Liu[135], K. Liu[136], M. Liu[60a], P. Liu[18], Y. Liu[15a,15d], Y. L. Liu[105], Y. W. Liu[60a], M. Livan[70a,70b], A. Lleres[58], J. Llorente Merino[15a], S. L. Lloyd[92], C. Y. Lo[63b], F. Lo Sterzo[42], E. M. Lobodzinska[46], P. Loch[7], S. Loffredo[73a,73b], T. Lohse[19], K. Lohwasser[149], M. Lokajicek[141], J. D. Long[173], R. E. Long[89], L. Longo[36], K. A. Looper[126], J. A. Lopez[147b], I. Lopez Paz[100], A. Lopez Solis[149], J. Lorenz[114], N. Lorenzo Martinez[5], M. Losada[22], P. J. Lösel[114], A. Lösle[52], X. Lou[46], X. Lou[15a], A. Lounis[132], J. Love[6], P. A. Love[89], J. J. Lozano Bahilo[174], M. Lu[60a], Y. J. Lu[64], H. J. Lubatti[148], C. Luci[72a,72b], A. Lucotte[58], C. Luedtke[52], F. Luehring[65], I. Luise[136], L. Luminari[72a], B. Lund-Jensen[154], M. S. Lutz[102], D. Lynn[29], R. Lysak[141], E. Lytken[96], F. Lyu[15a], V. Lyubushkin[79], T. Lyubushkina[79], H. Ma[29], L. L. Ma[60b], Y. Ma[60b], G. Maccarrone[51], A. Macchiolo[115], C. M. Macdonald[149], J. Machado Miguens[137], D. Madaffari[174], R. Madar[38], W. F. Mader[48], N. Madysa[48], J. Maeda[82], K. Maekawa[163], S. Maeland[17], T. Maeno[29], M. Maerker[48], A. S. Maevskiy[113], V. Magerl[52], N. Magini[78], D. J. Mahon[39], C. Maidantchik[80b], T. Maier[114], A. Maio[140a,140b,140d], O. Majersky[28a], S. Majewski[131], Y. Makida[81], N. Makovec[132], B. Malaescu[136], Pa. Malecki[84], V. P. Maleev[138], F. Malek[58], U. Mallik[77], D. Malon[6], C. Malone[32], S. Maltezos[10], S. Malyukov[36], J. Mamuzic[174], G. Mancini[51], I. Mandić[91], L. Manhaes de Andrade Filho[80a], I. M. Maniatis[162], J. Manjarres Ramos[48], K. H. Mankinen[96], A. Mann[114], A. Manousos[76], B. Mansoulie[145], I. Manthos[162], S. Manzoni[120], A. Marantis[162], G. Marceca[30], L. Marchese[135], G. Marchiori[136], M. Marcisovsky[141], C. Marcon[96], C. A. Marin Tobon[36], M. Marjanovic[38], Z. Marshall[18], M.U.F Martensson[172], S. Marti-Garcia[174], C. B. Martin[126], T. A. Martin[178], V. J. Martin[50], B. Martin dit Latour[17], L. Martinelli[74a,74b], M. Martinez[14,y], V. I. Martinez Outschoorn[102], S. Martin-Haugh[144], V. S. Martoiu[27b], A. C. Martyniuk[94], A. Marzin[36], S. R. Maschek[115], L. Masetti[99], T. Mashimo[163], R. Mashinistov[110], J. Masik[100], A. L. Maslennikov[122a,122b], L. H. Mason[104], L. Massa[73a,73b], P. Massarotti[69a,69b], P. Mastrandrea[71a,71b], A. Mastroberardino[41a,41b], T. Masubuchi[163], A. Matic[114], P. Mättig[24], J. Maurer[27b], B. Maček[91], D. A. Maximov[122a,122b], R. Mazini[158], I. Maznas[162], S. M. Mazza[146], S. P. Mc Kee[105], T. G. McCarthy[115], L. I. McClymont[94], W. P. McCormack[18], E. F. McDonald[104], J. A. Mcfayden[36], M. A. McKay[42], K. D. McLean[176], S. J. McMahon[144], P. C. McNamara[104], C. J. McNicol[178], R. A. McPherson[176,ae], J. E. Mdhluli[33c], Z. A. Meadows[102], S. Meehan[148], T. Megy[52], S. Mehlhase[114], A. Mehta[90], T. Meideck[58], B. Meirose[43], D. Melini[174], B. R. Mellado Garcia[33c], J. D. Mellenthin[53], M. Melo[28a], F. Meloni[46], A. Melzer[24], S. B. Menary[100], E. D. Mendes Gouveia[140a,140e], L. Meng[36], X. T. Meng[105], S. Menke[115], E. Meoni[41a,41b], S. Mergelmeyer[19], S. A. M. Merkt[139], C. Merlassino[20], P. Mermod[54], L. Merola[69a,69b], C. Meroni[68a], O. Meshkov[110,113], J. K. R. Meshreki[151], A. Messina[72a,72b], J. Metcalfe[6], A. S. Mete[171], C. Meyer[65], J. Meyer[160], J-P. Meyer[145], H. Meyer Zu Theenhausen[61a], F. Miano[156], M. Michetti[19], R. P. Middleton[144], L. Mijović[50], G. Mikenberg[180], M. Mikestikova[141], M. Mikuž[91], H. Mildner[149], M. Milesi[104], A. Milic[167], D. A. Millar[92], D. W. Miller[37], A. Milov[180],

D. A. Milstead[45a,45b], R. A. Mina[153,q], A. A. Minaenko[123], M. Miñano Moya[174], I. A. Minashvili[159b], A. I. Mincer[124], B. Mindur[83a], M. Mineev[79], Y. Minegishi[163], Y. Ming[181], L. M. Mir[14], A. Mirto[67a,67b], K. P. Mistry[137], T. Mitani[179], J. Mitrevski[114], V. A. Mitsou[174], M. Mittal[60c], A. Miucci[20], P. S. Miyagawa[149], A. Mizukami[81], J. U. Mjörnmark[96], T. Mkrtchyan[184], M. Mlynarikova[143], T. Moa[45a,45b], K. Mochizuki[109], P. Mogg[52], S. Mohapatra[39], R. Moles-Valls[24], M. C. Mondragon[106], K. Mönig[46], J. Monk[40], E. Monnier[101], A. Montalbano[152], J. Montejo Berlingen[36], M. Montella[94], F. Monticelli[88], S. Monzani[68a], N. Morange[132], D. Moreno[22], M. Moreno Llácer[36], C. Moreno Martinez[14], P. Morettini[55b], M. Morgenstern[120], S. Morgenstern[48], D. Mori[152], M. Morii[59], M. Morinaga[179], V. Morisbak[134], A. K. Morley[36], G. Mornacchi[36], A. P. Morris[94], L. Morvaj[155], P. Moschovakos[36], B. Moser[120], M. Mosidze[159b], T. Moskalets[145], H. J. Moss[149], J. Moss[31,n], K. Motohashi[165], E. Mountricha[36], E. J. W. Moyse[102], S. Muanza[101], J. Mueller[139], R. S. P. Mueller[114], D. Muenstermann[89], G. A. Mullier[96], J. L. Munoz Martinez[14], F. J. Munoz Sanchez[100], P. Murin[28b], W. J. Murray[144,178], A. Murrone[68a,68b], M. Muškinja[18], C. Mwewa[33a], A. G. Myagkov[123,ap], J. Myers[131], M. Myska[142], B. P. Nachman[18], O. Nackenhorst[47], A.Nag Nag[48], K. Nagai[135], K. Nagano[81], Y. Nagasaka[62], M. Nagel[52], E. Nagy[101], A. M. Nairz[36], Y. Nakahama[117], K. Nakamura[81], T. Nakamura[163], I. Nakano[127], H. Nanjo[133], F. Napolitano[61a], R. F. Naranjo Garcia[46], R. Narayan[42], D. I. Narrias Villar[61a], I. Naryshkin[138], T. Naumann[46], G. Navarro[22], H. A. Neal[105,*], P. Y. Nechaeva[110], F. Nechansky[46], T. J. Neep[21], A. Negri[70a,70b], M. Negrini[23b], C. Nellist[53], M. E. Nelson[135], S. Nemecek[141], P. Nemethy[124], M. Nessi[36,d], M. S. Neubauer[173], M. Neumann[182], P. R. Newman[21], Y. S. Ng[19], Y. W. Y. Ng[171], H. D. N. Nguyen[101], T. Nguyen Manh[109], E. Nibigira[38], R. B. Nickerson[135], R. Nicolaidou[145], D. S. Nielsen[40], J. Nielsen[146], N. Nikiforou[11], V. Nikolaenko[123,ap], I. Nikolic-Audit[136], K. Nikolopoulos[21], P. Nilsson[29], H. R. Nindhito[54], Y. Ninomiya[81], A. Nisati[72a], N. Nishu[60c], R. Nisius[115], I. Nitsche[47], T. Nitta[179], T. Nobe[163], Y. Noguchi[85], I. Nomidis[136], M. A. Nomura[29], M. Nordberg[36], N. Norjoharuddeen[135], T. Novak[91], O. Novgorodova[48], R. Novotny[142], L. Nozka[130], K. Ntekas[171], E. Nurse[94], F. G. Oakham[34,ay], H. Oberlack[115], J. Ocariz[136], A. Ochi[82], I. Ochoa[39], J. P. Ochoa-Ricoux[147a], K. O'Connor[26], S. Oda[87], S. Odaka[81], S. Oerdek[53], A. Ogrodnik[83a], A. Oh[100], S. H. Oh[49], C. C. Ohm[154], H. Oide[55a,55b], M. L. Ojeda[167], H. Okawa[169], Y. Okazaki[85], Y. Okumura[163], T. Okuyama[81], A. Olariu[27b], L. F. Oleiro Seabra[140a], S. A. Olivares Pino[147a], D. Oliveira Damazio[29], J. L. Oliver[1], M. J. R. Olsson[171], A. Olszewski[84], J. Olszowska[84], D. C. O'Neil[152], A. Onofre[140a,140e], K. Onogi[117], P. U. E. Onyisi[11], H. Oppen[134], M. J. Oreglia[37], G. E. Orellana[88], D. Orestano[74a,74b], N. Orlando[14], R. S. Orr[167], V. O'Shea[57], R. Ospanov[60a], G. Otero y Garzon[30], H. Otono[87], M. Ouchrif[35d], J. Ouellette[29], F. Ould-Saada[134], A. Ouraou[145], Q. Ouyang[15a], M. Owen[57], R. E. Owen[21], V. E. Ozcan[12c], N. Ozturk[8], J. Pacalt[130], H. A. Pacey[32], K. Pachal[49], A. Pacheco Pages[14], C. Padilla Aranda[14], S. Pagan Griso[18], M. Paganini[183], G. Palacino[65], S. Palazzo[50], S. Palestini[36], M. Palka[83b], D. Pallin[38], I. Panagoulias[10], C. E. Pandini[36], J. G. Panduro Vazquez[93], P. Pani[46], G. Panizzo[66a,66c], L. Paolozzi[54], C. Papadatos[109], K. Papageorgiou[9,h], A. Paramonov[6], D. Paredes Hernandez[63b], S. R. Paredes Saenz[135], B. Parida[166], T. H. Park[167], A. J. Parker[89], M. A. Parker[32], F. Parodi[55a,55b], E. W. P. Parrish[121], J. A. Parsons[39], U. Parzefall[52], L. Pascual Dominguez[136], V. R. Pascuzzi[167], J. M. P. Pasner[146], E. Pasqualucci[72a], S. Passaggio[55b], F. Pastore[93], P. Pasuwan[45a,45b], S. Pataraia[99], J. R. Pater[100], A. Pathak[181], T. Pauly[36], B. Pearson[115], M. Pedersen[134], L. Pedraza Diaz[119], R. Pedro[140a], T. Peiffer[53], S. V. Peleganchuk[122a,122b], O. Penc[141], H. Peng[60a], B. S. Peralva[80a], M. M. Perego[132], A. P. Pereira Peixoto[140a], D. V. Perepelitsa[29], F. Peri[19], L. Perini[68a,68b], H. Pernegger[36], S. Perrella[69a,69b], K. Peters[46], R. F. Y. Peters[100], B. A. Petersen[36], T. C. Petersen[40], E. Petit[101], A. Petridis[1], C. Petridou[162], P. Petroff[132], M. Petrov[135], F. Petrucci[74a,74b], M. Pettee[183], N. E. Pettersson[102], K. Petukhova[143], A. Peyaud[145], R. Pezoa[147b], L. Pezzotti[70a,70b], T. Pham[104], F. H. Phillips[106], P. W. Phillips[144], M. W. Phipps[173], G. Piacquadio[155], E. Pianori[18], A. Picazio[102], R. H. Pickles[100], R. Piegaia[30], D. Pietreanu[27b], J. E. Pilcher[37], A. D. Pilkington[100], M. Pinamonti[73a,73b], J. L. Pinfold[3], M. Pitt[180], L. Pizzimento[73a,73b], M.-A. Pleier[29], V. Pleskot[143], E. Plotnikova[79], D. Pluth[78], P. Podberezko[122a,122b], R. Poettgen[96], R. Poggi[54], L. Poggioli[132], I. Pogrebnyak[106], D. Pohl[24], I. Pokharel[53], G. Polesello[70a], A. Poley[18], A. Policicchio[72a,72b], R. Polifka[143], A. Polini[23b], C. S. Pollard[46], V. Polychronakos[29], D. Ponomarenko[112], L. Pontecorvo[36], S. Popa[27a], G. A. Popeneciu[27d], D. M. Portillo Quintero[58], S. Pospisil[142], K. Potamianos[46], I. N. Potrap[79], C. J. Potter[32], H. Potti[11], T. Poulsen[96], J. Poveda[36], T. D. Powell[149], G. Pownall[46], M. E. Pozo Astigarraga[36], P. Pralavorio[101], S. Prell[78], D. Price[100], M. Primavera[67a], S. Prince[103], M. L. Proffitt[148], N. Proklova[112], K. Prokofiev[63c], F. Prokoshin[79], S. Protopopescu[29], J. Proudfoot[6], M. Przybycien[83a], D. Pudzha[138], A. Puri[173], P. Puzo[132], J. Qian[105], Y. Qin[100], A. Quadt[53], M. Queitsch-Maitland[46], A. Qureshi[1], P. Rados[104], F. Ragusa[68a,68b], G. Rahal[97], J. A. Raine[54], S. Rajagopalan[29], A. Ramirez Morales[92], K. Ran[15a,15d], T. Rashid[132], S. Raspopov[5], M. G. Ratti[68a,68b], D. M. Rauch[46], F. Rauscher[114], S. Rave[99], B. Ravina[149], I. Ravinovich[180], J. H. Rawling[100], M. Raymond[36], A. L. Read[134], N. P. Readioff[58], M. Reale[67a,67b], D. M. Rebuzzi[70a,70b], A. Redelbach[177], G. Redlinger[29], K. Reeves[43], L. Rehnisch[19], J. Reichert[137], D. Reikher[161], A. Reiss[99], A. Rej[151], C. Rembser[36], M. Renda[27b], M. Rescigno[72a], S. Resconi[68a], E. D. Resseguie[137], S. Rettie[175], E. Reynolds[21], O. L. Rezanova[122a,122b], P. Reznicek[143], E. Ricci[75a,75b], R. Richter[115], S. Richter[46],

E. Richter-Was[83b], O. Ricken[24], M. Ridel[136], P. Rieck[115], C. J. Riegel[182], O. Rifki[46], M. Rijssenbeek[155], A. Rimoldi[70a,70b], M. Rimoldi[46], L. Rinaldi[23b], G. Ripellino[154], B. Ristić[89], E. Ritsch[36], I. Riu[14], J. C. Rivera Vergara[176], F. Rizatdinova[129], E. Rizvi[92], C. Rizzi[36], R. T. Roberts[100], S. H. Robertson[103,ae], M. Robin[46], D. Robinson[32], J. E. M. Robinson[46], C. M. Robles Gajardo[147b], A. Robson[57], E. Rocco[99], C. Roda[71a,71b], S. Rodriguez Bosca[174], A. Rodriguez Perez[14], D. Rodriguez Rodriguez[174], A. M. Rodríguez Vera[168b], S. Roe[36], O. Røhne[134], R. Röhrig[115], C. P. A. Roland[65], J. Roloff[59], A. Romaniouk[112], M. Romano[23a,23b], N. Rompotis[90], M. Ronzani[124], L. Roos[136], S. Rosati[72a], K. Rosbach[52], G. Rosin[102], B. J. Rosser[137], E. Rossi[46], E. Rossi[74a,74b], E. Rossi[69a,69b], L. P. Rossi[55b], L. Rossini[68a,68b], R. Rosten[14], M. Rotaru[27b], J. Rothberg[148], D. Rousseau[132], G. Rovelli[70a,70b], A. Roy[11], D. Roy[33c], A. Rozanov[101], Y. Rozen[160], X. Ruan[33c], F. Rubbo[153], F. Rühr[52], A. Ruiz-Martinez[174], A. Rummler[36], Z. Rurikova[52], N. A. Rusakovich[79], H. L. Russell[103], L. Rustige[38,47], J. P. Rutherfoord[7], E. M. Rüttinger[46,k], Y. F. Ryabov[138], M. Rybar[39], G. Rybkin[132], A. Ryzhov[123], G. F. Rzehorz[53], P. Sabatini[53], G. Sabato[120], S. Sacerdoti[132], H.F-W. Sadrozinski[146], R. Sadykov[79], F. Safai Tehrani[72a], B. Safarzadeh Samani[156], P. Saha[121], S. Saha[103], M. Sahinsoy[61a], A. Sahu[182], M. Saimpert[46], M. Saito[163], T. Saito[163], H. Sakamoto[163], A. Sakharov[124,ao], D. Salamani[54], G. Salamanna[74a,74b], J. E. Salazar Loyola[147b], P. H. Sales De Bruin[172], A. Salnikov[153], J. Salt[174], D. Salvatore[41a,41b], F. Salvatore[156], A. Salvucci[63a,63b,63c], A. Salzburger[36], J. Samarati[36], D. Sammel[52], D. Sampsonidis[162], D. Sampsonidou[162], J. Sánchez[174], A. Sanchez Pineda[66a,66c], H. Sandaker[134], C. O. Sander[46], I. G. Sanderswood[89], M. Sandhoff[182], C. Sandoval[22], D. P. C. Sankey[144], M. Sannino[55a,55b], Y. Sano[117], A. Sansoni[51], C. Santoni[38], H. Santos[140a,140b], S. N. Santpur[18], A. Santra[174], A. Sapronov[79], J. G. Saraiva[140a,140d], O. Sasaki[81], K. Sato[169], E. Sauvan[5], P. Savard[167,ay], N. Savic[115], R. Sawada[163], C. Sawyer[144], L. Sawyer[95,am], C. Sbarra[23b], A. Sbrizzi[23a], T. Scanlon[94], J. Schaarschmidt[148], P. Schacht[115], B. M. Schachtner[114], D. Schaefer[37], L. Schaefer[137], J. Schaeffer[99], S. Schaepe[36], U. Schäfer[99], A. C. Schaffer[132], D. Schaile[114], R. D. Schamberger[155], N. Scharmberg[100], V. A. Schegelsky[138], D. Scheirich[143], F. Schenck[19], M. Schernau[171], C. Schiavi[55a,55b], S. Schier[146], L. K. Schildgen[24], Z. M. Schillaci[26], E. J. Schioppa[36], M. Schioppa[41a,41b], K. E. Schleicher[52], S. Schlenker[36], K. R. Schmidt-Sommerfeld[115], K. Schmieden[36], C. Schmitt[99], S. Schmitt[46], S. Schmitz[99], J. C. Schmoeckel[46], U. Schnoor[52], L. Schoeffel[145], A. Schoening[61b], P. G. Scholer[52], E. Schopf[135], M. Schott[99], J. F. P. Schouwenberg[119], J. Schovancova[36], S. Schramm[54], F. Schroeder[182], A. Schulte[99], H-C. Schultz-Coulon[61a], M. Schumacher[52], B. A. Schumm[146], Ph. Schune[145], A. Schwartzman[153], T. A. Schwarz[105], Ph. Schwemling[145], R. Schwienhorst[106], A. Sciandra[146], G. Sciolla[26], M. Scodeggio[46], M. Scornajenghi[41a,41b], F. Scuri[71a], F. Scutti[104], L. M. Scyboz[115], C. D. Sebastiani[72a,72b], P. Seema[19], S. C. Seidel[118], A. Seiden[146], T. Seiss[37], J. M. Seixas[80b], G. Sekhniaidze[69a], K. Sekhon[105], S. J. Sekula[42], N. Semprini-Cesari[23a,23b], S. Sen[49], S. Senkin[38], C. Serfon[76], L. Serin[132], L. Serkin[66a,66b], M. Sessa[60a], H. Severini[128], F. Sforza[170], A. Sfyrla[54], E. Shabalina[53], J. D. Shahinian[146], N. W. Shaikh[45a,45b], D. Shaked Renous[180], L. Y. Shan[15a], R. Shang[173], J. T. Shank[25], M. Shapiro[18], A. Sharma[135], A. S. Sharma[1], P. B. Shatalov[111], K. Shaw[156], S. M. Shaw[100], A. Shcherbakova[138], Y. Shen[128], N. Sherafati[34], A. D. Sherman[25], P. Sherwood[94], L. Shi[158,au], S. Shimizu[81], C. O. Shimmin[183], Y. Shimogama[179], M. Shimojima[116], I. P. J. Shipsey[135], S. Shirabe[87], M. Shiyakova[79,ab], J. Shlomi[180], A. Shmeleva[110], M. J. Shochet[37], J. Shojaii[104], D. R. Shope[128], S. Shrestha[126], E. M. Shrif[33c], E. Shulga[180], P. Sicho[141], A. M. Sickles[173], P. E. Sidebo[154], E. Sideras Haddad[33c], O. Sidiropoulou[36], A. Sidoti[23a,23b], F. Siegert[48], Dj. Sijacki[16], M. Silva Jr.[181], M. V. Silva Oliveira[80a], S. B. Silverstein[45a], S. Simion[132], E. Simioni[99], R. Simoniello[99], S. Simsek[12b], P. Sinervo[167], V. Sinetckii[110,113], N. B. Sinev[131], M. Sioli[23a,23b], I. Siral[105], S. Yu. Sivoklokov[113], J. Sjölin[45a,45b], E. Skorda[96], P. Skubic[128], M. Slawinska[84], K. Sliwa[170], R. Slovak[143], V. Smakhtin[180], B. H. Smart[144], J. Smiesko[28a], N. Smirnov[112], S. Yu. Smirnov[112], Y. Smirnov[112], L. N. Smirnova[113,u], O. Smirnova[96], J. W. Smith[53], M. Smizanska[89], K. Smolek[142], A. Smykiewicz[84], A. A. Snesarev[110], H. L. Snoek[120], I. M. Snyder[131], S. Snyder[29], R. Sobie[176,ae], A. M. Soffa[171], A. Soffer[161], A. Søgaard[50], F. Sohns[53], C. A. Solans Sanchez[36], E. Yu. Soldatov[112], U. Soldevila[174], A. A. Solodkov[123], A. Soloshenko[79], O. V. Solovyanov[123], V. Solovyev[138], P. Sommer[149], H. Son[170], W. Song[144], W. Y. Song[168b], A. Sopczak[142], F. Sopkova[28b], C. L. Sotiropoulou[71a,71b], S. Sottocornola[70a,70b], R. Soualah[66a,66c,g], A. M. Soukharev[122a,122b], D. South[46], S. Spagnolo[67a,67b], M. Spalla[115], M. Spangenberg[178], F. Spanò[93], D. Sperlich[52], T. M. Spieker[61a], R. Spighi[23b], G. Spigo[36], M. Spina[156], D. P. Spiteri[57], M. Spousta[143], A. Stabile[68a,68b], B. L. Stamas[121], R. Stamen[61a], M. Stamenkovic[120], E. Stanecka[84], R. W. Stanek[6], B. Stanislaus[135], M. M. Stanitzki[46], M. Stankaityte[135], B. Stapf[120], E. A. Starchenko[123], G. H. Stark[146], J. Stark[58], S. H. Stark[40], P. Staroba[141], P. Starovoitov[61a], S. Stärz[103], R. Staszewski[84], G. Stavropoulos[44], M. Stegler[46], P. Steinberg[29], A. L. Steinhebel[131], B. Stelzer[152], H. J. Stelzer[139], O. Stelzer-Chilton[168a], H. Stenzel[56], T. J. Stevenson[156], G. A. Stewart[36], M. C. Stockton[36], G. Stoicea[27b], M. Stolarski[140a], P. Stolte[53], S. Stonjek[115], A. Straessner[48], J. Strandberg[154], S. Strandberg[45a,45b], M. Strauss[128], P. Strizenec[28b], R. Ströhmer[177], D. M. Strom[131], R. Stroynowski[42], A. Strubig[50], S. A. Stucci[29], B. Stugu[17], J. Stupak[128], N. A. Styles[46], D. Su[153], S. Suchek[61a], V. V. Sulin[110], M. J. Sullivan[90], D. M. S. Sultan[54], S. Sultansoy[4c], T. Sumida[85], S. Sun[105], X. Sun[3], K. Suruliz[156], C. J. E. Suster[157], M. R. Sutton[156], S. Suzuki[81], M. Svatos[141], M. Swiatlowski[37], S. P. Swift[2],

T. Swirski[177], A. Sydorenko[99], I. Sykora[28a], M. Sykora[143], T. Sykora[143], D. Ta[99], K. Tackmann[46,z], J. Taenzer[161], A. Taffard[171], R. Tafirout[168a], H. Takai[29], R. Takashima[86], K. Takeda[82], T. Takeshita[150], E. P. Takeva[50], Y. Takubo[81], M. Talby[101], A. A. Talyshev[122a,122b], N. M. Tamir[161], J. Tanaka[163], M. Tanaka[165], R. Tanaka[132], S. Tapia Araya[173], S. Tapprogge[99], A. Tarek Abouelfadl Mohamed[136], S. Tarem[160], G. Tarna[27b,c], G. F. Tartarelli[68a], P. Tas[143], M. Tasevsky[141], T. Tashiro[85], E. Tassi[41a,41b], A. Tavares Delgado[140a,140b], Y. Tayalati[35e], A. J. Taylor[50], G. N. Taylor[104], W. Taylor[168b], A. S. Tee[89], R. Teixeira De Lima[153], P. Teixeira-Dias[93], H. Ten Kate[36], J. J. Teoh[120], S. Terada[81], K. Terashi[163], J. Terron[98], S. Terzo[14], M. Testa[51], R. J. Teuscher[167,ae], S. J. Thais[183], T. Theveneaux-Pelzer[46], F. Thiele[40], D. W. Thomas[93], J. O. Thomas[42], J. P. Thomas[21], A. S. Thompson[57], P. D. Thompson[21], L. A. Thomsen[183], E. Thomson[137], Y. Tian[39], R. E. Ticse Torres[53], V. O. Tikhomirov[110,aq], Yu. A. Tikhonov[122a,122b], S. Timoshenko[112], P. Tipton[183], S. Tisserant[101], K. Todome[23a,23b], S. Todorova-Nova[5], S. Todt[48], J. Tojo[87], S. Tokár[28a], K. Tokushuku[81], E. Tolley[126], K. G. Tomiwa[33c], M. Tomoto[117], L. Tompkins[153,q], K. Toms[118], B. Tong[59], P. Tornambe[102], E. Torrence[131], H. Torres[48], E. Torró Pastor[148], C. Tosciri[135], J. Toth[101,ac], D. R. Tovey[149], A. Traeet[17], C. J. Treado[124], T. Trefzger[177], F. Tresoldi[156], A. Tricoli[29], I. M. Trigger[168a], S. Trincaz-Duvoid[136], W. Trischuk[167], B. Trocmé[58], A. Trofymov[132], C. Troncon[68a], M. Trovatelli[176], F. Trovato[156], L. Truong[33b], M. Trzebinski[84], A. Trzupek[84], F. Tsai[46], J.C-L. Tseng[135], P. V. Tsiareshka[107,ak], A. Tsirigotis[162], N. Tsirintanis[9], V. Tsiskaridze[155], E. G. Tskhadadze[159a], M. Tsopoulou[162], I. I. Tsukerman[111], V. Tsulaia[18], S. Tsuno[81], D. Tsybychev[155], Y. Tu[63b], A. Tudorache[27b], V. Tudorache[27b], T. T. Tulbure[27a], A. N. Tuna[59], S. Turchikhin[79], D. Turgeman[180], I. Turk Cakir[4b,v], R. J. Turner[21], R. T. Turra[68a], P. M. Tuts[39], S Tzamarias[162], E. Tzovara[99], G. Ucchielli[47], K. Uchida[163], I. Ueda[81], M. Ughetto[45a,45b], F. Ukegawa[169], G. Unal[36], A. Undrus[29], G. Unel[171], F. C. Ungaro[104], Y. Unno[81], K. Uno[163], J. Urban[28b], P. Urquijo[104], G. Usai[8], J. Usui[81], Z. Uysal[12d], L. Vacavant[101], V. Vacek[142], B. Vachon[103], K. O. H. Vadla[134], A. Vaidya[94], C. Valderanis[114], E. Valdes Santurio[45a,45b], M. Valente[54], S. Valentinetti[23a,23b], A. Valero[174], L. Valéry[46], R. A. Vallance[21], A. Vallier[36], J. A. Valls Ferrer[174], T. R. Van Daalen[14], P. Van Gemmeren[6], I. Van Vulpen[120], M. Vanadia[73a,73b], W. Vandelli[36], A. Vaniachine[166], D. Vannicola[72a,72b], R. Vari[72a], E. W. Varnes[7], C. Varni[55a,55b], T. Varol[42], D. Varouchas[132], K. E. Varvell[157], M. E. Vasile[27b], G. A. Vasquez[176], J. G. Vasquez[183], F. Vazeille[38], D. Vazquez Furelos[14], T. Vazquez Schroeder[36], J. Veatch[53], V. Vecchio[74a,74b], M. J. Veen[120], L. M. Veloce[167], F. Veloso[140a,140c], S. Veneziano[72a], A. Ventura[67a,67b], N. Venturi[36], A. Verbytskyi[115], V. Vercesi[70a], M. Verducci[74a,74b], C. M. Vergel Infante[78], C. Vergis[24], W. Verkerke[120], A. T. Vermeulen[120], J. C. Vermeulen[120], M. C. Vetterli[152,ay], N. Viaux Maira[147b], M. Vicente Barreto Pinto[54], T. Vickey[149], O. E. Vickey Boeriu[149], G. H. A. Viehhauser[135], L. Vigani[135], M. Villa[23a,23b], M. Villaplana Perez[68a,68b], E. Vilucchi[51], M. G. Vincter[34], V. B. Vinogradov[79], A. Vishwakarma[46], C. Vittori[23a,23b], I. Vivarelli[156], M. Vogel[182], P. Vokac[142], S. E. von Buddenbrock[33c], E. Von Toerne[24], V. Vorobel[143], K. Vorobev[112], M. Vos[174], J. H. Vossebeld[90], M. Vozak[100], N. Vranjes[16], M. Vranjes Milosavljevic[16], V. Vrba[142], M. Vreeswijk[120], T. Šfiligoj[91], R. Vuillermet[36], I. Vukotic[37], T. Ženiš[28a], L. Živković[16], P. Wagner[24], W. Wagner[182], J. Wagner-Kuhr[114], S. Wahdan[182], H. Wahlberg[88], K. Wakamiya[82], V. M. Walbrecht[115], J. Walder[89], R. Walker[114], S. D. Walker[93], W. Walkowiak[151], V. Wallangen[45a,45b], A. M. Wang[59], C. Wang[60b], F. Wang[181], H. Wang[18], H. Wang[3], J. Wang[157], J. Wang[61b], P. Wang[42], Q. Wang[128], R.-J. Wang[99], R. Wang[60a], R. Wang[6], S. M. Wang[158], W. T. Wang[60a], W. Wang[15c,af], W. X. Wang[60a,af], Y. Wang[60a,an], Z. Wang[60c], C. Wanotayaroj[46], A. Warburton[103], C. P. Ward[32], D. R. Wardrope[94], N. Warrack[57], A. Washbrook[50], A. T. Watson[21], M. F. Watson[21], G. Watts[148], B. M. Waugh[94], A. F. Webb[11], S. Webb[99], C. Weber[183], M. S. Weber[20], S. A. Weber[34], S. M. Weber[61a], A. R. Weidberg[135], J. Weingarten[47], M. Weirich[99], C. Weiser[52], P. S. Wells[36], T. Wenaus[29], T. Wengler[36], S. Wenig[36], N. Wermes[24], M. D. Werner[78], M. Wessels[61a], T. D. Weston[20], K. Whalen[131], N. L. Whallon[148], A. M. Wharton[89], A. S. White[105], A. White[8], M. J. White[1], D. Whiteson[171], B. W. Whitmore[89], F. J. Wickens[144], W. Wiedenmann[181], M. Wielers[144], N. Wieseotte[99], C. Wiglesworth[40], L. A. M. Wiik-Fuchs[52], F. Wilk[100], H. G. Wilkens[36], L. J. Wilkins[93], H. H. Williams[137], S. Williams[32], C. Willis[106], S. Willocq[102], J. A. Wilson[21], I. Wingerter-Seez[5], E. Winkels[156], F. Winklmeier[131], O. J. Winston[156], B. T. Winter[52], M. Wittgen[153], M. Wobisch[95], A. Wolf[99], T. M. H. Wolf[120], R. Wolff[101], R. W. Wölker[135], J. Wollrath[52], M. W. Wolter[84], H. Wolters[140a,140c], V. W. S. Wong[175], N. L. Woods[146], S. D. Worm[21], B. K. Wosiek[84], K. W. Woźniak[84], K. Wraight[57], S. L. Wu[181], X. Wu[54], Y. Wu[60a], T. R. Wyatt[100], B. M. Wynne[50], S. Xella[40], Z. Xi[105], L. Xia[178], D. Xu[15a], H. Xu[60a,c], L. Xu[29], T. Xu[145], W. Xu[105], Z. Xu[60b], Z. Xu[153], B. Yabsley[157], S. Yacoob[33a], K. Yajima[133], D. P. Yallup[94], D. Yamaguchi[165], Y. Yamaguchi[165], A. Yamamoto[81], T. Yamanaka[163], F. Yamane[82], M. Yamatani[163], T. Yamazaki[163], Y. Yamazaki[82], Z. Yan[25], H. J. Yang[60c,60d], H. T. Yang[18], S. Yang[77], X. Yang[58,60b], Y. Yang[163], W-M. Yao[18], Y. C. Yap[46], Y. Yasu[81], E. Yatsenko[60c,60d], J. Ye[42], S. Ye[29], I. Yeletskikh[79], M. R. Yexley[89], E. Yigitbasi[25], K. Yorita[179], K. Yoshihara[137], C. J. S. Young[36], C. Young[153], J. Yu[78], R. Yuan[60b,i], X. Yue[61a], S. P. Y. Yuen[24], B. Zabinski[84], G. Zacharis[10], E. Zaffaroni[54], J. Zahreddine[136], A. M. Zaitsev[123,ap], T. Zakareishvili[159b], N. Zakharchuk[34], S. Zambito[59], D. Zanzi[36], D. R. Zaripovas[57], S. V. Zeißner[47], C. Zeitnitz[182], G. Zemaityte[135], J. C. Zeng[173], O. Zenin[123], D. Zerwas[132], M. Zgubič[135], D. F. Zhang[15b], F. Zhang[181], G. Zhang[60a],

G. Zhang[15b], H. Zhang[15c], J. Zhang[6], L. Zhang[15c], L. Zhang[60a], M. Zhang[173], R. Zhang[60a], R. Zhang[24], X. Zhang[60b], Y. Zhang[15a,15d], Z. Zhang[63a], Z. Zhang[132], P. Zhao[49], Y. Zhao[60b], Z. Zhao[60a], A. Zhemchugov[79], Z. Zheng[105], D. Zhong[173], B. Zhou[105], C. Zhou[181], M. S. Zhou[15a,15d], M. Zhou[155], N. Zhou[60c], Y. Zhou[7], C. G. Zhu[60b], H. L. Zhu[60a], H. Zhu[15a], J. Zhu[105], Y. Zhu[60a], X. Zhuang[15a], K. Zhukov[110], V. Zhulanov[122a,122b], D. Zieminska[65], N. I. Zimine[79], S. Zimmermann[52], Z. Zinonos[115], M. Ziolkowski[151], G. Zobernig[181], A. Zoccoli[23a,23b], K. Zoch[53], T. G. Zorbas[149], R. Zou[37], L. Zwalinski[36]

[1] Department of Physics, University of Adelaide, Adelaide, Australia
[2] Physics Department, SUNY Albany, Albany, NY, USA
[3] Department of Physics, University of Alberta, Edmonton, AB, Canada
[4] [(a)]Department of Physics, Ankara University, Ankara, Turkey; [(b)]Istanbul Aydin University, Istanbul, Turkey; [(c)]Division of Physics, TOBB University of Economics and Technology, Ankara, Turkey
[5] LAPP, Université Grenoble Alpes, Université Savoie Mont Blanc, CNRS/IN2P3, Annecy, France
[6] High Energy Physics Division, Argonne National Laboratory, Argonne, IL, USA
[7] Department of Physics, University of Arizona, Tucson, AZ, USA
[8] Department of Physics, University of Texas at Arlington, Arlington, TX, USA
[9] Physics Department, National and Kapodistrian University of Athens, Athens, Greece
[10] Physics Department, National Technical University of Athens, Zografou, Greece
[11] Department of Physics, University of Texas at Austin, Austin, TX, USA
[12] [(a)]Faculty of Engineering and Natural Sciences, Bahcesehir University, Istanbul, Turkey; [(b)]Faculty of Engineering and Natural Sciences, Istanbul Bilgi University, Istanbul, Turkey; [(c)]Department of Physics, Bogazici University, Istanbul, Turkey; [(d)]Department of Physics Engineering, Gaziantep University, Gaziantep, Turkey
[13] Institute of Physics, Azerbaijan Academy of Sciences, Baku, Azerbaijan
[14] Institut de Física d'Altes Energies (IFAE), Barcelona Institute of Science and Technology, Barcelona, Spain
[15] [(a)]Institute of High Energy Physics, Chinese Academy of Sciences, Beijing, China; [(b)]Physics Department, Tsinghua University, Beijing, China; [(c)]Department of Physics, Nanjing University, Nanjing, China; [(d)]University of Chinese Academy of Science (UCAS), Beijing, China
[16] Institute of Physics, University of Belgrade, Belgrade, Serbia
[17] Department for Physics and Technology, University of Bergen, Bergen, Norway
[18] Physics Division, Lawrence Berkeley National Laboratory and University of California, Berkeley, CA, USA
[19] Institut für Physik, Humboldt Universität zu Berlin, Berlin, Germany
[20] Albert Einstein Center for Fundamental Physics and Laboratory for High Energy Physics, University of Bern, Bern, Switzerland
[21] School of Physics and Astronomy, University of Birmingham, Birmingham, UK
[22] Facultad de Ciencias y Centro de Investigaciónes, Universidad Antonio Nariño, Bogota, Colombia
[23] [(a)]Dipartimento di Fisica, INFN Bologna and Universita' di Bologna, Bologna, Italy; [(b)]INFN Sezione di Bologna, Bologna, Italy
[24] Physikalisches Institut, Universität Bonn, Bonn, Germany
[25] Department of Physics, Boston University, Boston, MA, USA
[26] Department of Physics, Brandeis University, Waltham, MA, USA
[27] [(a)]Transilvania University of Brasov, Brasov, Romania; [(b)]Horia Hulubei National Institute of Physics and Nuclear Engineering, Bucharest, Romania; [(c)]Department of Physics, Alexandru Ioan Cuza University of Iasi, Iasi, Romania ; [(d)]National Institute for Research and Development of Isotopic and Molecular Technologies, Physics Department, Cluj-Napoca, Romania; [(e)]University Politehnica Bucharest, Bucharest, Romania; [(f)]West University in Timisoara, Timisoara, Romania
[28] [(a)]Faculty of Mathematics, Physics and Informatics, Comenius University, Bratislava, Slovakia; [(b)]Department of Subnuclear Physics, Institute of Experimental Physics of the Slovak Academy of Sciences, Kosice, Slovak Republic
[29] Physics Department, Brookhaven National Laboratory, Upton, NY, USA
[30] Departamento de Física, Universidad de Buenos Aires, Buenos Aires, Argentina
[31] California State University, Long Beach, CA, USA
[32] Cavendish Laboratory, University of Cambridge, Cambridge, UK
[33] [(a)]Department of Physics, University of Cape Town, Cape Town, UK; [(b)]Department of Mechanical Engineering Science, University of Johannesburg, Johannesburg, South Africa; [(c)]School of Physics, University of the Witwatersrand, Johannesburg, South Africa

[34] Department of Physics, Carleton University, Ottawa, ON, Canada
[35] [(a)]Faculté des Sciences Ain Chock, Réseau Universitaire de Physique des Hautes Energies - Université Hassan II, Casablanca, Morocco; [(b)]Faculté des Sciences, Université Ibn-Tofail, Kénitra, Morocco; [(c)]Faculté des Sciences Semlalia, Université Cadi Ayyad, LPHEA-Marrakech, Marrakech, Morocco; [(d)]Faculté des Sciences, Université Mohamed Premier and LPTPM, Oujda, Morocco; [(e)]Faculté des sciences, Université Mohammed V, Rabat, Morocco
[36] CERN, Geneva, Switzerland
[37] Enrico Fermi Institute, University of Chicago, Chicago, IL, USA
[38] LPC, Université Clermont Auvergne, CNRS/IN2P3, Clermont-Ferrand, France
[39] Nevis Laboratory, Columbia University, Irvington, NY, USA
[40] Niels Bohr Institute, University of Copenhagen, Copenhagen, Denmark
[41] [(a)]Dipartimento di Fisica, Università della Calabria, Rende, Denmark; [(b)]INFN Gruppo Collegato di Cosenza, Laboratori Nazionali di Frascati, Frascati, Italy
[42] Physics Department, Southern Methodist University, Dallas, TX, USA
[43] Physics Department, University of Texas at Dallas, Richardson, TX, USA
[44] National Centre for Scientific Research "Demokritos", Agia Paraskevi, Greece
[45] [(a)]Department of Physics, Stockholm University, Stockholm, Sweden; [(b)]Oskar Klein Centre, Stockholm, Sweden
[46] Deutsches Elektronen-Synchrotron DESY, Hamburg and Zeuthen, Germany
[47] Lehrstuhl für Experimentelle Physik IV, Technische Universität Dortmund, Dortmund, Germany
[48] Institut für Kern- und Teilchenphysik, Technische Universität Dresden, Dresden, Germany
[49] Department of Physics, Duke University, Durham, NC, USA
[50] SUPA-School of Physics and Astronomy, University of Edinburgh, Edinburgh, UK
[51] INFN e Laboratori Nazionali di Frascati, Frascati, Italy
[52] Physikalisches Institut, Albert-Ludwigs-Universität Freiburg, Freiburg, Germany
[53] II. Physikalisches Institut, Georg-August-Universität Göttingen, Göttingen, Germany
[54] Département de Physique Nucléaire et Corpusculaire, Université de Genève, Geneva, Switzerland
[55] [(a)]Dipartimento di Fisica, Università di Genova, Genoa, Italy; [(b)]INFN Sezione di Genova, Genoa, Italy
[56] II. Physikalisches Institut, Justus-Liebig-Universität Giessen, Giessen, Germany
[57] SUPA-School of Physics and Astronomy, University of Glasgow, Glasgow, UK
[58] LPSC, Université Grenoble Alpes, CNRS/IN2P3, Grenoble INP, Grenoble, France
[59] Laboratory for Particle Physics and Cosmology, Harvard University, Cambridge, MA, USA
[60] [(a)]Department of Modern Physics and State Key Laboratory of Particle Detection and Electronics, University of Science and Technology of China, Hefei, China; [(b)]Institute of Frontier and Interdisciplinary Science and Key Laboratory of Particle Physics and Particle Irradiation (MOE), Shandong University, Qingdao, China; [(c)]School of Physics and Astronomy, Shanghai Jiao Tong University, KLPPAC-MoE, SKLPPC, Shanghai, China; [(d)]Tsung-Dao Lee Institute, Shanghai, China
[61] [(a)]Kirchhoff-Institut für Physik, Ruprecht-Karls-Universität Heidelberg, Heidelberg, Germany; [(b)]Physikalisches Institut, Ruprecht-Karls-Universität Heidelberg, Heidelberg, Germany
[62] Faculty of Applied Information Science, Hiroshima Institute of Technology, Hiroshima, Japan
[63] [(a)]Department of Physics, Chinese University of Hong Kong, Shatin, N.T., Hong Kong, Japan; [(b)]Department of Physics, University of Hong Kong, Hong Kong, Japan; [(c)]Department of Physics and Institute for Advanced Study, Hong Kong University of Science and Technology, Clear Water Bay, Kowloon, Hong Kong, China
[64] Department of Physics, National Tsing Hua University, Hsinchu, Taiwan
[65] Department of Physics, Indiana University, Bloomington, IN, USA
[66] [(a)]INFN Gruppo Collegato di Udine, Sezione di Trieste, Udine, Italy; [(b)]ICTP, Trieste, Italy; [(c)]Dipartimento Politecnico di Ingegneria e Architettura, Università di Udine, Udine, Italy
[67] [(a)]INFN Sezione di Lecce, Lecce, Italy; [(b)]Dipartimento di Matematica e Fisica, Università del Salento, Lecce, Italy
[68] [(a)]INFN Sezione di Milano, Milan, Italy; [(b)]Dipartimento di Fisica, Università di Milano, Milan, Italy
[69] [(a)]INFN Sezione di Napoli, Naples, Italy; [(b)]Dipartimento di Fisica, Università di Napoli, Naples, Italy
[70] [(a)]INFN Sezione di Pavia, Pavia, Italy; [(b)]Dipartimento di Fisica, Università di Pavia, Pavia, Italy
[71] [(a)]INFN Sezione di Pisa, Pisa, Italy; [(b)]Dipartimento di Fisica E. Fermi, Università di Pisa, Pisa, Italy
[72] [(a)]INFN Sezione di Roma, Rome, Italy; [(b)]Dipartimento di Fisica, Sapienza Università di Roma, Rome, Italy
[73] [(a)]INFN Sezione di Roma Tor Vergata, Rome, Italy; [(b)]Dipartimento di Fisica, Università di Roma Tor Vergata, Rome, Italy

[74] [(a)]INFN Sezione di Roma Tre, Rome, Italy; [(b)]Dipartimento di Matematica e Fisica, Università Roma Tre, Rome, Italy
[75] [(a)]INFN-TIFPA, Povo, Italy; [(b)]Università degli Studi di Trento, Trento, Italy
[76] Institut für Astro- und Teilchenphysik, Leopold-Franzens-Universität, Innsbruck, Austria
[77] University of Iowa, Iowa City, IA, USA
[78] Department of Physics and Astronomy, Iowa State University, Ames, IA, USA
[79] Joint Institute for Nuclear Research, Dubna, Russia
[80] [(a)]Departamento de Engenharia Elétrica, Universidade Federal de Juiz de Fora (UFJF), Juiz de Fora, Russia; [(b)]Universidade Federal do Rio De Janeiro COPPE/EE/IF, Rio de Janeiro, Russia; [(c)]Universidade Federal de São João del Rei (UFSJ), São João del Rei, Russia; [(d)]Instituto de Física, Universidade de São Paulo, São Paulo, Brazil
[81] KEK, High Energy Accelerator Research Organization, Tsukuba, Japan
[82] Graduate School of Science, Kobe University, Kobe, Japan
[83] [(a)]AGH University of Science and Technology, Faculty of Physics and Applied Computer Science, Krakow, Poland; [(b)]Marian Smoluchowski Institute of Physics, Jagiellonian University, Krakow, Poland
[84] Institute of Nuclear Physics Polish Academy of Sciences, Krakow, Poland
[85] Faculty of Science, Kyoto University, Kyoto, Japan
[86] Kyoto University of Education, Kyoto, Japan
[87] Research Center for Advanced Particle Physics and Department of Physics, Kyushu University, Fukuoka, Japan
[88] Instituto de Física La Plata, Universidad Nacional de La Plata and CONICET, La Plata, Argentina
[89] Physics Department, Lancaster University, Lancaster, UK
[90] Oliver Lodge Laboratory, University of Liverpool, Liverpool, UK
[91] Department of Experimental Particle Physics, Jožef Stefan Institute and Department of Physics, University of Ljubljana, Ljubljana, Slovenia
[92] School of Physics and Astronomy, Queen Mary University of London, London, UK
[93] Department of Physics, Royal Holloway University of London, Egham, UK
[94] Department of Physics and Astronomy, University College London, London, UK
[95] Louisiana Tech University, Ruston, LA, USA
[96] Fysiska institutionen, Lunds universitet, Lund, Sweden
[97] Centre de Calcul de l'Institut National de Physique Nucléaire et de Physique des Particules (IN2P3), Villeurbanne, France
[98] Departamento de Física Teorica C-15 and CIAFF, Universidad Autónoma de Madrid, Madrid, Spain
[99] Institut für Physik, Universität Mainz, Mainz, Germany
[100] School of Physics and Astronomy, University of Manchester, Manchester, UK
[101] CPPM, Aix-Marseille Université, CNRS/IN2P3, Marseille, France
[102] Department of Physics, University of Massachusetts, Amherst, MA, USA
[103] Department of Physics, McGill University, Montreal, QC, Canada
[104] School of Physics, University of Melbourne, Melbourne, VIC, Australia
[105] Department of Physics, University of Michigan, Ann Arbor, MI, USA
[106] Department of Physics and Astronomy, Michigan State University, East Lansing, MI, USA
[107] B.I. Stepanov Institute of Physics, National Academy of Sciences of Belarus, Minsk, Belarus
[108] Research Institute for Nuclear Problems of Byelorussian State University, Minsk, Belarus
[109] Group of Particle Physics, University of Montreal, Montreal, QC, Canada
[110] P.N. Lebedev Physical Institute of the Russian Academy of Sciences, Moscow, Russia
[111] Institute for Theoretical and Experimental Physics of the National Research Centre Kurchatov Institute, Moscow, Russia
[112] National Research Nuclear University MEPhI, Moscow, Russia
[113] D.V. Skobeltsyn Institute of Nuclear Physics, M.V. Lomonosov Moscow State University, Moscow, Russia
[114] Fakultät für Physik, Ludwig-Maximilians-Universität München, Munich, Germany
[115] Max-Planck-Institut für Physik (Werner-Heisenberg-Institut), Munich, Germany
[116] Nagasaki Institute of Applied Science, Nagasaki, Japan
[117] Graduate School of Science and Kobayashi-Maskawa Institute, Nagoya University, Nagoya, Japan
[118] Department of Physics and Astronomy, University of New Mexico, Albuquerque, NM, USA
[119] Institute for Mathematics, Astrophysics and Particle Physics, Radboud University Nijmegen/Nikhef, Nijmegen, The Netherlands
[120] Nikhef National Institute for Subatomic Physics and University of Amsterdam, Amsterdam, The Netherlands

[121] Department of Physics, Northern Illinois University, DeKalb, IL, USA
[122] [(a)]Budker Institute of Nuclear Physics and NSU, SB RAS, Novosibirsk, Russia; [(b)]Novosibirsk State University, Novosibirsk, Russia
[123] Institute for High Energy Physics of the National Research Centre Kurchatov Institute, Protvino, Russia
[124] Department of Physics, New York University, New York, NY, USA
[125] Ochanomizu University, , Otsuka, Bunkyo-ku, Tokyo, Japan
[126] Ohio State University, Columbus, OH, USA
[127] Faculty of Science, Okayama University, Okayama, Japan
[128] Homer L. Dodge Department of Physics and Astronomy, University of Oklahoma, Norman, OK, USA
[129] Department of Physics, Oklahoma State University, Stillwater, OK, USA
[130] Palacký University, RCPTM, Joint Laboratory of Optics, Olomouc, Czech Republic
[131] Center for High Energy Physics, University of Oregon, Eugene, OR, USA
[132] LAL, Université Paris-Sud, CNRS/IN2P3, Université Paris-Saclay, Orsay, France
[133] Graduate School of Science, Osaka University, Osaka, Japan
[134] Department of Physics, University of Oslo, Oslo, Norway
[135] Department of Physics, Oxford University, Oxford, UK
[136] LPNHE, Sorbonne Université, Paris Diderot Sorbonne Paris Cité, CNRS/IN2P3, Paris, France
[137] Department of Physics, University of Pennsylvania, Philadelphia, PA, USA
[138] Konstantinov Nuclear Physics Institute of National Research Centre "Kurchatov Institute", PNPI, St. Petersburg, Russia
[139] Department of Physics and Astronomy, University of Pittsburgh, Pittsburgh, PA, USA
[140] [(a)]Laboratório de Instrumentação e Física Experimental de Partículas-LIP, Coimbra, Portugal; [(b)]Departamento de Física, Faculdade de Ciências, Universidade de Lisboa, Lisbon, Portugal; [(c)]Departamento de Física, Universidade de Coimbra, Coimbra, Portugal; [(d)]Centro de Física Nuclear da Universidade de Lisboa, Lisbon, Portugal; [(e)]Departamento de Física, Universidade do Minho, Braga, Portugal; [(f)]Universidad de Granada, Granada, Spain; [(g)]Dep Física and CEFITEC of Faculdade de Ciências e Tecnologia, Universidade Nova de Lisboa, Caparica, Portugal
[141] Institute of Physics of the Czech Academy of Sciences, Prague, Czech Republic
[142] Czech Technical University in Prague, Prague, Czech Republic
[143] Charles University, Faculty of Mathematics and Physics, Prague, Czech Republic
[144] Particle Physics Department, Rutherford Appleton Laboratory, Didcot, UK
[145] IRFU, CEA, Université Paris-Saclay, Gif-sur-Yvette, France
[146] Santa Cruz Institute for Particle Physics, University of California Santa Cruz, Santa Cruz, CA, USA
[147] [(a)]Departamento de Física, Pontificia Universidad Católica de Chile, Santiago, Chile; [(b)]Departamento de Física, Universidad Técnica Federico Santa María, Valparaíso, Chile
[148] Department of Physics, University of Washington, Seattle, WA, USA
[149] Department of Physics and Astronomy, University of Sheffield, Sheffield, UK
[150] Department of Physics, Shinshu University, Nagano, Japan
[151] Department Physik, Universität Siegen, Siegen, Germany
[152] Department of Physics, Simon Fraser University, Burnaby, BC, Canada
[153] SLAC National Accelerator Laboratory, Stanford, CA, USA
[154] Physics Department, Royal Institute of Technology, Stockholm, Sweden
[155] Departments of Physics and Astronomy, Stony Brook University, Stony Brook, NY, USA
[156] Department of Physics and Astronomy, University of Sussex, Brighton, UK
[157] School of Physics, University of Sydney, Sydney, Australia
[158] Institute of Physics, Academia Sinica, Taipei, Taiwan
[159] [(a)]E. Andronikashvili Institute of Physics, Iv. Javakhishvili Tbilisi State University, Tbilisi, Taiwan; [(b)]High Energy Physics Institute, Tbilisi State University, Tbilisi, Georgia
[160] Department of Physics, Technion, Israel Institute of Technology, Haifa, Israel
[161] Raymond and Beverly Sackler School of Physics and Astronomy, Tel Aviv University, Tel Aviv, Israel
[162] Department of Physics, Aristotle University of Thessaloniki, Thessaloniki, Greece
[163] International Center for Elementary Particle Physics and Department of Physics, University of Tokyo, Tokyo, Japan
[164] Graduate School of Science and Technology, Tokyo Metropolitan University, Tokyo, Japan
[165] Department of Physics, Tokyo Institute of Technology, Tokyo, Japan
[166] Tomsk State University, Tomsk, Russia

[167] Department of Physics, University of Toronto, Toronto, ON, Canada
[168] [(a)]TRIUMF, Vancouver, BC, Canada; [(b)]Department of Physics and Astronomy, York University, Toronto, ON, Canada
[169] Division of Physics and Tomonaga Center for the History of the Universe, Faculty of Pure and Applied Sciences, University of Tsukuba, Tsukuba, Japan
[170] Department of Physics and Astronomy, Tufts University, Medford, MA, USA
[171] Department of Physics and Astronomy, University of California Irvine, Irvine, CA, USA
[172] Department of Physics and Astronomy, University of Uppsala, Uppsala, Sweden
[173] Department of Physics, University of Illinois, Urbana, IL, USA
[174] Instituto de Física Corpuscular (IFIC), Centro Mixto Universidad de Valencia - CSIC, Valencia, Spain
[175] Department of Physics, University of British Columbia, Vancouver, BC, Canada
[176] Department of Physics and Astronomy, University of Victoria, Victoria, BC, Canada
[177] Fakultät für Physik und Astronomie, Julius-Maximilians-Universität Würzburg, Würzburg, Germany
[178] Department of Physics, University of Warwick, Coventry, UK
[179] Waseda University, Tokyo, Japan
[180] Department of Particle Physics, Weizmann Institute of Science, Rehovot, Israel
[181] Department of Physics, University of Wisconsin, Madison, WI, USA
[182] Fakultät für Mathematik und Naturwissenschaften, Fachgruppe Physik, Bergische Universität Wuppertal, Wuppertal, Germany
[183] Department of Physics, Yale University, New Haven, CT, USA
[184] Yerevan Physics Institute, Yerevan, Armenia

[a] Also at Centre for High Performance Computing, CSIR Campus, Rosebank, Cape Town, South Africa
[b] Also at CERN, Geneva, Switzerland
[c] Also at CPPM, Aix-Marseille Université, CNRS/IN2P3, Marseille, France
[d] Also at Département de Physique Nucléaire et Corpusculaire, Université de Genève, Genève, Switzerland
[e] Also at Departament de Fisica de la Universitat Autonoma de Barcelona, Barcelona, Spain
[f] Also at Departamento de Física, Instituto Superior Técnico, Universidade de Lisboa, Lisboa, Portugal
[g] Also at Department of Applied Physics and Astronomy, University of Sharjah, Sharjah, United Arab Emirates
[h] Also at Department of Financial and Management Engineering, University of the Aegean, Chios, Greece
[i] Also at Department of Physics and Astronomy, Michigan State University, East Lansing, MI, USA
[j] Also at Department of Physics and Astronomy, University of Louisville, Louisville, KY, USA
[k] Also at Department of Physics and Astronomy, University of Sheffield, Sheffield, UK
[l] Also at Department of Physics, California State University, East Bay, USA
[m] Also at Department of Physics, California State University, Fresno, USA
[n] Also at Department of Physics, California State University, Sacramento, USA
[o] Also at Department of Physics, King's College London, London, UK
[p] Also at Department of Physics, St. Petersburg State Polytechnical University, St. Petersburg, Russia
[q] Also at Department of Physics, Stanford University, Stanford, CA, USA
[r] Also at Department of Physics, University of Adelaide, Adelaide, Australia
[s] Also at Department of Physics, University of Fribourg, Fribourg, Switzerland
[t] Also at Department of Physics, University of Michigan, Ann Arbor, MI, USA
[u] Also at Faculty of Physics, M.V. Lomonosov Moscow State University, Moscow, Russia
[v] Also at Giresun University, Faculty of Engineering, Giresun, Turkey
[w] Also at Graduate School of Science, Osaka University, Osaka, Japan
[x] Also at Hellenic Open University, Patras, Greece
[y] Also at Institucio Catalana de Recerca i Estudis Avancats, ICREA, Barcelona, Spain
[z] Also at Institut für Experimentalphysik, Universität Hamburg, Hamburg, Germany
[aa] Also at Institute for Mathematics, Astrophysics and Particle Physics, Radboud University Nijmegen/Nikhef, Nijmegen, The Netherlands
[ab] Also at Institute for Nuclear Research and Nuclear Energy (INRNE) of the Bulgarian Academy of Sciences, Sofia, Bulgaria
[ac] Also at Institute for Particle and Nuclear Physics, Wigner Research Centre for Physics, Budapest, Hungary
[ad] Also at Institute of High Energy Physics, Chinese Academy of Sciences, Beijing, China

[ae] Also at Institute of Particle Physics (IPP), Canada
[af] Also at Institute of Physics, Academia Sinica, Taipei, Taiwan
[ag] Also at Institute of Physics, Azerbaijan Academy of Sciences, Baku, Azerbaijan
[ah] Also at Institute of Theoretical Physics, Ilia State University, Tbilisi, Georgia
[ai] Also at Instituto de Fisica Teorica, IFT-UAM/CSIC, Madrid, Spain
[aj] Also at Istanbul University, Department of Physics, Istanbul, Turkey
[ak] Also at Joint Institute for Nuclear Research, Dubna, Russia
[al] Also at LAL, Université Paris-Sud, CNRS/IN2P3, Université Paris-Saclay, Orsay, France
[am] Also at Louisiana Tech University, Ruston, LA, USA
[an] Also at LPNHE, Sorbonne Université, Paris Diderot Sorbonne Paris Cité, CNRS/IN2P3, Paris, France
[ao] Also at Manhattan College, New York, NY, USA
[ap] Also at Moscow Institute of Physics and Technology State University, Dolgoprudny, Russia
[aq] Also at National Research Nuclear University MEPhI, Moscow, Russia
[ar] Also at Physics Department, An-Najah National University, Nablus, Palestine
[as] Also at Physics Dept, University of South Africa, Pretoria, South Africa
[at] Also at Physikalisches Institut, Albert-Ludwigs-Universität Freiburg, Freiburg, Germany
[au] Also at School of Physics, Sun Yat-sen University, Guangzhou, China
[av] Also at The City College of New York, New York, NY, USA
[aw] Also at The Collaborative Innovation Center of Quantum Matter (CICQM), Beijing, China
[ax] Also at Tomsk State University, Tomsk, and Moscow Institute of Physics and Technology State University, Dolgoprudny, Russia
[ay] Also at TRIUMF, Vancouver, BC, Canada
[az] Also at Universita di Napoli Parthenope, Naples, Italy
*Deceased